ON THE STABILITY OF NATURAL CIRCULATION LOOPS WITH PHASE CHANGE

by

Troy C. Haskin

A dissertation submitted in partial fulfillment of the requirements for the degree of

Doctor of Philosophy

(Nuclear Engineering and Engineering Physics)

at the

UNIVERSITY OF WISCONSIN–MADISON

2016

Date of final oral examination: September 20, 2016

The dissertation is approved by the following members of the Final Oral Committee:

Michael L. Corradini, *Professor*, *Engineering Physics*
Robert J. Witt, *Professor*, *Engineering Physics*
Jake Blanchard, *Professor*, *Engineering Physics*
Gregory A. Moses, *Professor*, *Engineering Physics*
Christopher Rutland, *Professor*, *Mechanical Engineering*

Abstract

The stability of a simple, closed-loop, water-cooled natural circulation system was characterized over a range of single phase and two-phase states. The motivation for this investigation is a Next Generation Nuclear Plant safety cooling system called the Reactor Cavity Cooling System (RCCS). One of the proposed designs for the RCCS is a closed-circuit of network piping using water as a working fluid. One of the safety considerations for such a system is the stability of the system at steady-state under a large number of unknown states. This work provides a derivation of the commonly used one-dimensional conservation laws used in thermohydraulic system modeling and a novel discretization scheme that allows for exact integration of the computational domain for accurate calculation of eigenvalues of a linearized system. The steady-state solution of the discretized equations is then performed using a fully nonlinear Jacobian-Free Newton Krylov Method for a number of temperatures, pressures, and heat loads both in single and two-phase conditions. All of the single and two-phase state exhibit linear stability to small perturbations in values. The linear stability is also found to increase with increasing heat load due to the greater inertia of the system damping out small perturbation effectively and with increasing pressure due to the greater stiffness of the fluid. Nonlinear stability was also examined for a point power insertion of varying intensity from two steady-states. The loop exhibited stability for all power insertions from both steady-states, returning to the initial steady value shortly after the pulse.

Acknowledgments

First and foremost, I would like to offer my sincerest thanks to my advisor Michael Corradini for his unending wisdom, guidance, and patience. His encouragement and understanding provided the bedrock on which this work stands. He has served as a paragon of knowledge, research, and achievement to which I will forevermore strive towards; a goal for which I am extremely appreciative.

I would also like to thank several colleagues for their years of camaraderie and support: Lewis, Gary, Ryan, Ryan, Billy, Mike, Brian, Amy, Megan, Tammy, Denise, and Aaron. Additionally, I would like to offer my heartfelt appreciation for the boundless friendship of Joe, Leah, Steph, Abby, Eric, Pat, Jordan, David, Gautam, Krissy, Sam, Arrielle, Louise, Ashley, David, David, Matt, Andrew, and so many more. Lastly, it's impossible to express how much I owe to my mother Mary, brother Bradley, and father Craig for all they have done for me as long as I can remember.

List of Contents

List of Tables

List of Figures

List of Acronyms

ANL	Argonne National Laboratory
EOS	equation of state
FDM	Finite Difference Method
FEM	Finite Element Method
FVM	Finite Volume Method
GMRES	Generalized Minimal Residual (Method)
HEM	Homogenous Equilibrium Model
IAPWS	International Association for the Properties of Water and Steam
IAPWS-95	IAPWS Formulation 1995 for the Thermodynamic Properties of Ordinary Water Substance for General and Scientific Use
MOL	Method of Lines
NGNP	Next Generation Nuclear Plant
NRC	Nuclear Regulatory Commission
ODE	Ordinary differential equation
PDE	Partial differential equation
RCCS	Reactor Cavity Cooling System
SFM	Separated Flow Model

Chapter 1

Introduction

Stability of two-phase natural circulation systems is not a novel subject in-and-of itself. However, this work aims to perform the analysis on a closed-loop geometry with unique characteristics to be discussed. Motivation for this effort will be given from examination of a physical system. Then, a literature review will be given that overviews the field of stability analysis in general. Finally, some concluding remarks will be given pertaining to the goals of this work.

1.1 Reactor Cavity Cooling System

The primary motivation behind this stability work is the so-called Reactor Cavity Cooling System (RCCS), which is a safety system for roposed Generation IV reactor designs. A definition and discussion of this safety system for full-scale application will be discussed first and followed by a description of an experimental test facility at the University of Wisconsin–Madison.

1.1.1 Full-Scale System

The Next Generation Nuclear Plant (NGNP) is a thermal-spectrum, gas-cooled reactor designed to be able to produce electricity as well as process heat for industrial applications. A novel feature of the NGNP is the RCCS. The RCCS is a natural circulation system of ducts designed to be NGNP's ultimate heat sink for decay heat under a number of accident scenarios. There are two main designs under consideration which vary mostly in their working fluid: air-cooled and water-cooled. This work will focus on the water-cooled RCCS design and leave air-cooled discussions left to the literature [1, 2].

A collaboration between Argonne National Laboratory (ANL) and the University of Wisconsin–Madison produced a base, full-scale RCCS system consisting of a two independent piping networks with each network having four main lines/tanks. Figure 1.1 outlines the basic design of system B but precludes any detail near the reactor. The elevation change of the system is on the order of several tens of meters with the reactor cavity portion being approximately twenty meters on its own. Within the reactor cavity, the eight cold lines of the RCCS split into approximately 200 so-called riser pipes that line the cavity wall and ensconce the reactor (see figure 1.2). The riser pipes then receive heat from the uninsulated reactor pressure vessel via convection and radiation. Due to the heating, the fluid that fills the pipes is subjected to a buoyancy force that results in upward flow.

During steady-state operation of the reactor, there is a persistent, parasitic heat loss from the reactor vessel to the RCCS of approximately 700 kW. If the reactor undergoes a loss-of-forced-flow accident with SCRAM, there is an expected peak decay heat load of 1.5 MW on the RCCS. If there is no loss of onsite or offsite power, the RCCS water storage tanks will be actively cooled, and the system is expected to maintain safe fuel temperatures for the duration of the accident. In the event of loss of onsite and offsite power (so-called station blackout),

Figure 1.1: ANL/UW-Madison water-cooled RCCS diagram. Water flows from a tank, through the cold leg (blue), through the reactor cavity system, and through the hot leg (red) to some tank on the train at the same conditions (a closed circuit).

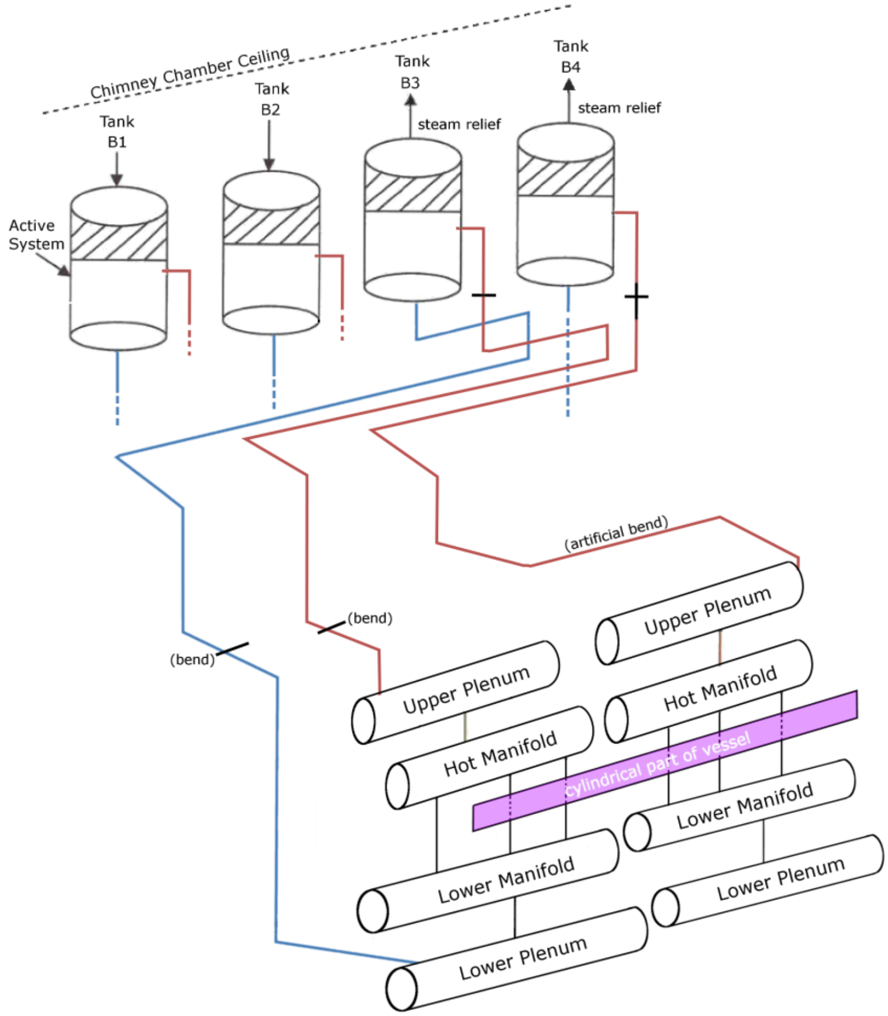

the RCCS can still continue to cool the reactor since the flow is naturally circulating, which is very important for the overall safety of the plant [3, §50.63].

However, without forced cooling, the reference temperature of the entire water system will continue to rise with continued decay heat exposure. At some point during the transient, the water leaving the riser system will reach the saturation temperature at atmospheric pressure. Due to the gravitational head of all the water on top of the risers, the water will not immediately boil. Rather, as the water flows to the top of the system, it will instantly boil as it passes into a region where the ambient pressure is below the saturation pressure; this process is called flashing. This sudden, discontinuous jump in substance properties results in flow oscillations because the steam produced from the flash is approximately 1,000 times less dense (i.e., lighter) than the liquid state on the cold side of the system.

Figure 1.3 shows a numerical simulation of the full-scale system. Before flashing, the mass flow rate is increasing and non-oscillatory. At the onset of flashing, the flow rate rapidly oscillates and evolves in a complicated manner. At some point in the evolution, the system's flow rate stabilizes and evolves just as the single phase system. The period, amplitude, and overall time evolution of these oscillations is subject to numerous factors and various linear and nonlinear effects. The oscillations are commonly referred to as density wave instabilities since they are driven by the density of the system [4]. These incessant perturbations could potentially lead to large, erratic flow excursions that could pose a safety risk via extreme mechanical or thermal damage.

Figure 1.2: Cutaway picture of reactor vessel, RCCS ducts/pipes in the reactor cavity. The low temperature fluid is in blue and the high temperature fluid is in red. The transparent boxes indicate network encasings. Credit: Darius Lisowski, University of Wisconsin–Madison.

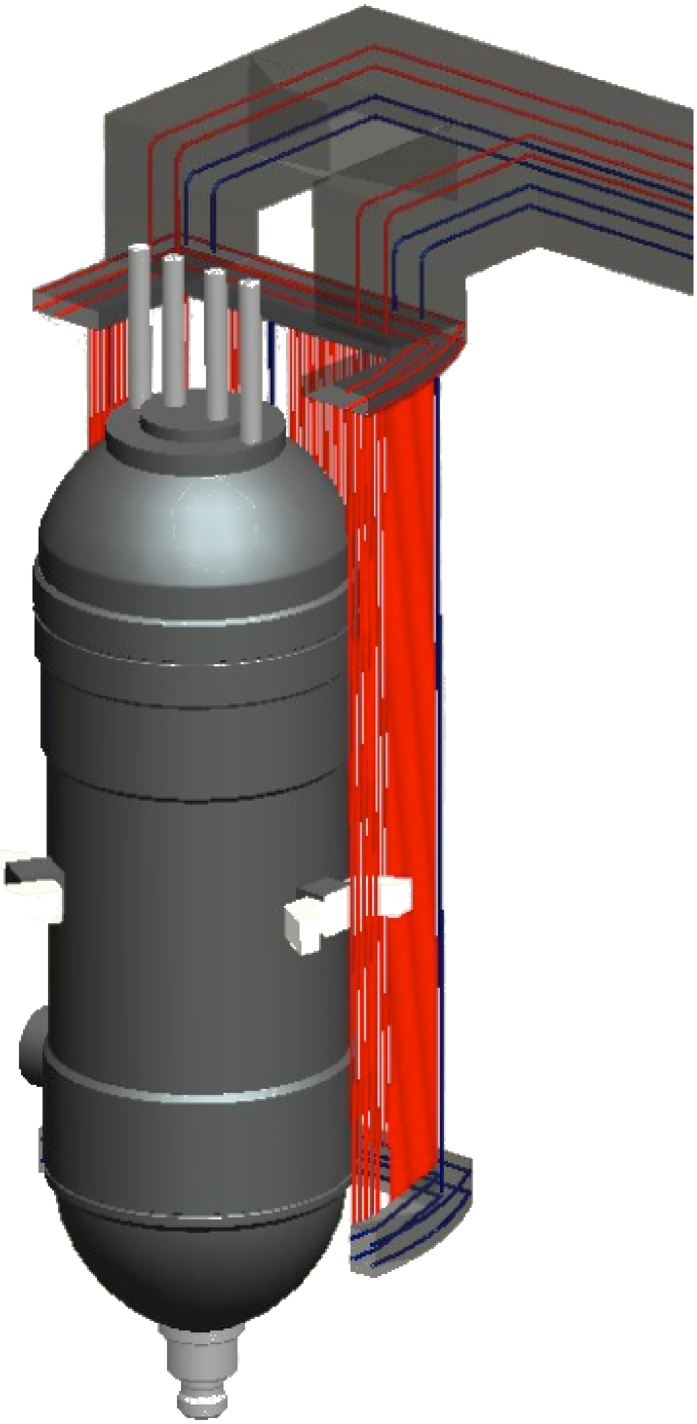

Figure 1.3: RCCS mass flow rate versus time under blackout conditions.

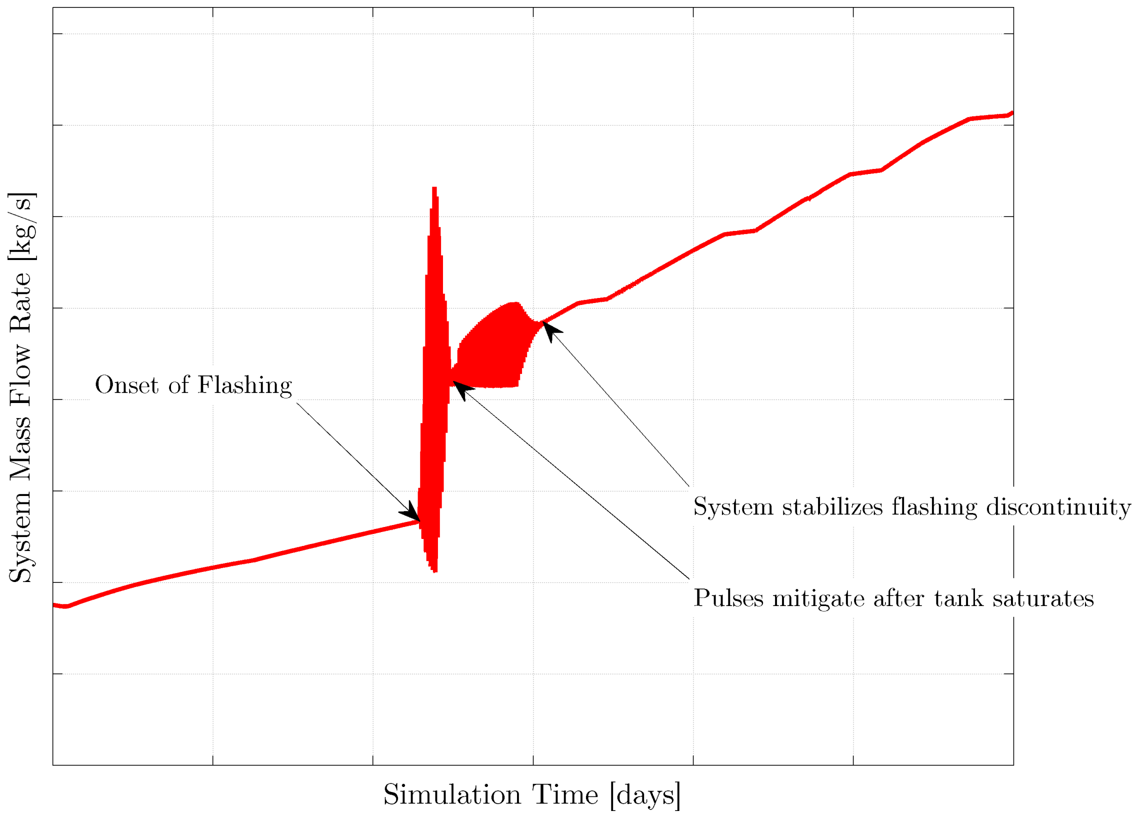

Figure 1.4: An overview of the whole RCCS experiment with important sections annotated.

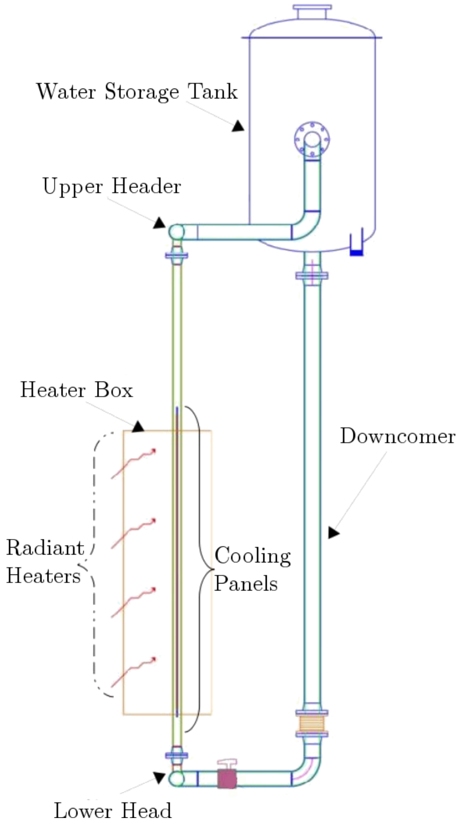

Figure 1.5: An overview of the RCCS experiment's three riser/radiant heater setup.

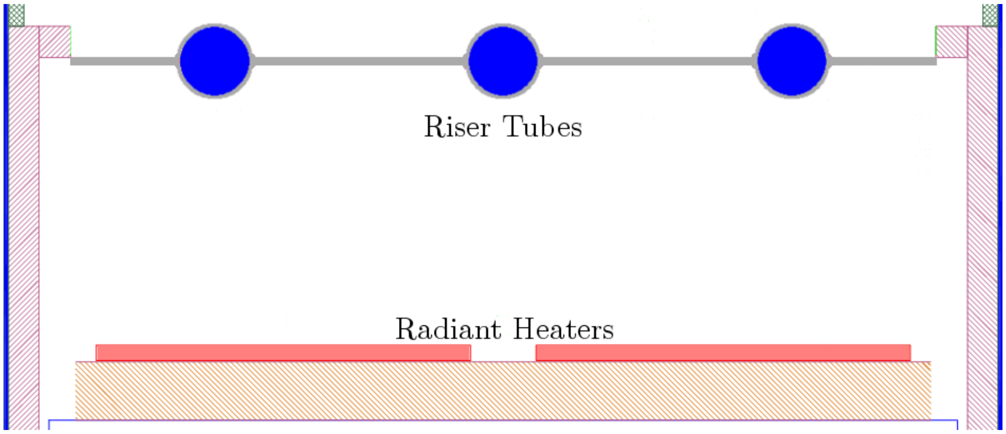

1.1.2 University of Wisconsin–Madison RCCS Experiment

While the RCCS discussed above was part of a full-scale reactor design, it has yet to be built. In part to aid in future endeavors to build such a reactor, an experiment was built at the University of Wisconsin–Madison to directly observe and measure the behavior of an RCCS-like system. The experiment, presented in-brief by figure 1.4, is a scaled version of the full-scale RCCS in terms of both dimension and number of risers. While the full-scale system spans tens of meters with hundreds of tubes, the experiment was scaled to a total height of approximately seven meters with three riser tubes. Heaters mounted opposite the riser tubes provide the power to drive the natural circulation of the system.

Due to the smaller scale and detailed design, a more precise numerical model could be made and benchmarked against data. The full convection/radiation enclosure for the heater box was used to simulate station blackout conditions as in the full-scale with a scaled heat flux. The mass flow rates from each of the risers for this accident simulation are shown in figure 1.6. The highly oscillatory nature of the flow rate after flashing begins is not only present but metastasized in this experiment. Additionally, reverse flows in two of the risers is present (though the total system mass flow rate is always positive). This local reversal of flow is more than likely systemic since short piping at the top allows a two-phase condition to exist at the top of the red riser. While not expected in the full-scale system, this flow reversal is an interesting feature of the experiment's design and is currently being investigated.

Figure 1.6: Mass flow rate versus time for the three riser tubes of the RCCS experiment with station blackout accident conditions. The colors of the plot lines correspond to the riser colors in figure 1.7.

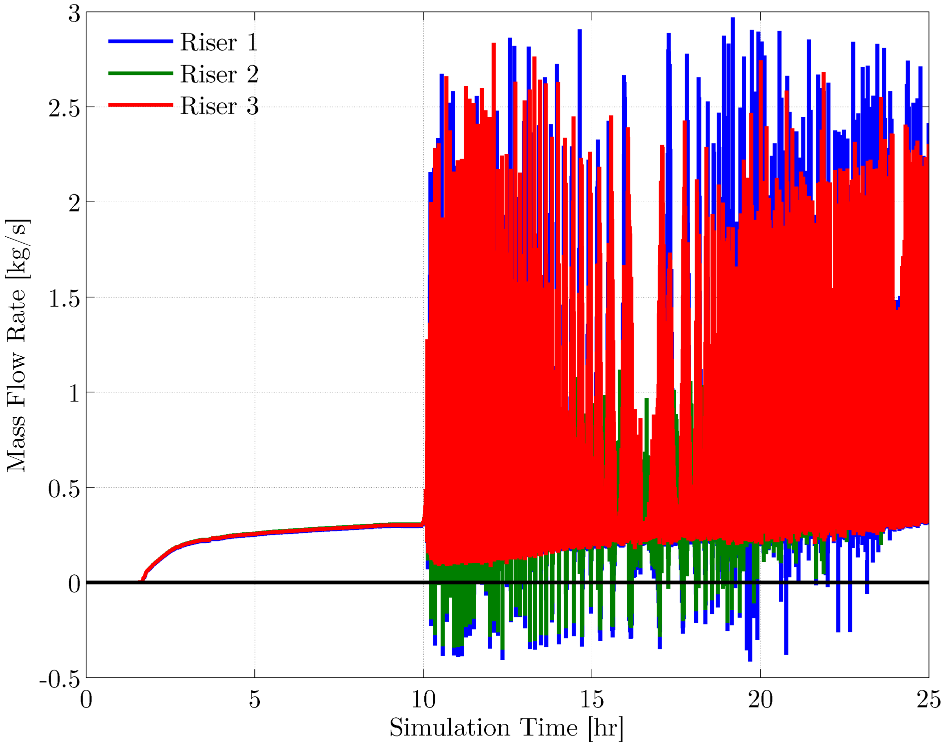

Figure 1.7: Basic layout of the RCCS experiment's numerical model. The blue and red outlines denote the cooling and heating zones, respectively.

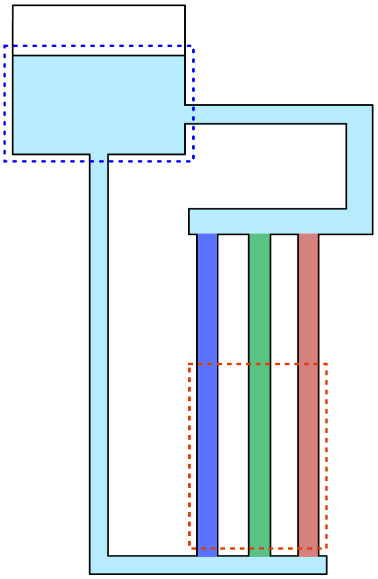

1.2 Literature

Two-phase flow instabilities have been extensively studied for numerous industrial applications, including thermosiphons and power cycle loops. Therefore, the literature of two-phase flow instabilities is extensive. It should be noted that single phase instabilities do exist and are researched [5], but an in-depth overview of those mechanisms will not be given. As such, an overview of two-phase instabilities, classifications, and definitions will be given. Then, specific discussion of efforts and techniques in the analysis will be discussed.

1.2.1 Two-Phase Flow Instabilities

There are a variety of ways to classify two-phase flow instabilities depending on geometry, spatial/temporal dependence, multiphase models, etc. Difficulties also arise when real world applications see a convergence of all of these parameters. Both Boure et al. and Kakac et al. provide extensive discussions of general two-phase flow instability characterization [6, 7], and their similar systems for describing two-phase systems will be used throughout this section. Tables 1.1 and 1.2 present a summary of general two-phase instabilities presented by the above authors; however, not all of them will be discussed in detail. Presad et al. [8] and Nayak et al. [9], while overlapping somewhat with the generic descriptions of instabilities, present and classify certain instabilities as natural circulation specific that should be described. Most of the following discussion concerns a flowing fluid undergoing phase transition in a channel which may require some familiarity with two-phase flow regimes; explanation of these regimes is left to the literature [10, 11, 12].

For clarity, key terms will be defined. If a system at steady-state is perturbed and eventually returns to its initial equilibrium, the system is described as stable. If a system at steady-state is perturbed into a neighborhood where no equilibrium exists near the initial state, the system possesses a static instability. A system has dynamic instabilities if there are inherently transient feedback mechanisms that may lead to a steady-state, though there is no guarantee of uniqueness. An instability that arises from another is referred to as a secondary phenomenon (the instigator being the primary). A compound instability is one that incorporates two or more mechanisms that confound analysis; fundamental instabilities are the opposite. Using a standard physical analogy, figure 1.8c is a stable system while figure 1.8d is an example of a system with a static instability.

One aspect of the stability the above definitions do not discuss is the magnitude of the system perturbations. The strength of the perturbation is important since it determines how much energy is imparted into the system and, therefore, how far the system will travel from its initial state. The importance can be seen in figures 1.8e and 1.8f where both systems exhibit different behavior depending how hard the system is “hit”. Figure 1.8e shows a linear instability while actually being nonlinearly stable with multiple equilibria. Figure 1.8f exhibits linear stability while being nonliearly stable These concepts are important to consider when looking at linear stability because the behavior beyond the system’s linear boundary is technically *terra incognita.* Actually performing a nonlinear analysis, if possible, is the only surefire tool for assessing stability.

Static Instabilities

Static instabilities are characterized by either a pure steady-state analysis or an analysis that foresees dynamic feedback from the steady-state system. The analysis tools used to derive stability boundaries for these instabilities will be discussed in section 2.4.

A flow excursion, also known as a Ledinegg instability, is the sudden drop in a steady flow rate

Figure 1.8: Ball-and-hill analogy of equilibrium descriptions. The ball represents some state at a given time and place, and the shapes supporting the ball dictate how the state moves when subjected to a perturbation. Troughs are considered stable while crests/runoffs are unstable.

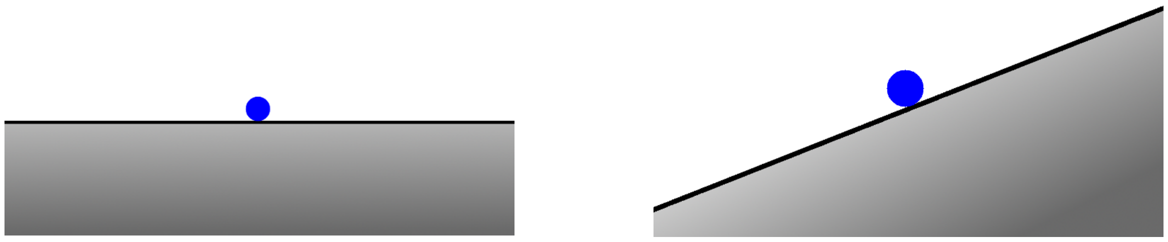

(a) Neutral equilibrium (infinitely many steady-states)

(b) No equilibrium (no steady-state)

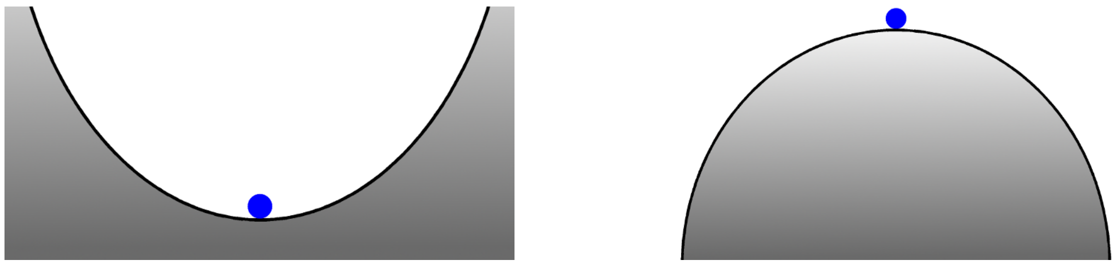

(c) Stable equilibrium

(d) Unstable equilibrium

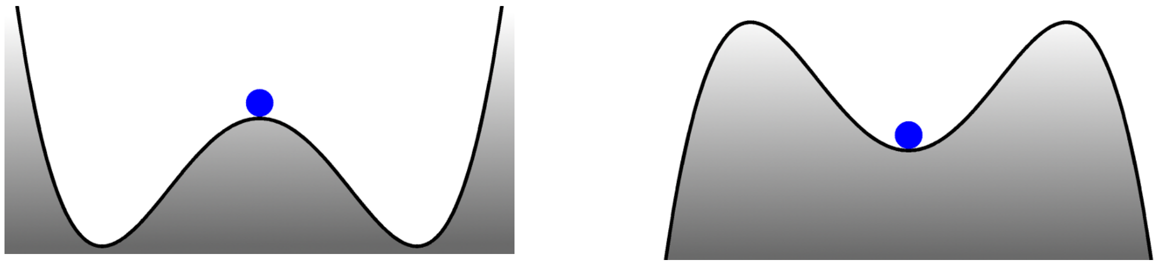

(e) Linearly unstable, nonlinearly stable equilibrium

(f) Linearly stable, nonlinearly unstable equilibrium

to a lower, steady value. This jump occurs when the pressure losses in a system decrease with increasing flow rate. For a liquid undergoing phase change in a channel, there is a complex, internal relationship between the buoyancy, friction, and acceleration momentum terms that must be taken into account for steady flow. If the flow is forced by external sources and the internal forces of the flow are not properly taken into account, then the pressure drop could rise with increasing flow; this is especially true for slightly sub-cooled flows entering a heated region where a sudden change in void fraction can have a large impact on the flow behavior with the system.

Fundamental relaxation instabilities occur when two or more flow regimes have state equilibriums close to each other. For example, a bubbly flow that experiences a small change in flow rate could transition to the annular regime. Then, the flow rate will experience an increase since annular flow has a relatively low pressure drop, and the flow regime transitions back to the bubbly regime. Given the right situation, this cycle could continue ad infinitum. The flow regime transitions act as a relaxation mechanism (in the dynamical system sense) that causes persistent, periodic behavior.

Chugging is an instability associated with the jetting of large vapor structures from a flow channel into larger space. This instability typically occurs with low velocities and moderate void fractions [11]. A flowing liquid receiving heat may develop large vapor bubbles in a coolant channel; this increases the flow rate due to the vapor-to-liquid ratio. After the bubbles have been expelled, or possibly quenched, at the channel exit, the flow rate will return to the pre-slug rate. As with the relaxation instability, this mechanism also has a periodic nature [13].

Dynamic Instabilities

Dynamic instabilities, unlike static, are inherently transient and primarily involve the transmission of information via waves. thermal hydraulic systems typically possess a material (density) wave and an acoustic (pressure) wave. For a non-ideal fluid, the acoustic wave's speed is primarily a function of the system's density and temperature while the material wave travels near the physical speed of the system.

Acoustic instabilities are typically of high frequency (10Hz–10kHz) and have been observed in various boiling regimes. The acoustic waves were found to cause large pressure drop oscillations relative to steady-state values. Even in situations where the lower frequency density waves were present, there was a clear superposition of high frequency acoustic waves with the material waves. At high pressure-and-temperature water experiments, the acoustic waves reached frequencies that were clearly audible (so-called whistler modes).

Material wave instabilities are the most common in two-phase flow and are a highly physical phenomenon that occur from a complex coupling of thermal hydraulic equations, constitutive relations, and geometry. These waves have also been described as “flow-void feedback instabilities” for boiling systems [14] and “time-delay oscillations” due to the relatively slow transmission of information at material speed [15]. Since the oscillation has its roots in the differing densities of a fluid's liquid and gas phases, vertical channel height (where the system pressure changes greatly with position), inlet conditions (thermodynamic and kinematic), and total heat transfer between the fluid and the surroundings are extremely important in the control and appearance of these flow oscillations. It has been found that by increasing the system pressure these oscillations can be mitigated or eliminated since the density ratio of the competing phases approach one another as the pressure increases.

These material oscillations can lead to oscillations in the boiling heat transfer processes at the wall and results in a compound thermal instability. The emphasis here is put on the highly variable nature of the two-phase heat transfer coefficient at the wall and how the information being propagated from the wall interacts with material wave oscillations. The effects of this interaction can be as bad as an oscillating dry point in the channel with large temperature oscillations.

Natural Circulation Instabilities

There are two natural circulation instabilities of primary interest: flashing and compound natural circulation. As mentioned in section 1.1, flashing occurs when a high temperature liquid flows into a region of lower pressure such that it enters a saturated or superheated state and immediately bursts into a two-phase mixture. This mechanism is a primary cause of material wave instabilities in natural circulation loops at low pressures or long vertical channels. This type of instability is currently under examination for one and two protypic fuel channels [16, 17].

The final instability is the compound natural circulation instability. This instability is the confluence of vertical channel heating, material wave oscillations (possibly due to flashing), chugging phenomenon, and flow regime transitions. Since the system's flow rate is not subject to any mechanical head contributions, all of these instabilities can occur concurrently and must be carefully analyzed to discern which of the mechanisms are present and which is dominant. These instabilities are extremely important for all types of nuclear reactors and are under continuously under investigation [18, 19, 20].

Table 1.1: *Summary of static flow instabilities due to [6]*

Name	**Class**	**Mechanism**	**Characteristics**
Flow excursion	Fundamental	$\frac{\partial \Delta P}{\partial(\rho u)}\Big\vert_{\text{int}} \leq \frac{\partial \Delta P}{\partial(\rho u)}\Big\vert_{\text{ext}}$	Sudden, large flow change to a new, stable state
Boiling crisis	Fundamental	Ineffective cooling	Wall temperature excursion and flow oscillation
Flow Regime Transition	Fundamental Relaxation	Varying ΔP between regimes	Cyclic flow pattern transitions and flow rate variations
Bumping, geysering, or chugging	Compound Relaxation	Periodic adjustment of metastable conditions	Periodic superheat and violent evaporation

Table 1.2: *Summary of dynamic flow instabilities due to [6]*

Name	**Class**	**Mechanism**	**Characteristics**
Acoustic Oscillations	Fundamental	Resonance of pressure waves	High frequency oscillations near the acoustic speeds
Density Wave Oscillations	Fundamental	Coupled mass, momentum, and energy feedback	Low frequency oscillations near the material speed
Thermal Oscillations	Compound	Variable heat transfer coefficient interacting with flow	Occurs during film boiling
BWR Instability	Compound	Hydraulic-neutronic coupling	Strong only for a small fuel time constant and low pressure
Parallel Channel Instability	Compound	Interaction among parallel channels	Various modes of flow redistribution
Pressure drop Oscillations	Secondary Compound	Flow excursions initiate interactions between channels and compressible volumes	Very low frequency, periodic process

Table 1.3: *Effects of parametric variation on instability for a flow entering a vertical channel sub-cooled or saturated due to [8]*

Parameter Increased	**Effect**	**Reason**
System pressure	Stability increases	Phase density difference lessens thus reducing the gravitational head gain.
Mass flow rate	Stability increases	Critical power for oscillation generation increases and avoids chugging.
Inlet sub-cooling	Destabilizes at small sub-coolings but stabilizes otherwise	For small sub-coolings,due to significant response delay in void formation with an increase in transit time. Otherwise, it reduces void fraction and increases non-boiling length.
Inlet resistance	Stability increases	Increases the single phase friction which has a damping effect upstream.
Exist resistance	Stability reduces	Increases two-phase friction which amplifies instabilities upstream
Riser height	Stability reduces	Increases two-phase gravitational pressure drop and phase transition as static head decreases

1.2.2 Previous Analysis Efforts

While the previous section discussed experimental observation, this section focuses on the analytical and numerical analysis of thermohydraulic stability. The two main types of analysis employed in stability analysis are linear and nonlinear (nonlinear being a superset of the other). Every analysis begins with a defined set of the conservation (i.e., balance) equations. These equations possess all of the modeling information and assumptions in the analysis to be performed. Three commonly used models are [21]:

- a Homogenous Equilibrium Model (HEM) where the distinct phases of a boiling fluid are treated as a single fluid with averaged properties;
- a Separated Flow Model (SFM) where an additional momentum equation is added to the HEM allowing phase slip;
- a two-fluid model where the distinct phases are treated as separate partitions of a total volume, have completely separate properties, and only communicate through their shared interface.

Chapter 2 discusses conservation laws in general and then focuses on the HEM equations, but for now, it suffices to say that these equations are nonlinear, coupled partial differential equations that do not, in general, admit analytical solutions.

After the model has been decided, authors either linearize the equations or not and assess the system's stability through various techniques. The specifics of the linear solution techniques are, for the most part, equivalent. What makes the approaches more interesting is the models used, approximations made, and geometry considered.

Wallis and Heasley present one of the earliest efforts to analytically tackle two-phase flow oscillations [22]. They investigated a simple, closed natural circulation loop with pentane as the working fluid. The analysis method looked at three sources of oscillations from a Lagrangian frame. The first source was changes in riser buoyancy resulting from velocity perturbations and an equation for the marginal stability was derived in terms of the friction factor's derivative with respect to some steady-state velocity. The second source was the heat input into the system with a theorized flow excursion for their loop. Lastly, they investigated parallel channels but did not complete the analysis due to the then intractability of the solution.

Welander, though not a study of two-phase instabilities, investigates a simple, closed loop with point sources and proportional constitutive relations.[23]. While the treatment is similar to Wallis and Heasley's, Welander's more mathematical approach is more in-line with this work's goals. Additionally, Welander derived an asymptotic steady-state solution and also compared the analytical neutral boundary with numerical experiments to confirm the boundary's validity. Zvirin and Greif continued this work by examining how an arbitrary initial condition evolved toward Welander's steady state [24]. They found that while the solution approached the analytical steady-state, the solution was without oscillation and concluded that the oscillation characteristics were strongly dependent on the shape of the initial condition.

Achard et al. investigated material wave oscillations in a horizontal boiling channel using both linear and nonlinear analysis [4]. They derived a lumped parameter integrodifferential equation. Upon linearizing the equation and using the friction and sub-cooling numbers as degrees of freedom, they found two absolutely unstable regions, several conditionally unstable regions, and one absolutely stable region. The conditionally unstable regions were found to depend on how actual system's state evolved in time and moved through the stability space. They also performed a nonlinear analysis where the parameter values to maintain stability were obtained by nonlinearly solving the lumped parameter equation for a given perturbation amplitude. The nonlinear analysis showed that stable parameter curves existed for their system, but the absolutely stable region shrank with increasing perturbation amplitude.

Lee and Ishii performed a linear analysis similar to Welander, but the system was explicitly two-phase, had a quadratic frictional dependence in velocity with a constant friction factor, and had a distributed heat load [25]. Additionally, as an extension of Zvirin and Greif's methodology, Lee and Ishii divided the loop into different regions with average properties and solved for the stability boundary using linear analysis.

Lee and Lee performed nearly the same analysis as Lee and Ishii with the added difficulty of a variable, flow regime-dependent friction factor [26]. Guanghui et al. also performed a similar analysis over a simple, closed loop that compared very well to experiments [27].

Knaani and Zvirin investigated the existence of multiple steady-states for a simple, closed loop undergoing boiling[28]. The analysis was done with HEM and incorporated a guess and check procedure for finding a solution to the nonlinear problem. They ultimately found multiple steady-states for the closed system due to the non-monotonic nature of the buoyancy term during phase change. Nayak et al. also performed analysis on a simple, closed loop but used a four equation model (two for mass and mixture equations for energy and momentum) and several different two-phase friction multipliers [29].

Lee and Pan undertook an HEM approach for a two-phase natural circulation system with two parallel, heated channels [30]. This treatment is the first work in this review to explicitly analyze a non-simple closed loop. Through a number of piece-wise integrations along the loop, the authors arrived at a set of ordinary differential equations that satisfied the zero pressure gradient requirement of the closed loop. Using the channel inlet sub-cooling as a parametric and a blackbox solver, the authors compared the steady-state channel flow rates with experimental data. The authors then found a stability curve for even heating of the channels that possessed two unstable regions and one stable region. The author concluded with a parametric study of how the stability region shifted with the addition of an orifice plate.

1.3 Research Purpose

The contribution of this work to the two-phase stability literature is a combination of topics in one analysis. First, this work uses a non-ideal, continuous equation of state (EOS) for water. Rather than approximating liquid water as a stiffened gas [31] or using tabulated values, a complete implementation of the equation of state of water from the International Association for the Properties of Water and Steam (IAPWS) is used. All thermodynamic and kinematic properties used in the simulations are calculated from the mechanically balanced mass and energy of the system. Second, this work uses an implementation of a modern, nonlinear solver that accurately and conservatively calculates all of the steady-states from which the linear stability calculations are made. The solver is based on Newton-Raphson methods but avoids the need to form the true Jacobian of the system during simulation, which greatly decreases the computational cost of the solution. Third, a modified discretization scheme is presented. It is a scheme that aims to allow complete physical coverage of the computational domain by a coarse, staggered grid and therefore allow complete and correct integration of the physical domain on both the conservation and momentum fields. This proper integration allows for a mathematically rigorous integration of the domain for accurate calculation of linear stability via full domain integration. The final result of these efforts is a stability analysis of a simple, closed-loop system under different power loads in both single and two-phase states.

Chapter 2

Theory

In this chapter, the theory of conservation laws, discretization of differential equations, solution of nonlinear equations, and calculation of linear stability are all discussed. Because the stability analysis in this work hinges upon the ability to accurately integrate the computational domain, the first three sections discuss the fully nonlinear equations and their solution. The last section then covers the final linearization process to create an eigenvalue problem from the thermohydraulic equations to gain insight into a system's stability.

2.1 Governing Equations

The governing equations to be solved for the fluid system will now be delineated. A general discussion of conservation laws is presented first and then the specific thermohydraulic equations. The section will follow with the constitutive relations used to close the system. The equations and relations will be presented in their most general forms appropriate to fluid modeling for theoretical completeness; however, the final section will discuss approximations made to the general forms that are used in the numerical solutions and final results for tractability.

2.1.1 Conservation Laws

A *conserved quantity* q is taken to be any physical property whose time evolution within an arbitrary, closed volume exactly balances with its surface fluxes and volume sources. For the purpose of mathematical discussion and analysis, the conserved quantity q will simultaneously represent a function of space and time that conforms to the requirements of the physical property. These definitions define the following scalar *conservation law* over a volume Ω with an enclosing surface Γ:

$$\frac{\mathrm{d}}{\mathrm{d}t}\int_{\Omega} q(x_i, t)\,\mathrm{d}\Omega = \int_{\Gamma} -f_i(q, x_i, t)n_i\,\mathrm{d}\Gamma + \int_{\Omega} s(q, x_i, t)\,\mathrm{d}\Omega, \tag{2.1}$$

where f_i is a vector of surface flux functions of q, n_i is the outward unit normal of the surface Γ, and s is the volume source of q. Such that the units in the equation agree, both q and s are taken on a per volume basis and f_i on a per area basis. The negative sign in the surface integral ensures that outward fluxes act as sinks and inward fluxes as sources to the time evolution of q's volume integral. Equation 2.1 is the most general scalar conservation law that will be presented and is always physically valid regardless of the functions' behaviors.

Differential Form

A general conservation law can also be presented in differential form (i.e., as a differential equation). First the Divergence Theorem is used to equate the surface integral in equation 2.1

to a volume integral:

$$\int_{\Gamma} -f_i(q, x_i, t) n_i \, \mathrm{d}\Gamma = \int_{\Omega} -\partial_i f_i(q, x_i, t) \, \mathrm{d}\Omega. \tag{2.2}$$

For simplicity, the volume Ω is now taken to be fixed in space for all time, although a time-varying derivation with the identical result is possible via the Reynolds Transport Theorem [32]. Substituting equation 2.2 into equation 2.1 and moving all terms to the left-hand side gives:

$$\int_{\Omega} \partial_t q(x_i, t) + \partial_i f_i(q, x_i, t) - s(q, x_i, t) \, \mathrm{d}\Omega = 0, \tag{2.3}$$

where the time derivative operator could be moved into the integral since the volume is time-independent. Since the integration volume in equation 2.3 is arbitrary, taking the limit of the equality as the volume shrinks to a zero gives

$$\operatorname*{Lim}_{\Omega \to 0} \left[\int_{\Omega} \partial_t q(x_i, t) + \partial_i f_i(q, x_i, t) - s(q, x_i, t) \, \mathrm{d}\Omega \right] = 0. \tag{2.4}$$

In this limit, the enforcement of the equality changes from one over a finite volume into one that is enforced at a particular point. To ensure point-wise enforcement over the domain of x_i, the integrand itself is required to be equally zero at every point in the domain; this yields the differential conservation law

$$\partial_t q(x_i, t) + \partial_i f_i(q, x_i, t) - s(q, x_i, t) = 0. \tag{2.5}$$

When equipped with adequate boundary and initial data, this differential equation defines the requirement for all sufficiently smooth functions that describe how the conserved quantity evolves at every point in space-time.

The differential form may seem cleaner than the integral form, but it is not valid for all functional forms of q. In transitioning from equation 2.4 to equation 2.5, it is assumed that all functions in the integrand remain bounded. If any of the terms within the limit become infinite, the balance cannot be satisfied. In particular, if q has an area where it undergoes a discontinuous jump, called a shock, the gradient of the flux is infinite and the differential form is rendered invalid. While methods that handle shocks in a robust fashion (shock-capturing schemes) are not the focus of this work, it is mentioned for completeness and consideration [33].

Vector Form

The simulation of real world problems often involves the solution of a system of conservation laws. In general, the systems are nonlinear and tightly coupled. The actual solution of these problems will be discussed in future sections, but the notation used will be introduced now.

The integral conservation law for a vector of conserved quantities q_i is

$$\frac{\mathrm{d}}{\mathrm{d}t}\int_\Omega q_i(x_i,t)\,\mathrm{d}\Omega = \int_\Gamma -f_{ij}(q_i,x_i,t)n_j\,\mathrm{d}\Gamma + \int_\Omega s_i(q_i,x_i,t)\,\mathrm{d}\Omega, \tag{2.6}$$

where f_{ij} is a matrix of surface fluxes of q_i in the j-th direction, n_j is the outward unit normal of the surface Γ, and s_i is the volume source of q_i. The integrals of the vector quantities represent element-wise integration. A process similar to the scalar case also yields the differential form of the system conservation law:

$$\partial_t q_i(x_i,t) + \partial_j f_{ij}(q_i,x_i,t) - s_i(q_i,x_i,t) = 0, \tag{2.7}$$

where $\partial_j f_{ij}$ represents a row-wise divergence operation.

2.1.2 Thermohydraulic Laws

The main equations of interest in thermohydraulics will be presented using the definitions above. Mass, momentum, and energy are the primary quantities, and their conservation laws will be presented for an assumed-flowing system. For all of the definitions, the following items are noted:

- As prescribed in section 2.1.1, all of the conserved quantities are taken to be continuous functions of space and time. Although fluids are actually composed of discrete, interacting molecules, taking the quantities to be everywhere-defined is a valid approximation as long as the length scales to be modeled are much greater than the mean free path of the local medium. [34]
- Also as prescribed in section 2.1.1, all of the conserved quantities will be considered on a per unit volume basis.
- For clarity, the dependence of all quantities and functions will often be omitted; however, they are all assumed to be dependent on any variable in the system.

Conservation of Mass

The net mass in a control volume or, rather, the volume-integrated density is conserved as a simple scalar. It is controlled by the background flow field advecting the mass through the boundary. Therefore, the integral conservation law for density is

$$\frac{\mathrm{d}}{\mathrm{d}t}\int_{\Omega} \rho \,\mathrm{d}\Omega = \int_{\Gamma} -(u_j \rho) n_j \,\mathrm{d}\Gamma + \int_{\Omega} s^{\rho} \,\mathrm{d}\Omega, \tag{2.8}$$

Conservation of Momentum

A control volume's momentum balance is more complicated than the simple in-out mass balance. It is inherently a vector quantity, so the combination of mass and the background flow field feed the momentum in a nonlinear fashion. Also, even though a continuum approximation has been made, physical molecular stresses on the boundary must still be modeled in some manner for physical solutions in all circumstances. Lastly, a body force is be added to account for buoyancy effects on the volume relative to the control volume's surroundings. With all of these nuances considered, the integral conservation of momentum is taken to be

$$\frac{\mathrm{d}}{\mathrm{d}t}\int_\Omega \rho u_i \,\mathrm{d}\Omega = \int_\Gamma (-u_j \rho u_i) n_j \,\mathrm{d}\Gamma + \int_\Gamma (-\delta_{ij} P + \tau_{ij}) n_j \,\mathrm{d}\Gamma + \int_\Omega \rho g_i + s_i^u \,\mathrm{d}\Omega \tag{2.9}$$

where ρu_i is the momentum in direction i, u_j is the velocity in direction j, δ_{ij} is the Kronecker delta, P is the thermodynamic pressure, τ_{ij} is the viscous stress tensor, and g_i is the gravitational acceleration in direction i. A more detailed discussion of the pressure and viscous stress tensor is presented in section 2.1.3.

Each of the terms on the right-hand side of equation 2.9 stems from the considerations made. The first integral represents how the background flow field transports the momentum across the volume's surface. The second integral accounts for the ever-present thermodynamic pressure of the fluid and all other non-equilibrium molecular friction via the tensor τ_{ij}. The last integral has a source of momentum due to the density of the volume in addition to a generic source s_i^u.

Conservation of Bulk Momentum While the above equation is three-dimensional, in thermohydraulic modeling, it is common practice to collapse the momentum equation to a single, dominant flow direction. The result of this dimensional collapse is an equation that conserves *bulk momentum.* The bulk flow equation is created by dotting the integral momentum equation with a constant unit vector z_i. The unit vector represents the physically dominant flow direction for the given volume. Performing the dot operation and letting $a_z = a_i z_i$ for any vector a_i, the bulk flow equation is

$$\frac{\mathrm{d}}{\mathrm{d}t}\int_{\Omega} \rho u_z \,\mathrm{d}\Omega = \int_{\Gamma} (-u_j \rho u_z) n_j \,\mathrm{d}\Gamma + \int_{\Gamma} -P n_z + \tau_{ij} z_i n_j \,\mathrm{d}\Gamma + \int_{\Omega} \rho g_z + s_z^u \,\mathrm{d}\Omega. \tag{2.10}$$

Conservation of Channel Momentum A further simplification that conserves *channel momentum* is also employed by a number of modeling tools. The channel flow equations are derived from bulk momentum conservation by placing the following restrictions on the integration volume:

- there are exactly two open surfaces that are parallel to each another and everywhere perpendicular to the bulk flow direction;
- the outward normal of the surface connecting the two openings and enclosing the volume is always perpendicular to the bulk flow direction.

By imposing these requirements, equation 2.10 takes on the simpler form

$$\frac{\mathrm{d}}{\mathrm{d}t}\int_{\Omega} \rho u_z \,\mathrm{d}\Omega = \int_{\Gamma_1+\Gamma_2} \pm(P + u_z \rho u_z) \,\mathrm{d}\Gamma + \int_{\Gamma_\mathrm{w}} \tau_{ij} z_i n_j \,\mathrm{d}\Gamma + \int_{\Omega} \rho g \,\mathrm{Cos}(\theta) + s_z^u \,\mathrm{d}\Omega, \tag{2.11}$$

where Γ_1 and Γ_2 are open surfaces one and two, Γ_w is the third (wetted) surface, and θ is the angle between the bulk flow direction and gravity with counter-clockwise sense. The plus-minus accounts for the sign flip which occurs between surfaces one and two, which embody inflow and outflow once the sense of the bulk flow direction is chosen.

Conservation of Energy

The energy equation is similar to the momentum equation since there are nonlinear and molecular components to the balance. The energy to be balanced is the *total energy* of the medium, where total means the sum of thermal, kinetic, and potential energies. The integral conservation for total energy is taken to be

$$\frac{\mathrm{d}}{\mathrm{d}t}\int_{\Omega} \rho e \, \mathrm{d}\Omega = \int_{\Gamma} [-(\rho e + P)u_j + u_i \tau_{ij} - q_j] n_j \, \mathrm{d}\Gamma + \int_{\Omega} \rho g_j u_j + s^e \, \mathrm{d}\Omega \tag{2.12}$$

where ρe is the total energy of the system and q_j is a conductive heat flux; all of the other terms have the same meaning as in the momentum equation. A more detailed discussion of the conductive heat flux is presented in section 2.1.3.

As in the momentum equation, all right-hand side terms serve a purpose. The first term, $\rho e + P$, represents the advected energy in addition to the associated flow work due to pressure. The second term accounts for thermal energy gain due to molecular friction, also referred to as *viscous dissipation*. The third term arises due to molecular diffusion of heat across the boundary. The final term acts as a source or sink of energy due to the buoyancy force from momentum.

Conservation of Energy Simplifications For the purposes of this work, several approximations were made to the general energy equation given above. Formally, the total energy would be a summation of internal, kinetic, and potential energy:

$$\rho e = \rho i + \frac{1}{2}\rho u_i u_i + \phi_{\text{poten}}. \tag{2.13}$$

This work assumes that the time rate-of-change of kinetic energy and potential energy is small compared to the internal, and therefore, ρi is synonymous to ρe for the remainder of this work. Further, the gradient of the advected enthalpy $(\rho i + P)u_j$ is taken to be of higher-order than both the viscous dissipation, heat diffusion, and the potential energy advection. The resulting energy equation is then

$$\frac{\mathrm{d}}{\mathrm{d}t}\int_\Omega \rho i \,\mathrm{d}\Omega = \int_\Gamma [-(\rho i + P)u_j]n_j \,\mathrm{d}\Gamma + \int_\Omega s^e \,\mathrm{d}\Omega. \tag{2.14}$$

Due to water's high density and thermal capacity, these assumptions hold for relatively slow flows and greatly eases the numerical modeling burden of defining velocities within a control volume or forming a diffusive grid. The ease is made apparent in the discussion of the discretization.

Differential Forms

All of the integral conservation laws shown above also have differential forms:

$$\partial_t \rho + \partial_j(u_j \rho) = s^\rho \tag{2.15}$$

$$\partial_t(\rho u_i) + \partial_j(u_j \rho u_i) = -\partial_i P + \partial_j \tau_{ij} + \rho g_i + s_i^u \tag{2.16}$$

$$\partial_t(\rho e) + \partial_j(u_j \rho e) = -\partial_j(u_j P) + \partial_j(u_i \tau_{ij} - q_j) + \rho g_i u_i + s^e \tag{2.17}$$

Given the same initial and boundary conditions, these differential equations and their integral counterparts are equivalent for sufficiently smooth solutions. As required by the equations listed, "sufficiently smooth" means that at least all first derivatives must be continuous over the entire solution domain; however, certain constitutive relations (e.g., the stress tensor) may place more stringent requirements on continuity.

2.1.3 Constitutive Relations

In deriving these conservation laws, a number of unknowns were introduced to account for different thermodynamic, molecular, and non-equilibrium phenomena. These unknowns have to be related to the system variables in some manner to make the system solvable. Equations that perform this task are called *constitutive relations*, *closure relations*, or simply *models*. The terms of interest are the thermodynamic pressure, viscous stress tensor, and conductive flux.

Pressure

Pressure is a macroscopic, thermodynamic property that arises from ensembles of particles exerting forces over some unit area. A constitutive relation that relates pressure to other system variables that define the system's state is what is called an EOS. An EOS can be constructed from first principle (microscopic) approaches or thermodynamic potential (macroscopic) approaches and may be composed of one or more equations. Regardless of the EOS's construction, it should be able to calculate all relevant thermodynamic properties given two independent properties for a pure fluid [35].

Since there are multiple avenues for creating an EOS, for any given fluid, several may exist; each one varying in complexity of formulation, range of validity, and fidelity to data. The choice of EOS is dependent on the importance of each of those three attributes. The EOS used for this work is the IAPWS Formulation 1995 for the Thermodynamic Properties of Ordinary Water Substance for General and Scientific Use (IAPWS-95). The IAPWS-95 formulation is extremely complex, but the range-of-validity and fidelity-to-data is second-to-none for water. The details of the formulation are left partially to appendix A and primarily to its publication [36].

Stress Tensor

The stress tensor requires a model that relates molecular friction, continuum deformation, and system variables. There are, like an EOS for a fluid, several different stress tensor models for any given system. These models vary in terms of the type of valid fluid, dimensionality of usage, and fidelity to data.

Newtonian fluid models are among the most popular stress tensor model choices and form the basis for the Navier-Stokes equations. From experiment, Newton observed that a proportional relationship exists between the shear stress exerted on a fluid and the fluid's uni-directional velocity gradient for a wide array of fluids. Stokes then extended this proportional relationship to higher dimensions by making three assumptions: the tensor is a linear function of strain, the fluid is isotropic, and the tensor's divergence must be zero for a fluid at rest such that pressure is the only extant surface force. With all of these observations and assumptions considered, the Newton stress tensor model (sometimes described as a compressible model) is defined by the equation:

$$\tau_{ij} = \mu\left(\frac{\partial u_i}{\partial x_j} + \frac{\partial u_j}{\partial x_i}\right) + \lambda\delta_{ij}\frac{\partial u_k}{\partial x_k} \tag{2.18}$$

where μ is the dynamic viscosity and λ is the bulk viscosity [37]. The dynamic viscosity term accounts for the pure shearing experienced by the fluid, and the bulk viscosity term accounts for the volumetric strain.

While the above relation is suitable for equation 2.9, the bulk and channel momentum conservation equations require a different relation since the multi-dimensional nature of the flow has been dotted away. One such relation is the Darcy friction factor which poses the traction from the walls as a loss of bulk kinetic energy:

$$\tau_{ij} z_i n_j = \Delta P_{\text{fric}} = \frac{1}{2} f_{\text{D}} \frac{L_{\text{char}}}{D_{\text{eff}}} \rho v^2, \tag{2.19}$$

where L_{char} is a characteristic (path) length, and D_{eff} is an effective flow diameter. The details of what densities and velocities to use is left to the numerical discretization portion that discusses the averaging process. The key kinematic property is the Darcy friction factor f_{D} that aims to encompass all of the molecular and wall traction experienced by the fluid using bulk properties. Similar to the prior EOS discussion, a full description of the relations used to calculate the friction factor is presented in appendix B, but all of the models used are fully nonlinear in conserved quantities and highly accurate to data.

Conductive Flux

The conductive flux is most often modeled by Fourier's Law:

$$q_j = -\kappa \partial_j T, \tag{2.20}$$

where κ is the thermal conductivity, and T is the thermodynamic Temperature [38]. The law is a simple but effective first order linear approximation of true conduction behavior and adds an explicit diffusive component to the conservation of energy equation.

2.1.4 Final Equations

The final set of equations to be discretized and solved are the conservation mass, conservation of bulk momentum, and the simplified conservation of energy:

$$\frac{\mathrm{d}}{\mathrm{d}t}\int_{\Omega} \rho \,\mathrm{d}\Omega = \int_{\Gamma} (-u_j \rho) n_j \,\mathrm{d}\Gamma + \int_{\Omega} s^{\rho} \,\mathrm{d}\Omega \tag{2.21a}$$

$$\frac{\mathrm{d}}{\mathrm{d}t}\int_{\Omega} \rho u_z \,\mathrm{d}\Omega = \int_{\Gamma} (-u_j \rho u_z) n_j \,\mathrm{d}\Gamma + \int_{\Gamma} -P n_z + \tau_{ij} z_i n_j \,\mathrm{d}\Gamma + \int_{\Omega} \rho g_z + s^{u}_{z} \,\mathrm{d}\Omega \tag{2.21b}$$

$$\frac{\mathrm{d}}{\mathrm{d}t}\int_{\Omega} \rho i \,\mathrm{d}\Omega = \int_{\Gamma} [-(\rho i + P) u_j] n_j \,\mathrm{d}\Gamma + \int_{\Omega} s^{e} \,\mathrm{d}\Omega \tag{2.21c}$$

2.2 Discretization

The conservation laws presented in the previous section will now be converted into a set of nonlinear, algebraic equations whose solution represents the system's evolution in space-time. In general, the purpose of this *discretization* is to transform the problem from finding a set of functions that have a defined value for every point of space-time to finding a set of unknown coefficients to chosen functions which represent the solution over a discrete subset of space-time. The motivation behind this conversion is that finding a vector of unknowns to balance a set of algebraic equations is easier, though still not trivial, than finding a continuous solution to a general, nonlinear differential equation. Of course, this process adds *discretization errors* to the obtained solution [39]; however, those errors are viewed as a necessary cost to effect a useful solution. Additionally, when the discretization is made carefully, it does not often undermine the underlying physical significance of the conservation laws.

The discussion of discretization is presented in two parts: choice of spatial discretization and choice

lines, also known as a *semi-discrete scheme*. The method of lines involves the discretization of the spatial dimension only, such that the system of equations becomes a system of coupled, ordinary differential equations. The system can then be solved using a standard and robust Ordinary differential equation (ODE) time integration method [40].

It is noted that most of the following discussion assumes the solution being found is one to a differential equation. As stated in the previous section, the conversion between differential and integral equations is valid as long as the solution has finite values of all required derivatives at every point in the domain. Because the topic of shockwaves is deemed beyond the scope of this work, the two forms are treated synonymously with a focus on the differential side since that is from where most of the relevant theory is acquired.

2.2.1 Spatial Discretization

The spatial discretization of a system of equations is taken to be both a concrete specification of how the solution is taken to vary in space and how the spatial domain of the system is partitioned. The first specification concerns what is called the *construction* of the solution, and the second concerns what is called the *partitioning* of the solution. For a single equation of unknowns, these choices are inexorably linked. However, a system of equations allows each of the equations to be partitioned differently despite having the same approximation, and thus the two concerns will be explained separately.

Construction

The construction of a solution to a system of differential equations involves the explicit selection of a functional form made to balance the system. Since the actual functional form of the solution is unknown globally, local functional forms of the solution with a varying number of undetermined coefficients (i.e., degrees of freedom) are assumed over a set of discrete points or sections of the domain. The coefficients are then calculated by requiring the functional forms to balance the system of equations in some manner and satisfy any compulsory compatibility conditions (such as global continuity). The union of these local functional forms with the determined coefficients then form the approximate global solution.

From that very general framework, there are three often-used methods of construction: finite difference, finite volume, and finite element. In brief, the main ideas behind these methods are:

- A Finite Difference Method (FDM) is derived from either local truncated Taylor expansions to approximate derivatives or from local polynomial interpolants with sufficient support[1] for the system being solved. The system is then required to be balanced at every point about which the construction is made.
- A Finite Volume Method (FVM) assumes the global solution to be a collection of disjoint partitions that only communicate at their boundaries via fluxes and are locally defined by an arbitrary polynomial. The equation is then required to be satisfied in an integral-sense over each of the partitions.
- A Finite Element Method (FEM) assumes the global solution to be a collection of

---

[1] In this instance, *support* means that the degree of the interpolating polynomial at least matches the differential order of the system such that all polynomial derivatives have non-trivial terms. For example, a third order differential equation requires a cubic interpolant because any lower degree polynomial would have a third derivative of 0 and could in no way balance (i.e., support) the differential equation.

contiguous partitions locally defined by an arbitrary polynomial. The equation is then required to be satisfied in a weighted integral-sense over the entire domain.

Finite differences are the oldest class of methods and easily allow for high-order approximations but are not easily extended to non-rectangular grids and may not exactly conserve quantities by construction. Finite volumes are easily extended to arbitrary grids due to their integral nature and can be guaranteed to ensure exact conservation but arbitrarily high-order approximations are difficult to form. Finite elements are easily extended to arbitrary grids due to their integral nature and are easily extended to arbitrarily high-order approximations but the global nature of the solution does not necessarily guarantee local conservation of quantities [41].

The method of approximation used for the remainder of this work will be FVM. The benefits of arbitrary geometry and exact conservation outweigh the lack of easy high-order methods. Further, only a first-order method will be pursued and concretely presented in the following section. Although first-order finite volume methods are known to be diffusive for source-less conservation laws, the method is always stable, even in the presence of shockwaves, and gives order-of-magnitude answers, as those sought in engineering level modeling. The latter assertion is demonstrated in the following example.

Consider numerically solving the following one-dimensional boundary value problem:

$$\frac{\mathrm{d}^2T}{\mathrm{d}x^2} = \frac{-\pi^2}{4}\,\mathrm{Cos}\left(\frac{\pi x}{2}\right); \qquad T(-1) = 0\,, \quad T(1) = \frac{1}{2} \tag{2.22}$$

For all three methods, the x dimension is divided by $n+1$ equidistant points between -1 and 1 with n internal partitions of width Δx. The algebraic equations from three different approximation methods are derived as follows:

- Approximating the unknown $T(x)$ at the i-th point by a quadratic polynomial defined by the values of T(x) at the points x_{i-1}, x_i, and x_{i+1}, the point-wise enforced finite difference equation is

$$\frac{T_{i+1} - 2T_i + T_{i-1}}{\Delta x^2} = \frac{-\pi^2}{4} \operatorname{Cos}\left(\frac{\pi x_i}{2}\right). \tag{2.23}$$

- Approximating the value of $T(x)$ over the j-th partition between x_{i-1} and x_i as a constant value $\overline{T}_j$, the partition-wise enforced finite volume equation is

  $$\left.\frac{\mathrm{d}\overline{T}}{\mathrm{d}x}\right|_i - \left.\frac{\mathrm{d}\overline{T}}{\mathrm{d}x}\right|_{i-1} = \frac{\overline{T}_{j+1} - 2\overline{T}_j + \overline{T}_{j-1}}{\Delta x} = \frac{-\pi^2}{4} \operatorname{Cos}\left(\frac{\pi}{2}\,\frac{(x_{i-1} + x_i)}{2}\right)\Delta x. \tag{2.24}$$

  The first expression emphasizes that the finite volume method integrates once to create flux-based difference equations. The fluxes are then formed using a chosen relationship between partition values, and the original right-hand is integrated in some approximate fashion over the partition. The choices leading to the second and third expressions are a piece-wise linear relationship between partition values and the mid-point integration rule for the right-hand side.

- Assuming the unknown $T(x)$ to behave linearly within the two partitions bounded by x_{i-1} and x_{i+1}, the partition-wise enforced finite element equation is

  $$\frac{T_{i+1} - 2T_i + T_{i-1}}{\Delta x^2} = \frac{4}{\Delta x^2} \operatorname{Cos}\left(\frac{\pi x_i}{2}\right) \operatorname{Sin}^2\left(\frac{\pi x_i}{4}\right), \tag{2.25}$$

  where the right-hand side was integrated exactly over the partitions.

The approximate and analytical solutions are shown in figure 2.1. As can be seen, despite the extremely similar difference equations between the three methods, the underlying choice of construction leads to very different approximate solutions. Furthermore, as seen in figure 2.2, the FVM's assumption of partition-wise constant data leads to a first-order convergent method instead of the second-order convergence shown by FDM and FEM. However, regardless of its first-order nature, the solution provided by FVM still qualitatively reproduces the analytical

Figure 2.1: Solutions of equation 2.22 for the approximation methods discussed using six partitions.

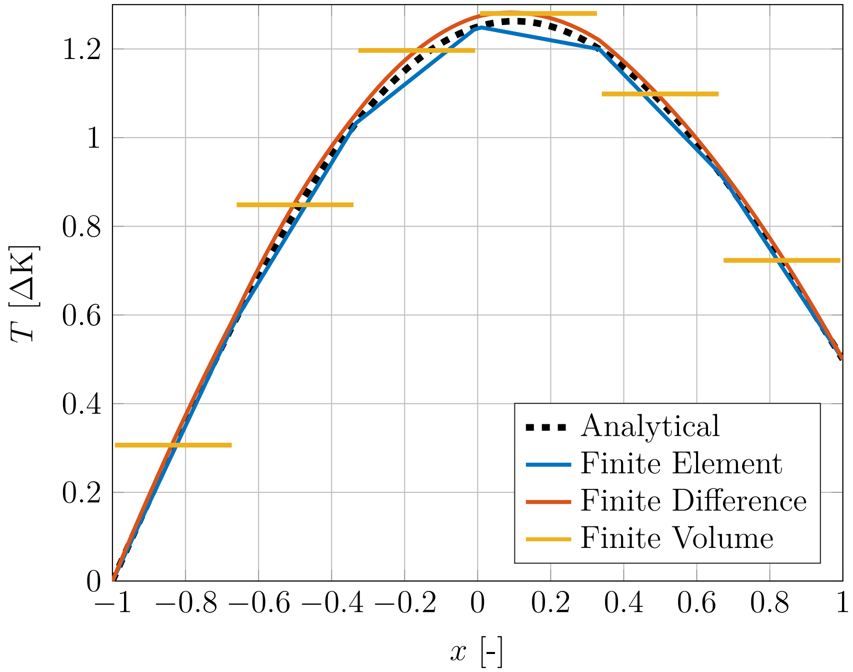

solution. And because the end goal of this work is not a rigorous resolution of the spatial domain at all scales but a conservative, system-integrated stability analysis, the first-order FVM method is viewed as the best compromise between the FDM and FEM methodologies.

Partitioning

Partitioning, alternatively known as *meshing*, involves selecting a collection of partitions whose union recreates the problem geometry as closely as possible. In general, the partitioning is not unique and may be vary between equations in the system. For FVM, partitions are commonly referred to as *control volumes*. Control volumes can be any shape needed to cover the physical domain but, for simplicity, are often limited to polyhedra or a natural differential element in the coordinate system being used.

Figure 2.2: L_2 norm error plots versus partition count. FEM and FDM exhibit second order convergence; FVM exhibits first order.

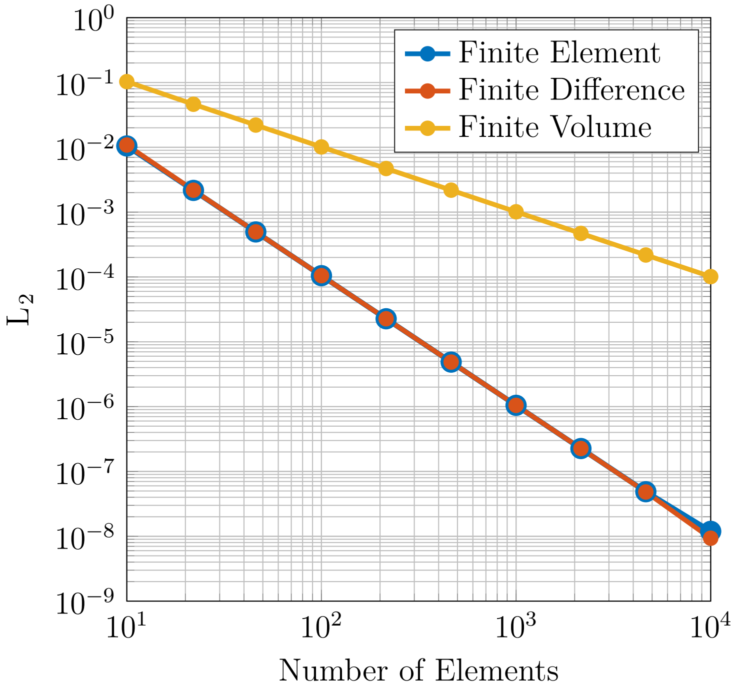

This work will make use control volumes with completely flat bounding faces. The flat bounding faces make approximating the surface integrals in the conservation laws more straightforward. While this may appear limiting, evaluation of the surface integral is only performed where there is a non-zero flux of a conserved quantity. And since the velocity is assumed to be zero on all solid surfaces within the model assuming no-slip and impermeability, the control volumes can be deformed to fit the bounding physical surface with only the artificial flux exchange surfaces required to be flat.

Additionally, this work employs a so-called *staggered scheme* with two different partitionings: one for the conservation of energy and mass and another for the conservation of bulk momentum. The staggered scheme overcomes a problem introduced by solving a single, bulk momentum equation: the control volumes used to solve the bulk momentum equation have an inherent flow direction z_i, but the mass and energy control volumes are exposed to fluxes

Figure 2.3: A simple, two-dimensional partition diagram of a tee-branch; red arrows indicate a dominant flow direction.

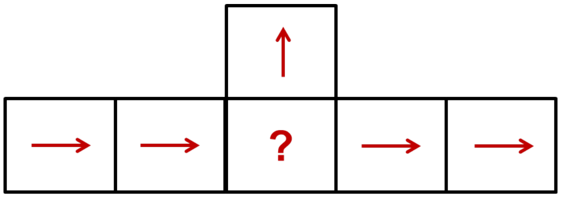

of material from any direction.

If the partitionings were the same for all equations, more approximations would need to be introduced to calculate the surface velocities not to mention the burden of having to define an exchange scheme for branching flows. To exemplify that point, consider figure 2.3. The dominant flow directions, indicated with red arrows, are all apparent aside from the partition where the flow splits in two. If the momentum equations were partitioned on the same grid as the mass and energy equations, the flexibility of the code to model real world situations would be greatly limited. This single choice of partition is to be contrasted with the one shown in figure 2.4. By off-setting the center points of the momentum equation's partition, velocities at any direction are able to be calculated as long as the boundaries of the partitions are adjusted appropriately.

Furthermore, the values of the partition-wise constant momentum maybe taken to exist directly at the bounding face of the control volumes. If chosen in this manner, then the surface flux values for the mass and energy conservation equations have a known advection velocity. This choice is similar to selecting a single location within an integration rectangle and using the value of the function at that point multiplied by the rectangle's width to approximate the integral.

Semi-discrete Conservation Laws

Using the partition-wise constant constructions and staggered scheme from the previous section, the semi-discrete form of the equations will now be presented. For efficiency, some terminology will be discussed first. The system of ordinary differential equations will then be given.

For any model, the spatial domain is partitioned into discrete *control volumes* that will hold the mass and energy of the system. In order to create a connection between two control volumes through which mass may transfer, identification numbers are used to form a “from” and “to” relationship between the control volumes; this “from” and “to” connection creates a partition for the momentum equation called a *momentum cell*. The connection also carries the bulk flow direction information and forms an exchange surface between the control volumes that is orthogonal to the dominant flow direction. Lastly, each surface shared by two momentum cells between which momentum may be transferred are called *interfaces*. For each interface, an “upwind” and a “downwind” momentum cell must be specified along with the interfaces unit normal, which is assumed to point away from the upwind cell.

The creation of the connections is programmatically done with identification numbers associated with the control volumes and all other numbers induced by those connections. A physical diagram with identification numbers is shown in figure 2.5. The connection information is

Figure 2.4: A staggered, two-dimensional diagram of a tee-branch.

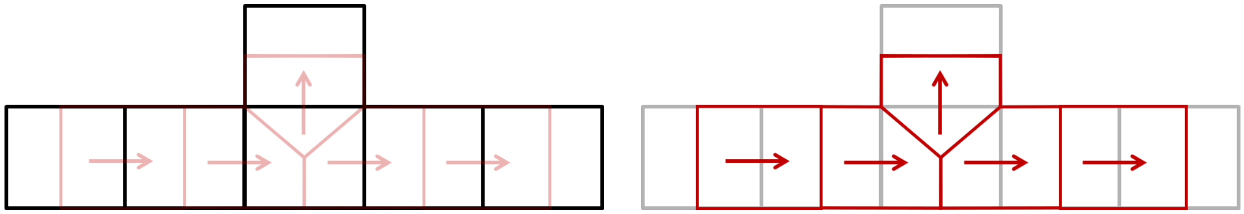

(a) Mass and Energy Partition

(b) Momentum Partition

shown in table 2.1. These physical connections, flow directions, flow areas, and volumes give enough information to form the semi-discrete form of the equations.

The spatially discretized mass equation for the k-th control volume has the form

$$\frac{\mathrm{d}}{\mathrm{dt}}\int_{\Omega}\rho_k\,\mathrm{d}\Omega = s_k^{\rho}V_k + \sum_{n=1}^{N} u_n\rho_{d,n}A_n \tag{2.26}$$

where s_k^{ρ} is a source term, V_k is the volume of the control volume, u_n is the exchange velocity, $\rho_{d,n}$ is the donor density, and A_n is the exchange surface area. The index n runs from 1 to however many other control volumes are connected to k. The donor density $\rho_{d,n}$ is the density of the “from” volume if Sign(u_n) is positive or the density of the “to” volume otherwise. This donor approach ensures exact conservation of mass.

The spatially discretized energy equation for the k-th control volume has the form

$$\frac{\mathrm{d}}{\mathrm{dt}}\int_{\Omega}\rho i_k\,\mathrm{d}\Omega = s_k^{e}V_k + \sum_{n=1}^{N} u_n\rho h_{d,n}A_n \tag{2.27}$$

where s_k^{e} is a source term, V_k is the volume of the control volume, u_n is the exchange velocity, $\rho h_{d,n}$ is the donor enthalpy, and A_n is the exchange surface area. The donor enthalpy $\rho h_{d,n}$ is equal to $\rho i_{d,n} + P_{d,n}$ is the enthalpy of the “from” volume if Sign(u_n) is positive or the density of the “to” volume otherwise. This donor approach ensures exact conservation of energy.

Figure 2.5: A staggered, two-dimensional diagram of a tee-branch with identification numbers and interface normals.

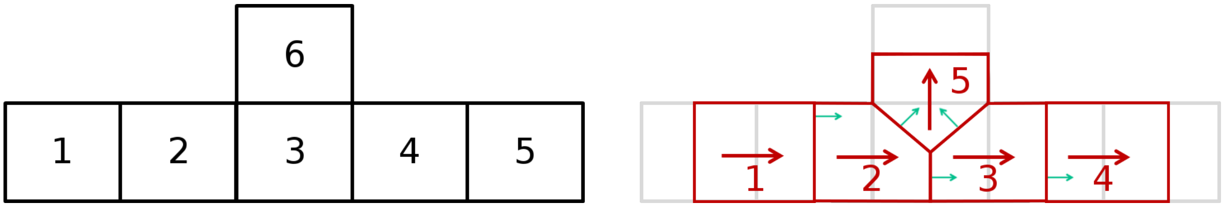

(a) Mass and Energy Partition

(b) Momentum Partition

The spatially discretized momentum equation for the k-th momentum cell has the form

$$\frac{\mathrm{d}}{\mathrm{d}t}\int_{\Omega} \rho u_k \,\mathrm{d}\Omega = \left(\rho_k g_k + s_k^u\right) V_k - \sum_{n=1}^{N} (P_n z_n + u_{\mathrm{I},n} \rho u_{d,n}) A_n - \frac{1}{2} f_{\mathrm{D,k}} \frac{L_{\mathrm{char,k}}}{D_{\mathrm{eff,k}}} \,\mathrm{Abs}(\rho u_k) u_k A_k \quad (2.28)$$

where ρ_k is the average mass density of the control volumes spanned by the k-th momentum cell, g_k is the dot product of gravity with the dominant flow direction of the cell, s_k^u is the source, V_k is the volume of the cell, P_n is the pressure along the n-th interface, z_n is the dot product of the interface's unit normal with the dominant flow direction, $u_{\mathrm{I},n}$ is the interface exchange velocity, $\rho u_{d,n}$ is the donor momentum, A_n is the area of the interface, f is the friction factor, L is the friction exchange length, D is the effective diameter, ρu_k is the intensive bulk momentum, u_k is the bulk velocity, and A_k is the flow area of the momentum cell. The interface exchange velocity is a simple average of the upwind and downwind momentums following their dot with the interface normal. The donor momentum is, as previously done for exact conservation, either the upwind or downwind momentum dependent on the sign of the interface exchange velocity. All of the intensive quantities are derived from the extensive properties through standard arithmetic relations.

TABLE 2.1: *Summary tables of the connection information used to programmatically construct the example tee-branch.*

(A) *From-To Connections*

From	To	Momentum Cell Number	Dominant Flow Direction
1	2	1	$1\hat{\imath}$
2	2	2	$1\hat{\imath}$
3	3	3	$1\hat{\imath}$
4	5	4	$1\hat{\imath}$
3	6	5	$1\hat{\jmath}$

(B) *Upwind-Downwind Connections*

Upwind	Downwind	Interface Number	Unit Normal
1	2	1	$1\hat{\imath}$
2	3	2	$1\hat{\imath}$
2	5	3	$\frac{1}{\sqrt{2}}\hat{\imath} + \frac{1}{\sqrt{2}}\hat{\jmath}$
3	4	4	$1\hat{\imath}$
3	5	5	$-\frac{1}{\sqrt{2}}\hat{\imath} + \frac{1}{\sqrt{2}}\hat{\jmath}$

2.2.2 Temporal Discretization

For a model consisting of N_{CV} control volumes and N_{MC} momentum cells, equations 2.26 to 2.27 constitute a system of $2\,N_{\text{CV}} + N_{\text{MC}}$ ordinary differential equations. This can be simply expressed as

$$\frac{\mathrm{d}q_i}{\mathrm{d}t} = f_i(t, q_i). \tag{2.29}$$

In order to turn the above ODE into an algebraic system, another discretization choice must be made. There are many different types of discretizations to choose from, but this work employs the Implicit Euler Method. This method was chosen because it is an extremely stable, first-order method that does not necessarily have a restriction on the time-step size for advancement of the equations. Although, a small time-step is used in practice for accuracy and quick solution of the system.

The Implicit Euler Method approximates the left-hand time derivative as a first-order finite difference and evaluates the right-hand side at the next time-step value:

$$\frac{q_i^{p+1} - q_i^p}{t^{p+1} - t^p} = f_i(t^{p+1}, q_i^{p+1}) \tag{2.30}$$

which upon re-arranging yields the residual form:

$$r_i(t^{p+1}, q^{p+1}) = q_i^{p+1} - q_i^p + (t^{p+1} - t^p) f_i(t^{p+1}, q_i^{p+1}). \tag{2.31}$$

The next time-step value q^{p+1} is unknown and must be found by driving the residual function $r_i(t^{p+1}, q^{p+1})$ to or near zero. The manner chosen to solve this nonlinear, algebraic equation is presented in detail in the next section.

2.3 Jacobian-Free Newton-Krylov Solver

A Jacobian-Free Newton-Krylov (JFNK) solver is a general name for an algorithm that solves a system of nonlinear equations. As implied by the name, these solvers are characterized by two main features: lack of a need to form the exact Jacobian and Newton-like updates obtained from a Krylov method. The need for a Jacobian and an explanation of Newton updates will be discussed first. An overview of Krylov methods and the more specific Generalized Minimal Residual (GMRES) method will follow. The section will conclude with an approximation that allow the pieces to fit together and form a JFNK solver.

2.3.1 Newton's Method

Systems of coupled, nonlinear equations are pervasive across all disciplines of science and engineering. They are also one of the most important and difficult class of problems to analyze and solve. While there are numerous analytical and numerical techniques for solving such problems, Newton's method is the singular option that will be explored here.

Problem Statement

The problem under consideration is defined as follows [42]: given an $n \times 1$ vector of nonlinear equations $r(x)$, determine an $n \times 1$ vector x_n such that

$$r(x_n) = 0. \tag{2.32}$$

Because each row of the equation vector is sought to be identically zero in this definition, the problem is sometimes referred to as a multi-dimensional root-finding problem. A different but similar statement can be formed by viewing the solution as the result of a minimization procedure: given an $n \times 1$ vector of nonlinear equations $r(x)$, determine an $n \times 1$ vector x_n such that

$$x_n = \underset{x}{\mathrm{ArgMin}} \, \|r(x)\| \tag{2.33}$$

in any valid norm of $r(x)$, where ArgMin_x is a function that returns the argument which minimizes $\|r(x)\|$ over the domain of x. The minimization problem is equivalent to the root-finding problem as long as $r(x)$ admits a root in the domain of x. If it does not, as in $r(x) = x^2 + 1$ where $x \in \mathbb{R}$, the minimization problem still has a well-defined solution. However, because many engineering problems posed in the manner of equation 2.32 arise from a physical balance of left- and right-hand sides involving x, a root most often exists within its domain.

Either problem is still difficult to solve in practice. Even for a modest value of n, because the function $r(x)$ is taken to be nonlinear, a closed-form solution to either variation may be impractical, if not impossible, to find. Therefore, numerical techniques like Newton's method are frequently used to solve the problem approximately.

Newton Update

In an effort to satisfy equation 2.32, Newton's method forms a solution from a recursive series of linear approximations. The method begins with some initial value x_0. Assuming $r(x)$ has a root in the domain of x, if $\|r(x_0)\|$ is not sufficiently close to zero, there may be a direction δx_0 in which the norm decreases, called a *descent direction*. Such a direction can be found by considering the function's Taylor series about x_0 evaluated at $x_0 + \delta x_0$:

$$r(x_0 + \delta x_0) = r(x_0) + J_r(x_0)\delta x_0 + c(x_0, \delta x_0) \tag{2.34}$$

where $J_r(x_0)$ is an $n \times n$ Jacobian matrix and $c(x_0, \delta x_0)$ is an $n \times 1$ vector of higher-order corrections that ensure the equality [43]. Near the expansion point, the higher-order corrections are small relative to the linear term and may be neglected. Further, to both drive $r(x)$ toward zero and yield a solvable system, the function value $r(x_0 + \delta x_0)$ is taken to be zero. This procedure can be thought of as assuming the direction and magnitude of δx_0 leads to the exact solution of the problem. The resulting linear system used to solve for the descent direction is

$$J_r(x_0)\delta x_0 = -r(x_0). \tag{2.35}$$

The above procedure yields a locally linear system whose solution is the descent direction δx_0 as long as the Jacobian is non-singular. Any search direction calculated from the above formula is called a *Newton direction.* Of course, since the higher-order corrections were ignored in attaining the linear system, this δx_0 will unlikely lead to an acceptable solution. However, if δx_0 leads to a new point with a norm smaller than that of the initial guess, it is arguably a better point at which to form the Taylor expansion.

From the new point $x_1 = x_0 + \delta x_0$, another linear system can be formed, a new descent direction calculated, and the process repeated. As such, the k-th new point from the current expansion location x_{k-1} moving in the Newton direction δx_{k-1} is

$$x_k = x_{k-1} - J_r^{-1}(x_{k-1}) r(x_{k-1}) = x_{k-1} + \delta x_{k-1} \tag{2.36}$$

As long as each successive point from the locally linear system yields a norm smaller than its predecessor, the repetition is forming a sequence of points that is approaching a solution to the nonlinear problem. Moreover, if each successive point decreases the residual's norm, the norms of the descent directions and the higher-order correction terms are decreasing as well. So if the sequence of points is convergent to a solution, the linear approximation becomes increasingly valid as the Newton step decreases. Setting aside algorithmic flow, stopping criteria, and other details, this update procedure is Newton's method.

As an example of the above procedure, the residual function is taken to be

$$r(x) = \mathrm{Exp}\left[-\left(x + \frac{1}{4}\right)^2\right] - \frac{3}{4} \tag{2.37}$$

While the function admits a simple analytical solution, Newton's method may be applied to find one of the solutions. Graphical results of applying the method to the residual with a starting guess of 1 are shown in figure 2.6. As can be seen, each successive iteration of the method results in a decrease of the norm and a decrease of the length of the Newton update.

Figure 2.6: The first few Newton updates of equation 2.45 *with a starting guess of* $x_0 = 1$. *Solid lines, aside from the residual's, indicate tangents, and dashed lines indicate update locations from the roots of the tangents.*

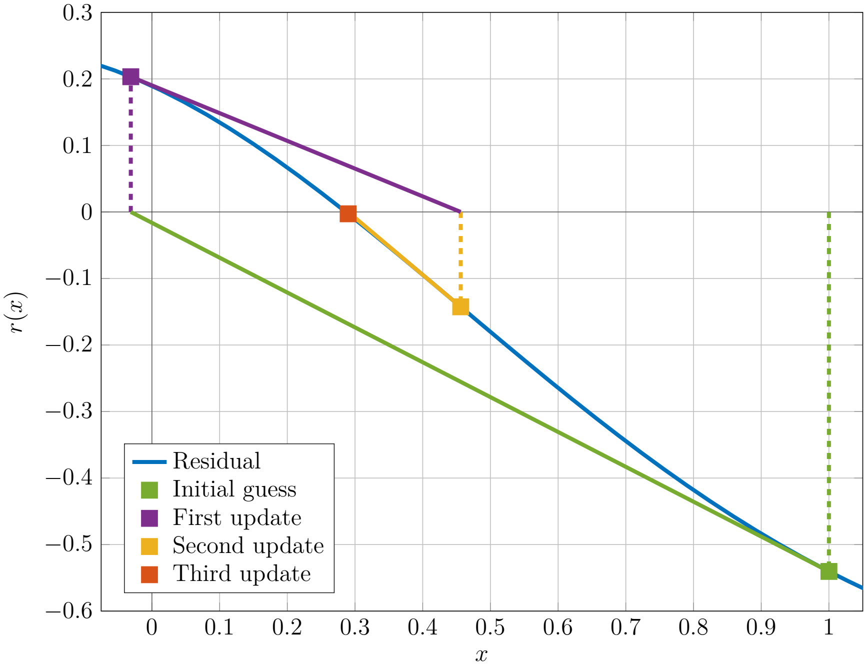

It is noted that because this residual is nonlinear, it does have another solution which is not found in this example because the initial guess is further from it than the one found. In accordance with the discussion above, Newton's method finds *a solution* of the problem but not all of the solutions.

Line Search

While the solution of equation 2.35 is a descent direction and figure 2.6 shows smooth convergence with full Newton steps, reduction of the norm is only guaranteed close to the point of expansion where preclusion of the higher-order terms in the Taylor expansion is valid. As such, the magnitude of δx_{k-1} may result in an x_k with a higher norm due to stepping outside the neighborhood of descent. To remedy this problem, implementations of Newton's method often introduce a step fraction α such that equation 2.36 becomes

$$x_k(\alpha) = x_{k-1} + \alpha\delta x_{k-1}. \tag{2.38}$$

Using this formulation, after solving for the descent direction δx_{k-1} as normal, the scaling parameter is calculated from

$$\alpha = \underset{\alpha^*}{\text{ArgMin}} \, \|r(x_k(\alpha^*))\| \tag{2.39}$$

This problem is referred to as a *line search* and is solved by finding the scalar value α which minimizes the norm of the residual along the Newton direction [42]. Because the linear assumption is valid near the expansion point, the minimization often results in an α bounded between 0 and 1, meaning that the Newton direction is often underrelaxed. However, if the norm of the function exhibits positive convexity along the entire descent direction, an overrelaxtion of the step fraction may be possible and can lead to faster convergence.

While finding the exact minimum of a residual along the search direction is an admirable goal in theory, it can be computationally disadvantageous. Therefore, instead of strictly adhering to equation 2.39, which is called an *exact line search*, less stringent criteria that guarantee acceptable advancement of the solution are often employed in practice. These criteria form the basis for an *inexact line search*. The most obvious criterion to impose would be a reduction in the residual's norm after the step:

$$\|r(x_{k-1} + \alpha\, \delta x_{k-1})\|_2 < \|r(x_{k-1})\|_2 \tag{2.40}$$

Another option is one often employed in routines for finding extrema: the *Armijo Rule*. This criterion requires the step to generate a residual value that falls below a relaxed tangent line of the norm of the residual [44]:

$$\|r(x_{k-1} + \alpha\, \delta x_{k-1})\|_2 < \|r(x_{k-1})\|_2 + \alpha\, \beta\, \left.\frac{\partial \|r(x_{k-1})\|_2}{\partial \alpha}\right|_{\alpha=0}. \tag{2.41}$$

The relaxation parameter β is often taken to be small such that α is not restricted to small values for steep residuals and that the criterion is similar to the former, pure reduction one for modestly decreasing residuals. The derivative along the step fraction α is

$$\left.\frac{\partial \|r(x_{k-1})\|_2}{\partial \alpha}\right|_{\alpha=0} = \frac{r(x_{k-1})^{\intercal}\, J_r(x_{k-1}) \delta x_{k-1}}{\|r(x_{k-1})\|_2} = -\|r(x_{k-1})\|_2. \tag{2.42}$$

The latter reduction comes from equation 2.35 and succinctly shows that the Newton direction is a descent direction since the value of the derivative is always negative. Inserting the value of the derivative into equation 2.41 shows that the Armijo rule is stricter than equation 2.40 because the reduction requirement is below unity if α is non-zero. However, the criterion is still a simple reduction requirement with a free parameter β that can be used to control the overall strictness:

$$\|r(x_{k-1} + \alpha\, \delta x_{k-1})\|_2 < (1 - \alpha\, \beta)\|r(x_{k-1})\|_2. \tag{2.43}$$

It is noted that the simplification of the Armijo rule to this form does not arise in its optimization uses because those routines solve a linear system involving the Hessian and gradient of the residual's norm. For the rest of this work, the criterion for acceptance of the step fraction α will be one of strict reduction with a multiplier of unity.

There are a number of algorithms that could be used to perform the line search to meet the imposed criterion. The methods vary in their complexity, run-time, and robustness. The following is a small, non-exhaustive list of line search methods:

- *Proportional back-tracking*: iteratively multiply the current step fraction by some factor less then one until a reduction in the norm is found. While extremely simple, the method only requires evaluation of the residual and is guaranteed to converge since α will eventually be reduced into the local area of descent.

- *Interpolation back-tracking*: use any known values of the residual or Jacobian to form a polynomial whose minimum can be easily found and, if necessary or desired, iterate using the new information. Since the calculated residual is assumed to be higher than the expansion point's and the initial derivative is downward, at least one minimum of the polynomial will exist within the interval. This procedure is typically applied iteratively with a quadratic or a cubic polynomial since their minima are readily computed. As long as all of the residuals used are higher than the expansion point's, the interval over which the polynomial is constructed will shrink and eventually be reduced into the local area of descent.

- *Golden Section Search*: starting from two bounding points and two interior points of an interval, find the new interval which guarantees a minimum is contained within itself, sample a new interior point, and iterate until convergence. The "golden" part of the name comes from the interior points being chosen such that they are a relative distance of one over the golden ratio (~ 0.618) from the interval bounds. This method is most useful for exact line searches since an exact minimum in the relaxation regime of α may potentially be exactly found, as opposed to the previous back-tracking methods. However, the search is only guaranteed to find the true minimum if the residual is unimodal (i.e., only has one minimum) within the initial interval and only converges linearly to a minimum. As such, either the proportional and interpolation back-tracking methods are most frequently used. This method is mentioned for an example of a non-back-tracking algorithm.

The method implemented in this work is quadratic-cubic interpolation back-tracking.

As an example to motivate the use of line searches, consider the following vector-valued

Figure 2.7: Residual value of equation 2.45 as a function of α for several values of μ.

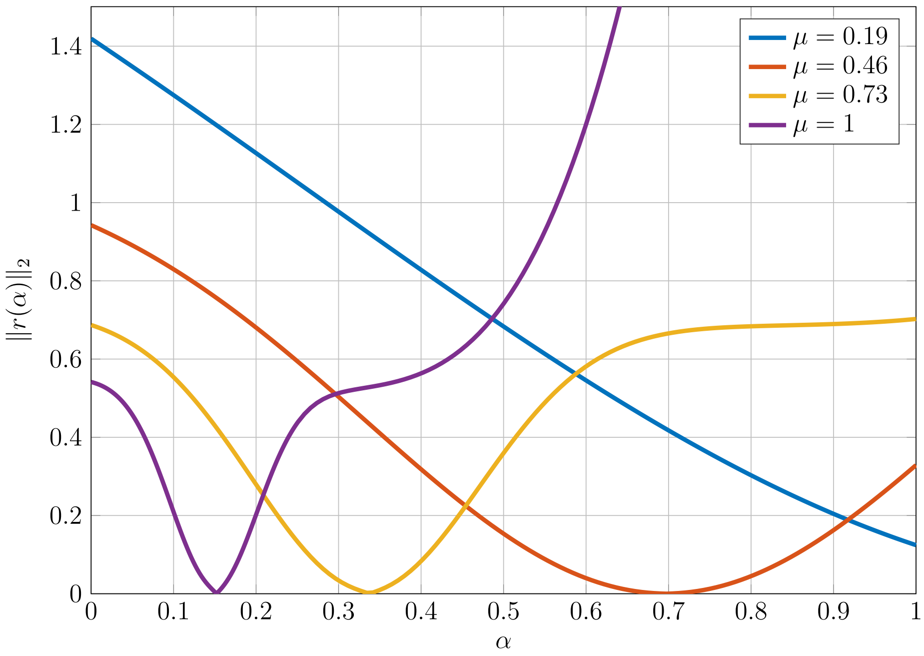

function:

$$f(x;\mu) = \begin{bmatrix} (2\mu)^{-1}\ \text{Exp}\Big[-\mu(x_1 + x_2)^2\Big] \\ (x_1^2 + 1)^{-1}\ \text{Cosh}[x_2] \end{bmatrix}, \tag{2.44}$$

where $x = [x_1\,, x_2]^{\intercal}$ and the scalar parameter μ is used to adjust the function's convexity near the origin. The associated residual is taken to be

$$r(x;\mu) = f(x;\mu) - f([0\,,0]^{\intercal};\mu), \tag{2.45}$$

whose solution is then $x_n = [0\,,0]^{\intercal}$ by construction. Figure 2.7 shows the residual norms for the first Newton step from the initial point $x_0 = [1\,,1]^{\intercal}$ for several values of μ. For the lowest value of μ, the norm is decreasing along the entire length of the Newton step while the residual quickly explodes to over twenty-times its initial value for the highest μ. The intermediate parameters exhibit mild features of the extremes: one that reduces the norm at the full Newton step but not as much as possible and the other results in a slight increase in the norm but does showcase a promising minimum near a step fraction of 0.33.

Even for this simple example, some form of line search would be required to ensure convergence across all values of μ. The two highest values are prime candidates for one of the back-tracking schemes since they have multiple extrema. The second smallest value is a candidate for a golden section search since it is unimodal with a better optimum than the full step at around 0.75. Finally, the lowest μ value can actually be over-relaxed to a value around 1.3. However, these observations and determinations can only be made since the true residual was also observed. In practice, a back-tracking algorithm is employed only if the residual does not reduce enough and the Newton iteration is continued automatically.

Algorithm

An outline of the nonlinear solving algorithm is given in algorithm 1. The function introduces two more parameters that have been implied but not fully addressed since they are independent of the mathematics. The first parameter is the *absolute residual tolerance* ε. The Newton iteration is considered complete when the residual's norm falls below ε. If the system is scaled to around an order of one, common default values of ε fall in the range of 10^{-6} to 10^{-8}. The second parameter is the constant used in the proportional back-tracker τ. The value of τ is arbitrary but a good value has been found to be 0.5.

The motivation and derivation of Newton's method for solving non-linear equations is now complete. The next item to be explained is how to efficiently solve the linear system, as shown on line 5 of algorithm 1, and how the manner in which the system is solved will allow the preclusion of calculating and inverting the Jacobian.

Algorithm 1: Nonlinear solve with Newton's Method

```
function newtonSolve($x_0, r(x), J(x), \varepsilon, \tau$)
    $x_{k-1} = x_0$    % Initialization
    $r_{k-1} = r(x_{k-1})$
    while $\|r_{k-1}\|_2 > \varepsilon$ do    % begin linear solves
        Solve $J(x_{k-1})\,\delta x_{k-1} = -r_{k-1}$
        $x_k = x_{k-1} + \delta x_{k-1}$
        $r_k = r(x_k)$
        if $\|r(x_k)\|_2 > \|r(x_{k-1})\|_2$    % back-track if needed
            $\alpha = \tau$
            while $\|r(x_k)\|_2 > \|r(x_{k-1})\|_2$ do
                $x_k = x_{k-1} + \alpha\,\delta x_{k-1}$
                $r_k = r(x_k)$
                $\alpha = \tau\,\alpha$
            end
        end
        $x_{k-1} = x_k$
        $r_{k-1} = r_k$
    end
    Return $x_k$
end
```

2.3.2 Krylov Methods

Krylov methods are a class of techniques used to solve linear systems of the form

$$Ax = b \tag{2.46}$$

where x and b are $n \times 1$ vectors and A is an $n \times n$ nonsingular matrix [45]. Different methods place other limitations on A, but a required condition for all methods is that the coefficient matrix A be invertible. The exact solution to equation 2.46 is simply

$$x = A^{-1}b. \tag{2.47}$$

Although trivially , the exact inversion of A can be computationally and memory intensive if n is large. The computational cost of inverting A is only exacerbated when solving nonlinear problems with a Newton-like scheme since several, if not many, linear solves are required to make one nonlinear advancement.

Krylov methods aim to provide an approximate solution to equation 2.46 without ever forming the inverse of A explicitly. To explain the procedure used, first, the solution will be written in an inverse-free form. Then, a general explanation of Krylov subspaces and methods will be given. The section will conclude with the particular Krylov method used for this work: GMRES.

Inverse-free Form

Let x_n represent the exact solution to equation 2.46 and x_0 represent an initial guess to the solution. Assuming the problem is solvable, there exists some δx such that $x_n = x_0 + \delta x$. Therefore, the residual vector for the initial guess from the solution is

$$r_0 = b - Ax_0 \tag{2.48}$$

Isolating b on the left-hand side and multiplying through by A^{-1} then gives

$$A^{-1}b = x_0 + A^{-1}r_0 \tag{2.49}$$

Substituting this into equation 2.47 gives

$$x_n = x_0 + A^{-1}r_0. \tag{2.50}$$

The burden of calculating A's inverse is still present. To avoid this burden, we use a result of the Cayley-Hamilton theorem: the inverse of a square $n \times n$ matrix can be expressed as a linear combination of the matrix's powers from 0 to $n-1$ [46]. To wit, given the proper weights c_i, the equality $A^{-1} = \sum c_i A^i$ is satisfied and equation 2.50 can be re-written to

$$x_n = x_0 + \sum_{i=0}^{n-1} c_i A^i r_0. \tag{2.51}$$

The true solution to the problem is now in a form that incorporates some initial guess and is free of matrix inversions. However, the weights c_i, which are required for the equality to hold, are based on A's characteristic polynomial. Calculating these weights exactly are, as in the explicit calculation of the inverse, difficult to efficiently compute for large n and an approximation must be made for tractability.

Generic Krylov Methods

The set of vectors $\{A^i r_0\}$ present in equation 2.51 is called the Krylov subspace of A, denoted $\mathcal{K}_n(A, r_0)$, and is the basis of all Krylov methods [45]. The set is of dimension n and will hereafter be referred to as the full subspace. Typically, the methods to be discussed use a variable number m of lower dimensional spaces that will likewise be denoted $\mathcal{K}_m(A, r_0)$.

The approximate solution formed by Krylov methods is based on one simplification to equation 2.51: only form a subset of the full subspace; the idea being that the true solution in the full subspace may not be far from the subset. At every m-th iteration of a Krylov method, a new vector from the Krylov subspace is generated through the application of the matrix A to the previous vector and is then added to the current vector set $\mathcal{K}_m(A, r_0)$. An overdetermined problem from a linear combination of the vector set with m undetermined coefficients is then solved to create a new approximate solution. The set is grown and approximate solution updated until the norm of the residual is sufficiently low. The maximum number of basis vectors needed varies by problem, but it is guaranteed that the approximation will reach the true solution once the full subspace is formed since the number of degrees of freedom will equal the dimension of A.

In terms of linear algebra, let $Z_m = [\, z_1 \,, z_2 \,, \dots , z_m]$ be an $n \times m$ matrix whose columns form a basis for $\mathcal{K}_m(A, r_0)$ and $w_m = [\omega_1 \,, \omega_2 \,, \dots , \omega_m]^{\mathsf{T}}$ be an $m \times 1$ weight vector (analogous to the aforementioned c_i). Starting with $z_1 = r_0 / \|r_0\|$, at every m-th iteration, generate a new vector in the Krylov subspace by applying A to the previous vector: $z_m = A z_{m-1}$. A new solution direction δx_m is then found by calculating the weight vector w_m with z_m added into the Krylov expansion. Therefore, the m-th approximate solution is

$$x_m = x_0 + \delta x_m = x_0 + Z_m w_m \tag{2.52}$$

with the associated residual

$$r_m = r_0 - A \delta x_m = r_0 - A Z_m w_m . \tag{2.53}$$

Two side effects of iteratively growing the basis matrix Z_m are that the weights are no longer based on A's characteristic polynomial and the resulting system to solve for the weights is overdetermined as long as $m < n$. To remedy this problem, Krylov methods define an optimality condition that results in weights that attempt to reduce the residual every iteration.

Since Krylov methods are a family, a specific method arises from consideration of A's structure, choice of optimality condition, and choice of the basis vectors for Z_m [45]. GMRES will give concreteness to these three choices.

GMRES

First presented by Saad and Schultz in 1986, GMRES is a Krylov method designed to solve any linear system with an invertible matrix A [47]. Because GMRES does not require any other special structure, it is well-suited for generic, unsymmetrical problems. Of course, with the power to solve any invertible system comes a burden of mathematical and computational complexity when compared to more specialized Krylov methods.

The algorithm is developed with the goal of solving the minimization problem

$$\delta x_m = \underset{\delta x_m^*}{\operatorname{ArgMin}} \|r_0 - A\delta x_m^*\|_2^2. \tag{2.54}$$

Therefore, the m-th solution direction is the one which minimizes the associated residual r_m. If the solution direction has n free parameters, the minimization problem is equivalent to exactly solving the full linear system. However, if the direction is limited to $m < n$ free parameters, the problem is one of least squares. The least squares problem is the one to be solved because GMRES aims to solve the linear system without a full matrix inversion.

The least squares problem is solved by finding the m-th residual vector r_m that lies orthogonal

Figure 2.8: Two-dimensional analogue of the n-dimensional triangle that motivates the optimality condition: the length of r_m is minimal when it is orthogonal to $A\delta x_m$.

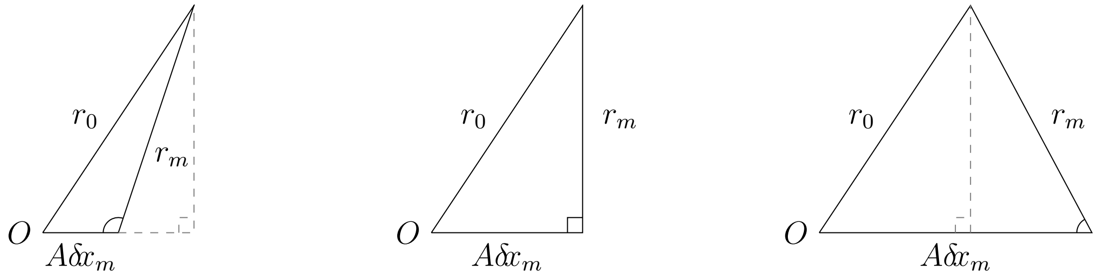

to the A-combination of the current Krylov subspace:

$$r_m \perp A\mathcal{K}_m(A, r_0) \tag{2.55}$$

Noting that $\delta x_m \in \mathcal{K}_m(A, r_0)$, the requirement of orthogonality can be seen by considering the equality $r_0 = r_m + A\delta x_m$. If r_0 lies within the plane $A\mathcal{K}_m(A, r_0)$, it can be exactly found as a linear combination of the basis vectors Z_m, and r_m must be exactly 0 to honor the balance. If it lies outside of the plane, the closest $A\delta x_m$ can approach r_0 is its orthogonal projection onto the plane with r_m representing the components that lie outside the current subspace. Figure 2.8 shows a simple two-dimensional triangle analogue of this situation: assuming r_0 is not parallel to $A\delta x_m$, r_m has its shortest, non-zero length when it is perpendicular to $A\delta x_m$.

The final choice to be made for the implementation of GMRES is that of the vectors used to form Z_m. The so-called classic GMRES of Saad and Schultz proposed an iteratively grown orthonormal basis for $\mathcal{K}_m(A, r_0)$ and used those vectors to form Z_m [47]. The choice of basis is natural since the solution lies in the Krylov subspace. However, this choice of basis leads to a least squares problem involving a Hessenberg matrix which itself requires a QR decomposition for an efficient solution. As such, a version called Simpler GMRES was later developed by Walker and Zhou that builds an orthonormal basis for $A\mathcal{K}_m(A, r_0)$ and uses those basis vectors to form Z_m [48]. The choice of vectors in Simpler GMRES leads directly to a QR factorization and is therefore simpler to implement; however, the choice was proven to result in an ill-conditioned R-factor and therefore be far less numerically stable than the classic method [49]. The stability problem was resolved by a method called Adaptive Simpler GMRES (ASGMRES) due to Jiránek and Rozložník. ASGMRES switches between the basis of Simpler GMRES and a basis formed from the sequence of residuals from the iterative solution [50]. Specifically, at the m-th iteration of the solution, given a Simpler GMRES basis vector q_{m-1} and residuals from two previous iterations r_{m-1} , r_{m-2}, the vector z_m is assigned thusly:

$$z_m = \begin{cases} r_{m-1}/\|r_{m-1}\|_2 & \text{if } \|r_{m-1}\|_2 < \nu\|r_{m-2}\|_2 \\ q_{m-1} & \text{otherwise} \end{cases}. \tag{2.56}$$

The reasoning behind switching between the two sets is that one is more stable if the residuals are decreasing sharply and the other is more stable if the residuals are decreasing slowly. The parameter ν, which is bounded between 0 and 1, is used to determine what decrease is sufficient enough to warrant the use of the residual vectors.

With the choice of basis vector for Z_m complete, the problem of solving the least squares problem is all that remains. From equation 2.53, an equivalent form of equation 2.54 is

$$w_m = \underset{w_m^*}{\text{ArgMin}} \|r_0 - AZ_m w_m^*\|_2^2. \tag{2.57}$$

The QR factorization of the $n \times m$ coefficient matrix AZ_m has the form

$$AZ_m = \widetilde{Q}_m \widetilde{R}_m = \begin{bmatrix} Q_m & Q_{n-m} \end{bmatrix} \begin{bmatrix} R_m \\ 0 \end{bmatrix} = Q_m R_m \tag{2.58}$$

where $\widetilde{Q}_m$ is an $n \times n$ orthogonal matrix, $\widetilde{R}_m$ is an $n \times m$ full rank rectangle, Q_m is an $n \times m$ orthogonal rectangle, Q_{n-m} is an $n \times (n-m)$ orthogonal rectangle, and R_m is an $m \times m$ upper-triangular matrix. The matrices $\widetilde{Q}_m$ and $\widetilde{R}_m$ comprise what is called the full factorization, and Q_m and R_m comprise the reduced factorization.

The minimization problem can be reduced to a solvable, square system using the QR factorization. Three key properties of the orthogonal matrix $\widetilde{Q}_m$ aid in this reduction: the transpose $\widetilde{Q}_m^T$ is also the inverse, the transpose is also orthogonal, and orthogonal matrices do not change the 2-norm of a vector ($\|Qx\|_2 = \|x\|_2$) [51]. Introducing the full QR factorization into the minimization problem and using the properties of $\widetilde{Q}_m$, equation 2.57 has the equivalent form

$$w_m = \operatorname{ArgMin}\left\| \widetilde{Q}_m^T r_0 - \widetilde{R}_m w_m \right\|_2^2. \tag{2.59}$$

The problem can be further simplified using the reduced factorization to yield

$$\begin{aligned} w_m &= \operatorname{ArgMin}\left\| \begin{bmatrix} Q_m^T r_0 - R_m w_m \\ Q_{n-m}^T r_0 \end{bmatrix} \right\|_2^2 \\ &= \operatorname{ArgMin}\left(\left\| Q_m^T r_0 - R_m w_m \right\|_2^2 + \left\| Q_{n-m}^T r_0 \right\|_2^2 \right). \end{aligned}$$

Since the quantity $\|Q_{n-m}^T r_0\|_2^2$ is independent of the weights, the minimization is achieved by solving the term involving the reduced factorization to render its norm zero. The weights are therefore calculated from the square, linear system

$$R_m w_m = Q_m^T r_0. \tag{2.60}$$

With the weights now known, an approximate solution can be found and the residual checked for convergence against some tolerance.

While calculating the weights and explicitly evaluating the residual every iteration is possible, that procedure will slow down the solution as R_m becomes large. A way around this problem is to recall that r_m lies perpendicular to $A\mathcal{K}_m(A, r_0)$ and the columns of $Q_m = [\, q_1 \,, q_2 \,, \dots \,, q_m]$ form an orthonormal basis for $A\mathcal{K}_m(A, r_0)$ [50]. As such, r_m can be calculated by an orthogonal projection using Q_m:

$$r_m = (I - Q_m Q_m^{\mathsf{T}}) r_0 = (I - q_m q_m^{\mathsf{T}}) r_{m-1} = r_{m-1} - (q_m^{\mathsf{T}} r_{m-1})\, q_m. \tag{2.61}$$

This formula allows for the calculation of the m-th residual without explicitly calculating w_m and will therefore increase the efficiency of the implementation.

Algorithm

A full outline of an implementation of ASGMRES is given in algorithm 2. The absolute convergence tolerance ε and residual decrease ratio ν are two additional inputs to the required pieces of the linear system itself. A full explanation of the QR factorization as shown on lines 4 and 15 is omitted for brevity; however, this work makes use of a QR implementation based on Householder reflectors as described in [52]. The final solution of the linear system for the weights will also be omitted, but since R_m is upper-triangular, the solution is simply one of back-substitution.

Algorithm 2: Solve a linear system using Adaptive Simple GMRES

```
function asgmres($x_0$, $A$, $b$, $\varepsilon$, $\nu$)
    $r_0 = b - Ax_0$    % Initialization
    $z_1 = r_0/\|r_0\|_2$
    UpdateQR $AZ_1 = Q_1R_1$
    $r_1 = r_0 - (q_1^\intercal r_0)\, q_1$
    $m = 2$
    $r_{m-2} = r_0$
    $r_{m-1} = r_1$
    while $\|r_{m-1}\|_2 > \varepsilon$ do    % begin building the Krylov solution
        if $\|r_{m-1}\| < \nu\|r_{m-2}\|$    % choose the next basis vector
            $z_m = r_{m-1}/\|r_{m-1}\|_2$
        else
            $z_m = q_{m-1}$
        end
        UpdateQR $AZ_m = Q_mR_m$
        $r_{m-2} = r_{m-1}$
        $r_{m-1} = r_{m-1} - (q_m^\intercal r_{m-1})\, q_m$
        $m = m + 1$
    end
    Solve $R_m\, w_m = Q_m^\intercal r_{m-1}$
    $x_m = x_0 + Z_m w_m$
    Return $x_m$
end
```

2.3.3 Jacobian-Free Augmentation

With both Newton's method and ASGMRES explained, a Jacobian-free non-linear solver can now be discussed. Using the ASGMRES implementation discussed to solve the linear system for the Newton direction, the QR factorization in ASGMRES becomes $J_r(x_k)Z_m = Q_mR_m$. This is the only manner in which the Jacobian affects ASGMRES; it only appears as a sequence of matrix-vector products on the left-hand side of the QR factorization:

$$J_r(x_k)Z_m = [\, J_r(x_k)z_1\, , J_r(x_k)z_2\, , \dots\, , J_r(x_k)z_m\,] \tag{2.62}$$

Because each row of the Jacobian is a gradient of the associated function from $r(x_k)$, the matrix-vector product results in a dot product of the vector z_m with all of the gradients which produces a vector of directional derivative values. Therefore, the resulting product is in some sense a directional derivative and may be approximated by a finite difference:

$$J_r(x_k)z_m \approx \frac{r(x_k + \sigma\, z_m) - r(x_k)}{\sigma}, \tag{2.63}$$

where σ is a small number. Formally, the approximation is a finite application of the Gâteaux derivative [53] and can be seen as valid through a multivariate Taylor expansion of $r(x_k + \sigma\, z_m)$ about x_k

$$r(x_k + \sigma\, z_m) = r(x_k) + J_r(x_k)\sigma\, z_m + c(x_k, \sigma\, z_m). \tag{2.64}$$

Substituting this expansion into equation 2.63 sans the higher-order terms yields the first-order finite difference approximation. Therefore, the m-th column of the left-hand side of the QR factorization can be approximately computed without explicit presence of the Jacobian matrix. And because everything is being solved approximately to a tolerance anyways, one more approximation, especially one that greatly reduces the computational complexity of the solution, is not detrimental to the overall solution.

Knoll and Keyes provide a much wider and in-depth discussion of JFNK methods in [54], but only two of the items they presented will be mentioned. First, they mention a centered, second-order finite difference scheme may be used in place of equation 2.63 but note it has not gained much popularity, and indeed, any standard differencing scheme may be used as the approximation as long as the residual is defined on the stencil. The apparent aversion to such schemes may stem from the need to evaluate the residual function two or more times per loop instead of the single evaluation for the first-order scheme and due to little gain in effectiveness since σ must be adjusted according to the order of the method to balance finite difference truncation error and floating-point round-off error. The second item a discussion of a good choice of σ. If the system is scaled to around unity, a choice of around 10^{-8} is standard for finite differences since smaller values succumb to the limitation 64-bit floating-point precision. If the system is not scaled that nicely, a number of recommendations are given, such as

$$\sigma = \frac{\sqrt{\left(1 + \|x_k\|_2\right) \sigma_{\mathrm{mach}}}}{\|z_m\|_2}, \tag{2.65}$$

where σ_{mach} is the machine epsilon. If the norm of the expansion point is particularly large, this is the value of σ used and 10^{-8} is used for norms close to unity.

A modified ASGMRES algorithm is presented in algorithm 3. The non-linear residual function is denoted as r_{NL} in order to clearly distinguish it from the residuals of the linear solve r_m. Also, the first-order finite difference is denoted

$$Dr_{\mathrm{NL}}(z_m;\, x_k, \sigma) = \frac{r(x_k + \sigma\, z_m) - r(x_k)}{\sigma} \tag{2.66}$$

both for cleanliness and to emphasize that the first-order approximation is only a function of the Krylov vector with the expansion point and difference step size acting as a parameters. The only major change from algorithm 2 is instead of performing the matrix-matrix product AZ_m, a new matrix L is introduced that holds the matrix-vector columns generated from the

Dr_{NL} function. Also, since the Jacobian doesn't explicitly exist, the true initial linear residual $r_0 = -r_{\text{NL}}(x_K) - J_r(x_k)\delta x_k$ cannot be calculated, so the guess value is taken to be the zero vector.

Algorithm 3: Solve for a Newton update using ASGMRES with no Jacobian

```
function jfgmres($x_k$, $r_{\text{NL}}$, $\varepsilon$, $\nu$, $\sigma$)
    $r_0 = -r_{\text{NL}}(x_k)$    % Initialization
    $z_1 = r_0 / \|r_0\|_2$
    $L = Dr_{\text{NL}}(z_1; x_k, \sigma)$    % Store the first approximate column of $J_r(x_k) z_1$
    UpdateQR $L = Q_1 R_1$
    $r_1 = r_0 - (q_1^{\mathsf{T}} r_0)\, q_1$
    $m = 2$
    $r_{m-2} = r_0$
    $r_{m-1} = r_1$
    while $\|r_{m-1}\|_2 > \varepsilon$ do    % begin building the Krylov solution
        if $\|r_{m-1}\| < \nu \|r_{m-2}\|$    % choose the next basis vector
            $z_m = r_{m-1} / \|r_{m-1}\|_2$
        else
            $z_m = q_{m-1}$
        end
        $L = [L\,,\, Dr_{\text{NL}}(z_1; x_k, \sigma)]$    % augment $L$ with the new column
        UpdateQR $L = Q_m R_m$
        $r_{m-2} = r_{m-1}$
        $r_{m-1} = r_{m-1} - (q_m^{\mathsf{T}} r_{m-1})\, q_m$
        $m = m + 1$
    end
    Solve $R_m\, w_m = Q_m^{\mathsf{T}} r_{m-1}$
    $x_m = x_0 + Z_m w_m$
    Return $x_m$
end
```

2.4 Stability Analysis

A stability analysis is an umbrella term for studying the basic structure of solutions to differential equations. The concerns of stability analysis include oscillations in solutions, sensitivity of solutions to perturbations, solution uniqueness dependent upon system parameters, and solution divergence (i.e., blow-up). This section focuses on the tractable subject of the linear stability. A full discussion of nonlinear stability theory is beyond the scope of this work and is left to the literature (e.g., [55, 56]).

At the heart of linear stability analysis is the solution of an eigenvalue problem. Through manipulation and simplification of the conservation laws, the ultimate goal of linear stability is to find the eigenvalues of a coefficient matrix a_{ij} present in the ordinary differential equation

$$\partial_t \delta q_i = a_{ij} \delta q_j, \tag{2.67}$$

where δq_i are small, system-wide perturbations off of a steady-state solution, as will be discussed. The eigenvalues determine the asymptotic behavior of the perturbations in time. If the perturbations eventually decay toward zero, the system with the associated a_{ij} is said to be *stable*. If the perturbations grow, it is *unstable*. These aspects will be explored again in the following subsection in more depth.

The section proceeds with a general discussion and derivation of the above equation and finishes with the particular application of the analysis to the system of equations presented in previous sections.

2.4.1 The Perturbation Equation

The differential form of the conservation law of primary concern for this work is

$$\partial_t q_i(x_i,t) + \partial_j f_{ij}(q_i,x_i,t) - s_i(q_i,x_i,t) = 0 \tag{2.68}$$

where f_{ij} and s_i are taken to be nonlinear functions of the system parameters q_i. The assumed nonlinearity in the flux and source functions makes analytical solutions of the equation extremely difficult to acquire and analyze in a rigorous manner. Linear stability analysis remedies this shortcoming by Taylor expanding the nonlinear problem about an equilibrium point. A solution of the form

$$q_i(x_i,t) = q_i^{\text{ss}}(x_i) + \delta q_i(x_i,t) \tag{2.69}$$

is assumed. That is to say, the total solution is taken to be the linear combination of a steady-state solution $q^{\text{ss}}(x_i)$ and a transient, perturbation solution $\delta q(x_i,t)$. Substituting this ansatz into the conservation law gives the following:

$$\partial_t \delta q_i(x_i,t) + \partial_j f_{ij}(q_i^{\text{ss}} + \delta q_i; x_i, t) - s_i(q_i^{\text{ss}} + \delta q_i; x_i, t) = 0. \tag{2.70}$$

The still-extant nonlinearity is then removed via a Taylor expansion about the steady-state solution. Since all surface fluxes exactly balance all sources at steady-state, the zero-th order terms in the Taylor expansion cancel, and only the first-order Jacobian terms remain with all higher orders neglected:

$$\partial_t \delta q_i(x_i,t) + \partial_j \left[\frac{\partial f_{ij}}{\partial q_k^{\text{ss}}} \delta q_k \right] = \frac{\partial s_i}{\partial q_k^{\text{ss}}} \delta q_k. \tag{2.71}$$

This linear, partial differential equation for the perturbation solution forms the fundamental basis for linear stability analysis.

Despite the perturbation equation being linear, it is still a partial differential equation with a spatially dependent coefficient matrix under the gradient on the left-hand side that does not lend itself easily toward a closed-form solution. Further, the differential form will only give a point-wise perspective on the perturbations' evolution and not a more important, system-wide perspective. The solution to these problems is to integrate the perturbation equation over the entire computational domain to turn the partial differential equation into an ordinary differential equation:

$$\partial_t \int_\Omega \delta q_i(x_i, t)\, \mathrm{d}\Omega + \int_\Gamma \frac{\partial f_{ij}}{\partial q_k^{\mathrm{ss}}} \delta q_k n_j\, \mathrm{d}\Gamma = \int_\Omega \frac{\partial s_i}{\partial q_k^{\mathrm{ss}}} \delta q_k\, \mathrm{d}\Omega. \tag{2.72}$$

While this procedure bares resemblance to the earlier outlined FVM, there are two key differences. The first difference is that the integration should be done over the entire system and not broken into pieces. Breaking the integration into pieces will allow local tracking of perturbations, but the resulting coefficient matrix will have possibly spurious positive eigenvalues associated with the positive advection of material across control volume boundaries; therefore, the integration should not be partitioned.

The second difference is that some simple spatial form of the perturbations should be chosen such that they can be removed from the integrals to generate the ordinary differential equations presented at the beginning of this section. This step is needed since the domain cannot be partitioned without corrupting the eigenvalue calculation. The two simplest choices for the spatial dependence of the perturbations is point sources or everywhere-constant sources. The point sources are arguably the least severe to consider given their local nature and would require a volume-by-volume tracking scheme to determine where to perform the integration; therefore, point sources will not be considered in this work. Everywhere-constant sources, while not physically correct, would likely provide bounding behavior for the system given the size and coverage of the disturbances. Furthermore, it would allow the perturbations to be pulled directly out of the integrals and naturally lead to a system of ordinary differential equations. This is the choice of spatial perturbations that will be explored for the rest of this work. With this choice of basis and some minor manipulations, equation 2.72 becomes

$$\partial_t \delta q_i(t) = \frac{1}{\int_\Omega \mathrm{d}\Omega} \left[\int_\Omega \frac{\partial s_i}{\partial q_k^{\mathrm{ss}}} \,\mathrm{d}\Omega - \int_\Gamma \frac{\partial f_{ij}}{\partial q_k^{\mathrm{ss}}} n_j \,\mathrm{d}\Gamma \right] \delta q_k(t); \tag{2.73}$$

this is the general conservation law for linear stability analysis. Now, the specific sources and fluxes of the system of equations described in section 2.1 will be put into this equation.

2.4.2 Thermohydraulic Stability Equation

To give concreteness to the above generics, we consider equation 2.21 in their differential form:

$$\frac{\mathrm{d}}{\mathrm{d}t} \begin{bmatrix} \rho \\ \rho i \\ \rho u_z \end{bmatrix} = -\partial_j \begin{bmatrix} \rho u_j \\ (\rho i + P) u_j \\ u_j \rho u_z + P z_i - \tau_{ij} z_i \end{bmatrix} + \begin{bmatrix} s^\rho \\ s^e \\ \rho g_z + s_z^u \end{bmatrix} \tag{2.74}$$

Linearizing these equations about a steady-state solution and canceling the balancing zero-th order terms gives

$$\frac{\mathrm{d}}{\mathrm{d}t} \begin{bmatrix} \delta\rho \\ \delta\rho i \\ \delta\rho u_z \end{bmatrix} = -\partial_j \left(\begin{bmatrix} \partial_{q_k}(\rho u_j) \\ \partial_{q_k}[(\rho i + P) u_j] \\ \partial_{q_k}(u_j \rho u_z + P \delta_{ij} z_i - \tau_{ij} z_i) \end{bmatrix} \delta q_k \right) + \left(\begin{bmatrix} \partial_{q_k}(s^\rho) \\ \partial_{q_k}(s^e) \\ \partial_{q_k}(\rho g_z + s_z^u) \end{bmatrix} \delta q_k \right), \tag{2.75}$$

where $\delta q_k = [\delta\rho \,, \delta\rho i \,, \delta\rho u_z]^\intercal$.

A fair bit of the apparent mess in calculating the derivatives can be avoided by carrying out the system-wide integration at this stage. As opposed to the FVM solution discussed earlier, there is no material transfer across any of the system boundaries and all advection terms immediately integrate to zero regardless of value. Further, since the bulk flow direction is always perpendicular to the outward surface normals for the simulations under consider, the pressure surface integrals will likewise be zero. Finally, the only external source of material is the heat addition and removal from the system which is constant; therefore, all of the source terms differentiate to zero as well. All of these arguments lead to the perturbation equation of

$$\frac{\mathrm{d}}{\mathrm{d}t}\begin{bmatrix}\delta\rho \\ \delta\rho i \\ \delta\rho u_z\end{bmatrix} = \frac{1}{V_{\mathrm{sys}}}\begin{bmatrix}0 & 0 & 0 \\ 0 & 0 & 0 \\ \alpha_\rho & \alpha_{\rho i} & \alpha_{\rho u_z}\end{bmatrix}\begin{bmatrix}\delta\rho \\ \delta\rho i \\ \delta\rho u_z\end{bmatrix}, \tag{2.76}$$

where

$$\begin{aligned}
\alpha_\rho &= -\int_\Gamma \partial_\rho \Delta P_{\mathrm{dar}}\,\mathrm{d}\Gamma + \int_\Omega g_z\,\mathrm{d}\Omega \\
\alpha_\rho &= -\int_\Gamma \partial_{\rho i} \Delta P_{\mathrm{dar}}\,\mathrm{d}\Gamma \\
\alpha_\rho &= -\int_\Gamma \partial_{\rho u_z} \Delta P_{\mathrm{dar}}\,\mathrm{d}\Gamma
\end{aligned}$$

By way of the matrix exponential, this system of differential equations has the solution

$$\begin{bmatrix}\delta\rho(t) \\ \delta\rho i(t) \\ \delta\rho u_z(t)\end{bmatrix} = \begin{bmatrix}1 & 0 & 0 \\ 0 & 1 & 0 \\ \frac{\alpha_\rho}{\alpha_{\rho u_z}}(e^{\tilde{\alpha}t}-1) & \frac{\alpha_{\rho i}}{\alpha_{\rho u_z}}(e^{\tilde{\alpha}t}-1) & e^{\tilde{\alpha}t}\end{bmatrix}\begin{bmatrix}\delta\rho(0) \\ \delta\rho i(0) \\ \delta\rho u_z(0)\end{bmatrix}, \tag{2.77}$$

where $\tilde{\alpha} = \alpha_{\rho u_z}/V_{\mathrm{sys}}$. And we see that the solution makes sense in relation to all of the assumptions that have been made up to now. Since the system was assumed to be perfectly isolated, there are no mechanisms to dissipate excess mass or energy perturbed into the system. As such, any non-zero initial perturbations in mass and energy will remain but with no dynamic behavior on either the mass or energy components of the system; they will simply be constant additions to the system.

Further, the time dependence on the $\alpha_{\rho u_z}$ parameter is shown through the exponential functions. If the value of the parameter is negative, the system will be asymptotically stable in that all perturbations will eventually decay to zero or another finite value dependent on any non-zero mass and energy perturbations introduced into the system. The calculation of the sign of these parameters, the eigenvalues of the above system, is what ultimately determines the stability of the system. And in order to calculate them properly, an accurate integration of the entire system is required. Accurate integration of the entire system necessitates local values attained from a FVM solution of the system.

Chapter 3

Simulations

The model used to test all of the aforementioned theory is a simple, closed loop model with 14 control volume and 14 momentum cells. The model's steady-states and stability were characterized and tested both in single and two-phase states. The single phase tests were performed in the subcooled liquid regime of water over a chosen rectangle in pressure-temperature space at several different heating loads. The two-phase tests were performed along the saturated liquid line of the vapor dome over several saturation temperatures and heating loads.

Figure 3.1: Test loop geometry. Black lines enclose control volumes, dashed red lines indicate the extents of the momentum cells, the blue control volume is removing the heat load, and the yellow control volume is receiving the heat load.

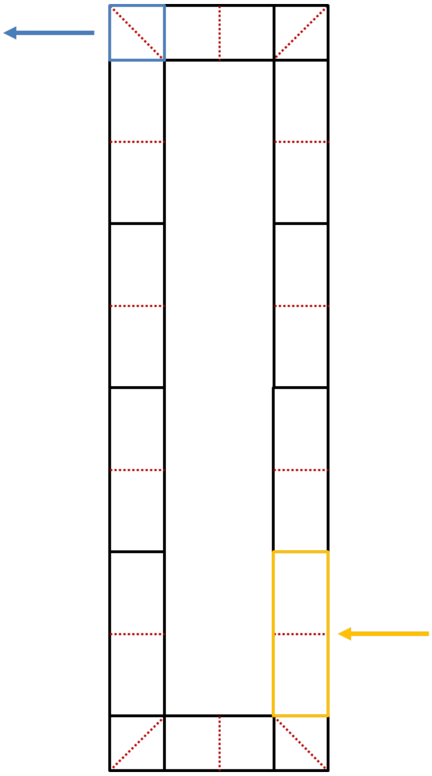

3.1 Geometry

The loop geometry and problem set-up are summarized in figure 3.1. All of the control volumes have a hydraulic diameter or 0.1 m and exchange surface flow areas of $1 \times 10^{-2}\,\mathrm{m}^2$. The lengths of the corner volumes are 0.1 m on all sides, the horizontal bridges are 0.2 m in length, and the vertical volumes are 0.3 m tall. The total volume of the system is $0.032\,\mathrm{m}^3$ with an aspect ratio of 3.5.

The geometry was chosen to be a smaller scale version of the UW–Madison RCCS experiment.

The size of the model, number of control volumes, and total amount of water in the system has an enormous impact on the current performance of the code used to solve the problems. As such, a small numerical experiment was settled upon to allow efficient investigation into both the single and two-phase systems before any in-depth efforts were made to improve performance beyond the code optimizations of the implementation language and platform.

3.2 Solution Methodology

Despite the simple geometry, the steady-state solutions required for the stability analysis are not easily solved because any closed-loop system presents an inherently singular steady-state balance between fluxes and sources. Therefore, all of the steady-states that will be presented were acquired from transient simulations that were run until the absolute value of the time rate-of-change of all system variables fell below 10. The limiting variable using that metric was the energy of the control volumes since their values were on the order of 1×10^5 J to 1×10^6 J with all other system variables being driven to very small rates-of-change relative to their inherent scales. A time evolution of some system parameters can be seen in figures 3.2 and 3.3.

To aid in proper gauging of the system, the cooling volume for steady-state simulations was set to a fixed state. This Dirichlett condition allowed for exact specification of a state within the system such that a map of states could be precisely traversed for the linear stability analysis. The system was changed to one with pure Neumann boundary conditions when the transient, pulsed simulations were performed to more adequately simulate the dynamics of the loop.

The eigenvalue calculations were performed using a central finite difference on the momentum value to approximate the required derivatives. A numerical approximation was chosen to overcome the complexities of the derivatives due to models used in single phase and primarily those in two-phase for the friction factor multiplier (see appendix B).

3.3 Linear Stability Results

3.3.1 Single Phase

The single phase simulations were carried out by setting the cooling corner of the model to a set temperature and pressure and letting the simulation run to a steady-state. Steady-states were generated using a grid of temperatures ranging from 300 K to 372 K and pressure ranging from 101 325 Pa to 202 650 Pa and heat loads of 1, 2, 4, 8 and 16 kW. Pertinent average parameters and a crude energy balance for comparison are presented in table 3.1.

The results of the eigenvalue calculations for each of the power levels over the computational rectangle can be found in appendix C.1. As show in figure 3.4, all of the individual stability maps have been compressed into a single multiple-surface plot to facilitate the summary of results and notice trends. As can be seen, all of the computed eigenvalues are below zero, and thus the system doesn't exhibit any instabilities in the single phase region. The lack of a boundary is not all that shocking given that water is an extremely dense and robust fluid while it is in the subcooled regime. Additionally, since the only remaining system-wide terms in the perturbation equations were dissipative in nature, the absolute stability of the simulations is not that surprising.

It is also noted that the eigenvalues become more negative as either the heat load increases or the system pressure increases and remains relative constant with varying temperature.

Figure 3.2: Steady-state time evolutions of the test loop with the cooled control volume fixed at a saturated liquid state at 372 K.

(a) Maximum Quality

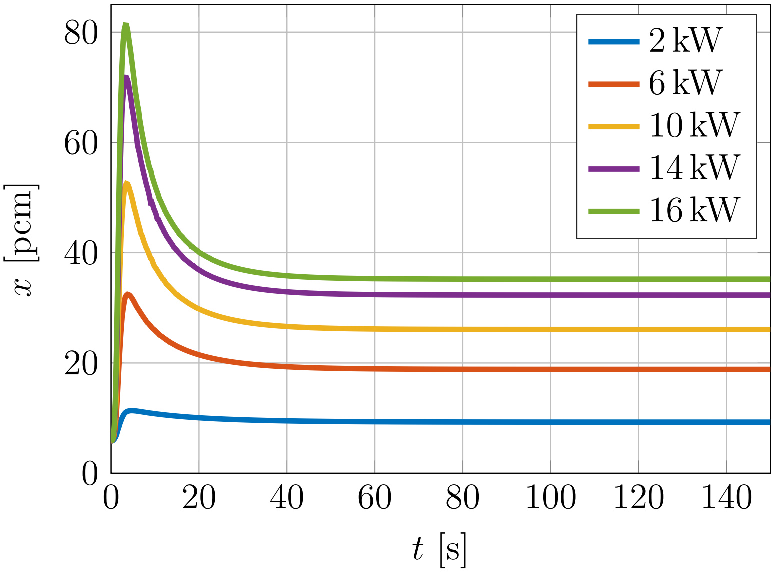

(b) Maximum Void Fraction

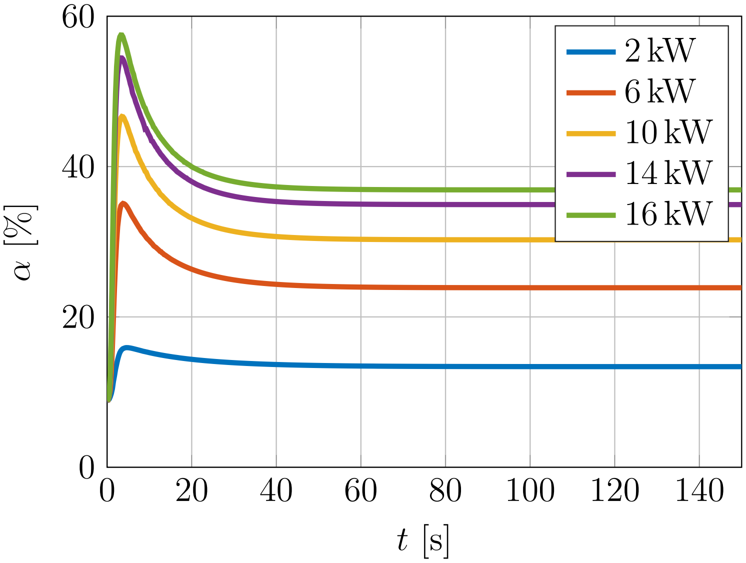

Figure 3.2: (cont.) Steady-state time evolutions of the test loop with the cooled control volume fixed at a saturated liquid state at 372 K.

(c) System Temperature Rise

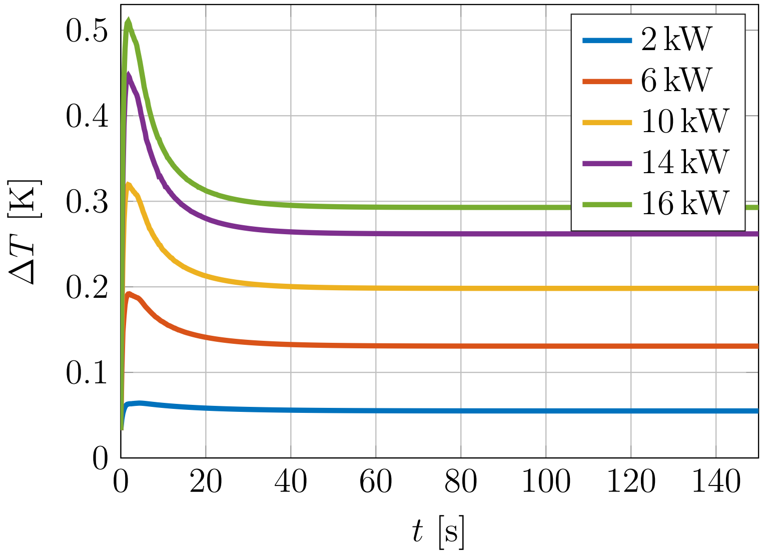

(d) System Pressure Difference

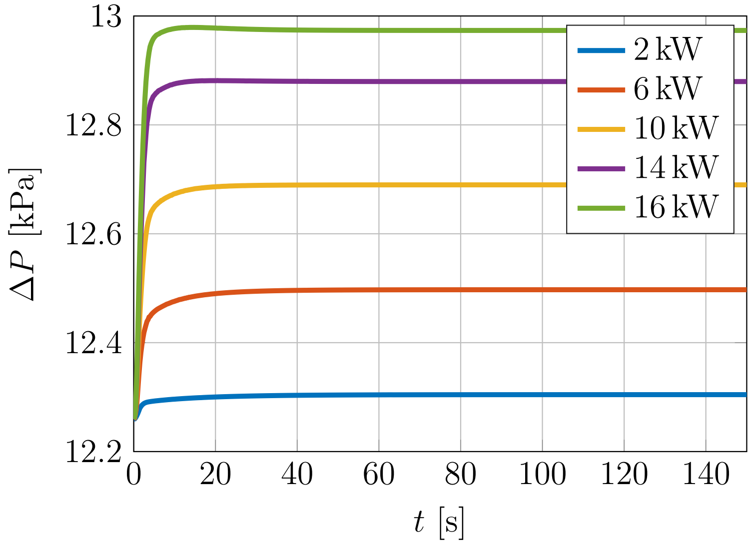

Figure 3.3: Steady-state time evolutions of the test loop with the cooled control volume fixed at a saturated liquid state at 390 K.

(a) Maximum Quality

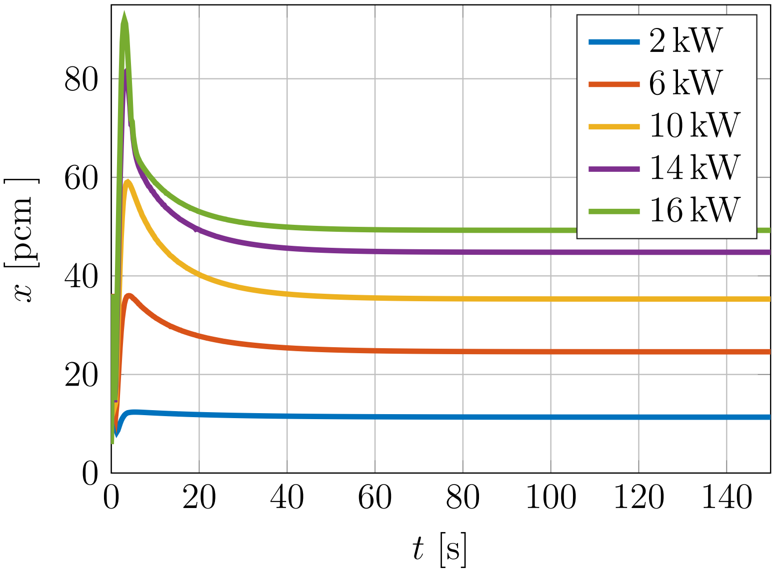

(b) Maximum Void Fraction

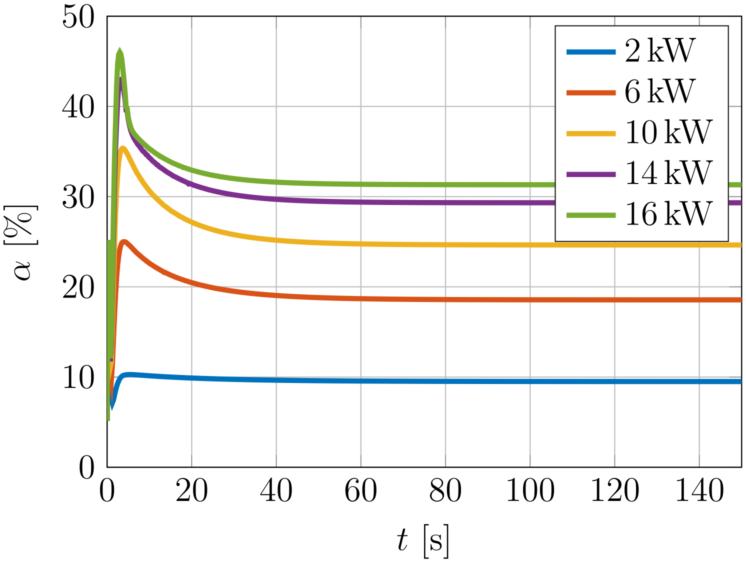

Figure 3.3: (cont.) Steady-state time evolutions of the test loop with the cooled control volume fixed at a saturated liquid state at 390 K*.*

(c) System Temperature Rise

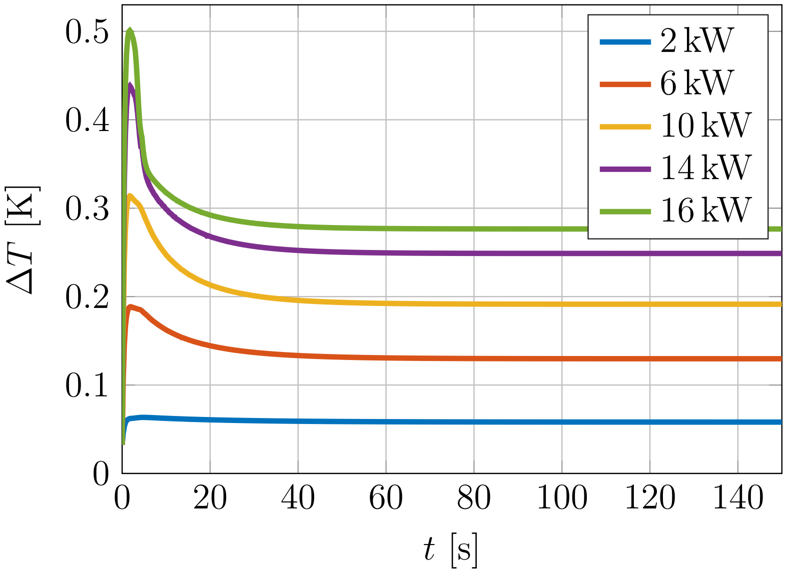

(d) System Pressure Difference

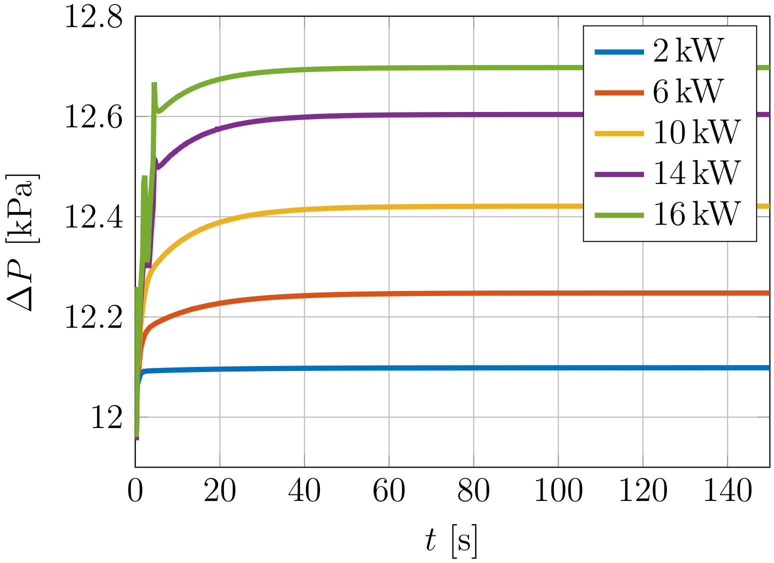

Figure 3.4: Eigenvalue maps of the simple, closed loop over the chosen state space at varying heat loads; the top most surface is the 1 kW *simulation and the bottom surface is the* 16 kW *simulation. All eigenvalues are negative.*

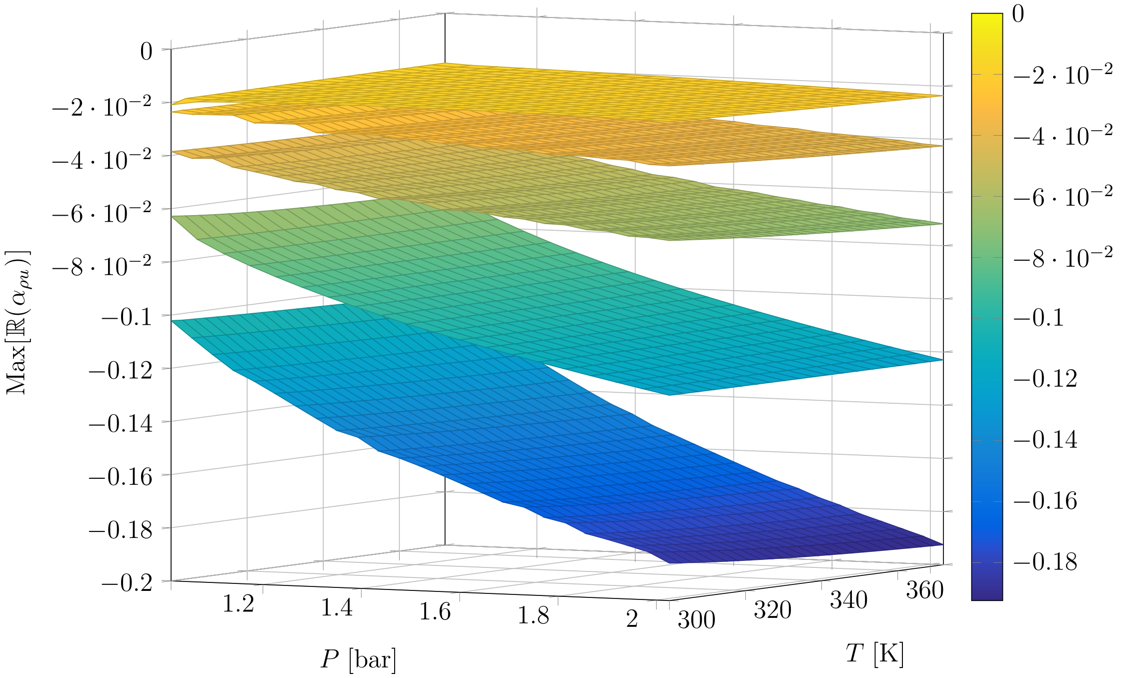

Considering the power variation, the increase in system stability is attributed to the ever-increasing mass flow. As the system's fluid travels faster, the greater inertia works to damp out small perturbations more effectively than a slower system. Likewise, an increase in pressure stiffens the water system and allows for a more potent mitigation of small perturbations in the system. These trends will also be seen in the two-phase results.

3.3.2 Two-Phase

The two-phase simulations were carried out by setting the cooling corner of the model to a saturation temperature with the associated pressure and liquid density; the system was then heated and allowed to evolve to a steady-state. Steady-states were generated using saturation temperatures ranging from 372 K to 390 K, which corresponds to a pressure range of 97.33 kPa to 179.64 kPa, with heat loads of 1 kW and from 2 to 16 kW by increments of 2. Pertinent average parameters and a crude energy balance for comparison are presented in table 3.1. Although the usage of heat capacity isn't valid with two-phase results, it should provide a close estimate for a hand-calculation comparison to the simulation given the small maximum quality of the system.

The results of the eigenvalue calculations over the saturation temperatures and across the powers is presented in figure 3.5. As can be seen, all of the computed eigenvalues are below zero, and thus the system doesn't exhibit any instabilities when portions of the upper hot leg undergo flashing. The lack of any positive eigenvalues is a little surprising given the chaotic nature two-phase flashing is known to have. As in the single phase results, the two-phase system becomes more stable as either the heat load or the saturation pressure (parametrized by the saturation temperature) are increased. The pressure dependence is more clear for the two-phase results as it will result in a smaller latent heat and, thus, more liquid water in the system to act as a stabilizing force. The heat load dependence is analogous to the single phase case in that a faster flowing system will damp out small perturbations very well.

As a side note, the eigenvalue map shown has a corrugated shape and is not smooth like the single phase maps. The behavior is attributed to the extra complications introduced by the presence of another phase: the nonlinear system solver, the nonlinear solution of the saturation state, the nonlinear nature of the two-phase friction factor in the flashing portions, and the numerical approximation of the eigenvalues. Since eigenvalues are a smooth function of the system parameters, all of the delineated numerical facets are taken to be the primary culprit and indicate nothing more.

Figure 3.5: Eigenvalue map of the simple, closed loop undergoing phase-change along the liquid saturation line at various heating loads. All eigenvalues are negative.

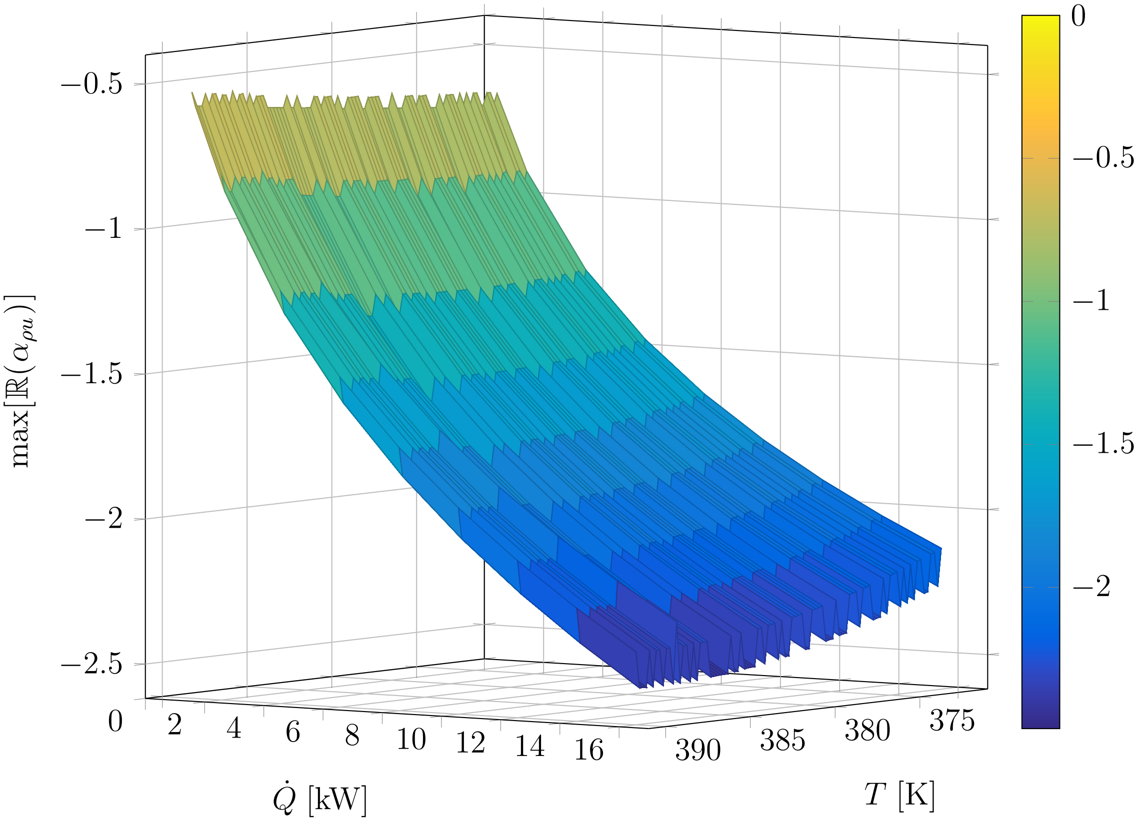

Table 3.1: *Summary of pertinent average system parameters (indicated by an overbar) for the single and two-phase simulations: heat load $\dot{Q}$, temperature rise ΔT, Pressure difference ΔP, mass flow rate $\dot{m}$, and a naive heat balance. The two-phase results also contain values for the quality x (vapor mass fraction) and void α (homogeneous vapor volume fraction) as defined in appendix A.3.*

Phases	$\dot{Q}$ [kW]	$\overline{T}$ [ΔK]	$\overline{P}$ [ΔkPa]	$\overline{\dot{m}}$ [$\mathrm{kg\,s^{-1}}$]	$\overline{x}$ [pcm]	$\overline{\alpha}$ [%]	$\overline{\dot{m}}\, c_\mathrm{p}\, \overline{\Delta T}$ [kW]*
1	1	0.239	12.504	1.01	–	–	1.02
	2	0.368	12.501	1.33	–	–	2.05
	4	0.543	12.501	1.80	–	–	4.08
	8	0.794	12.500	2.44	–	–	8.10
	16	1.260	12.500	3.08	–	–	16.2
2	1	0.034	12.166	6.89	6.49	7.46	0.981
	2	0.056	12.202	8.34	10.5	11.5	1.97
	4	0.095	12.287	9.92	16.8	17.2	3.94
	6	0.130	12.378	10.9	22.2	21.5	5.92
	8	0.163	12.472	11.6	27.0	25.0	7.90
	10	0.195	12.567	12.1	31.4	27.9	9.88
	12	0.225	12.663	12.6	35.6	30.5	11.9
	14	0.255	12.759	13.0	39.5	32.7	13.8
	16	0.285	12.855	13.3	43.3	34.7	15.8

* $c_\mathrm{p} = 4182\,\mathrm{J\,kg^{-1}\,K^{-1}}$

3.4 Nonlinear Pulsed Stability

This section aims to show that the test loops is nonlinearly stable when subject to relatively large perturbations off of the steady-state. The simulations done to show this stability all have the cooling volume at about 372 K at saturated conditions; the “about” is added because these simulations are purely Neumann in nature with no fixed state. From steady-states acquired with heat loads of 1 and 16 kW and possessing a 372 K saturated cooled volume, the heated volume was subjected to a point pulse one second into the simulation of 1, 2, 5, 10, and 15 kW. Various system parameters for all the simulations are plotted in figures 3.6 and 3.7 for the first ten seconds of simulation (fifty second results are given in appendix C.3).

As can be seen, the system exhibits extremely strong stability when exposed to large perturbations off of the steady-state. The system at 1 kW experiences a pulse fifteen times its nominal value and quickly returns to the initial state; the system at 16 kW experiences a pulse to almost double its nominal value and returns to the initial state quickly as well. Whereas the previous section showed the system to be stable for small perturbation in general, these simulations show that the test loop is extremely stable even in the face of large injections while operating at steady-state.

Figure 3.6: Nonlinear response of the 1 kW *system to various point-power insertions.*

(a) Maximum Quality

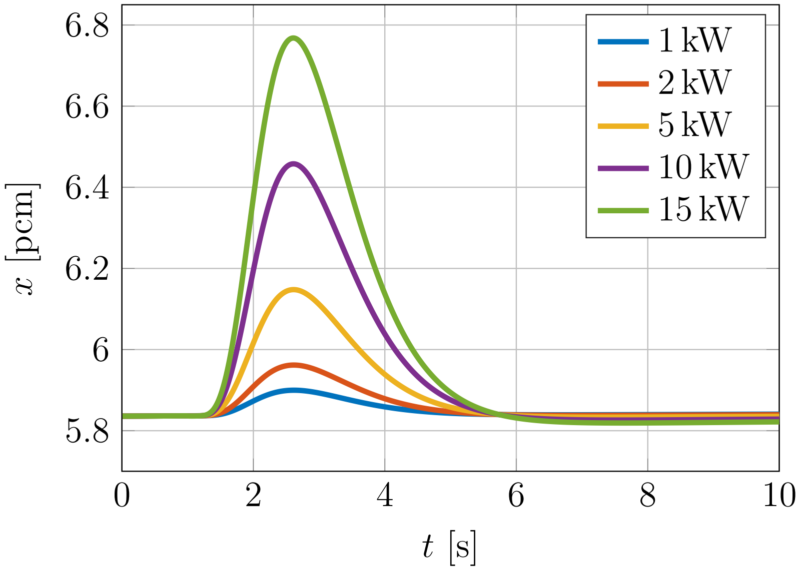

(b) Maximum Void Fraction

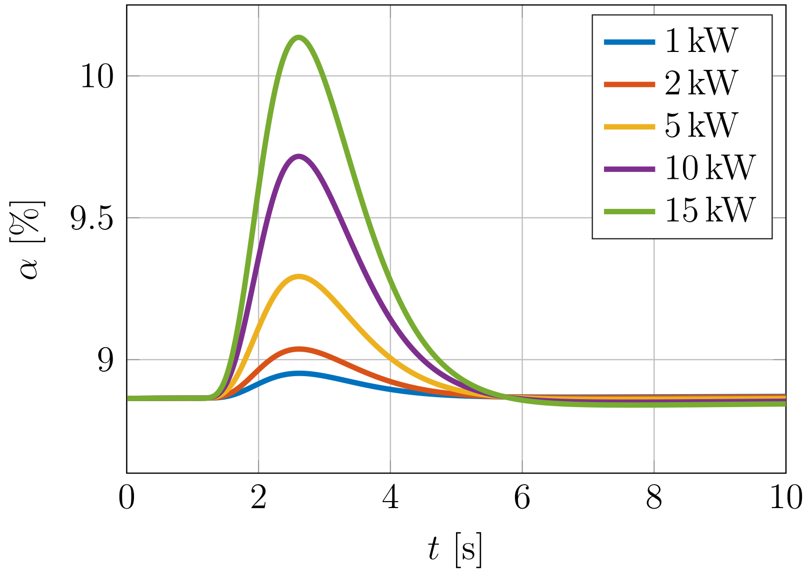

Figure 3.6: (cont.)Nonlinear response of the 1 kW *system to various point-power insertions.*

(c) System Temperature Rise

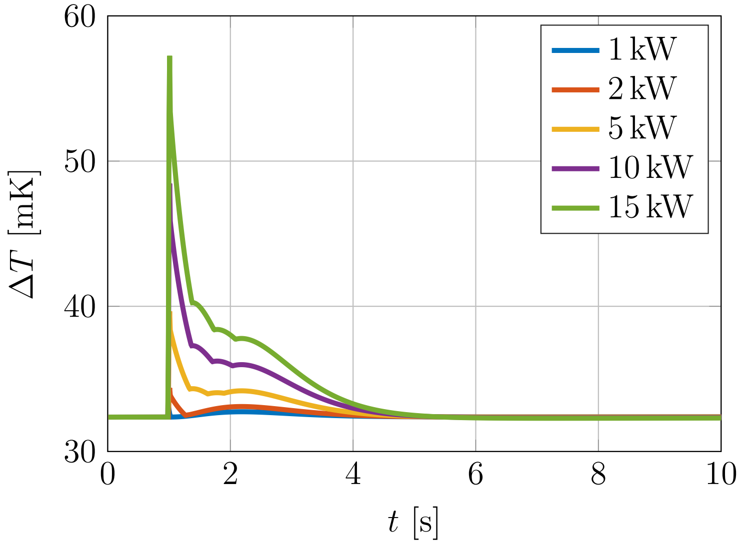

(d) System Pressure Difference

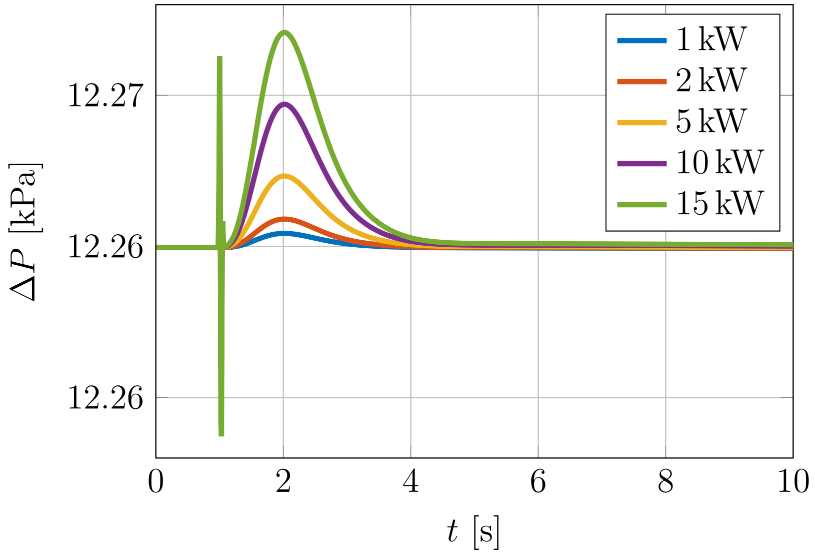

Figure 3.7: Nonlinear response of the 16 kW *system to various point-power insertions.*

(a) Maximum Quality

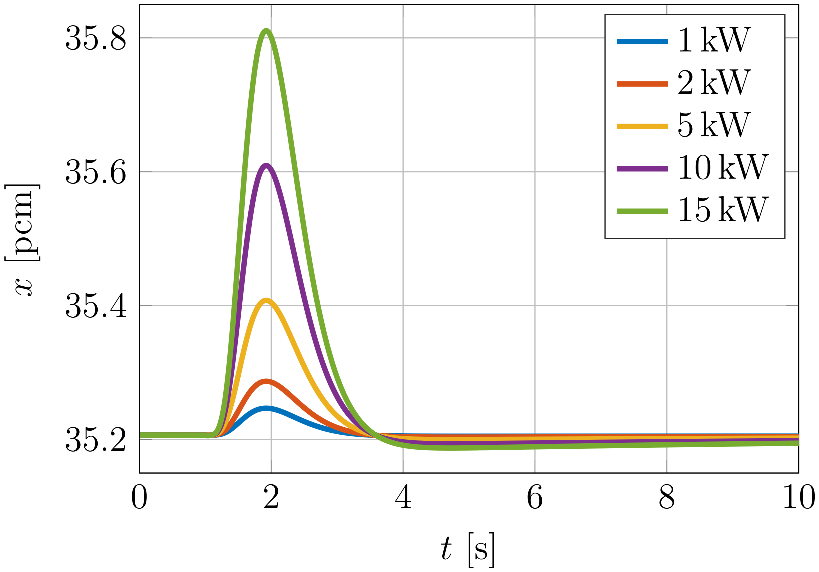

(b) Maximum Void Fraction

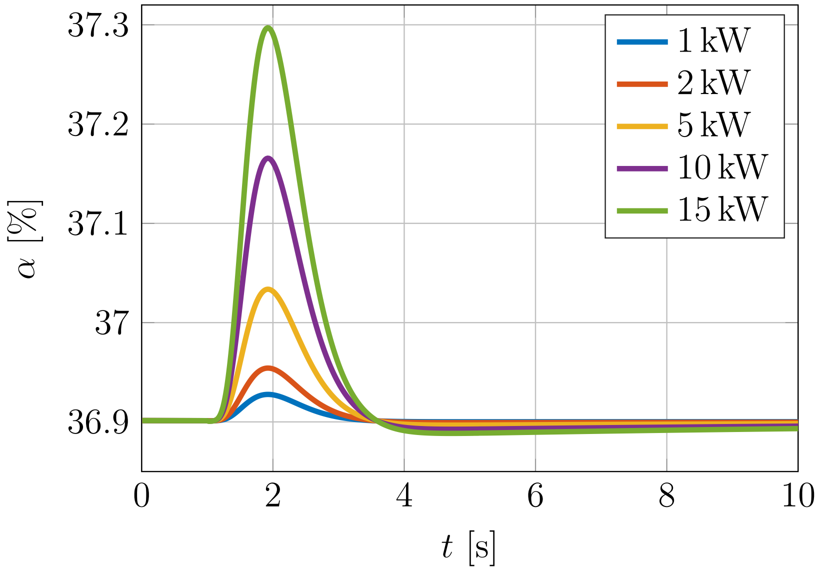

Figure 3.7: (cont.)Nonlinear response of the 16 kW *system to various point-power insertions.*

(c) System Temperature Rise

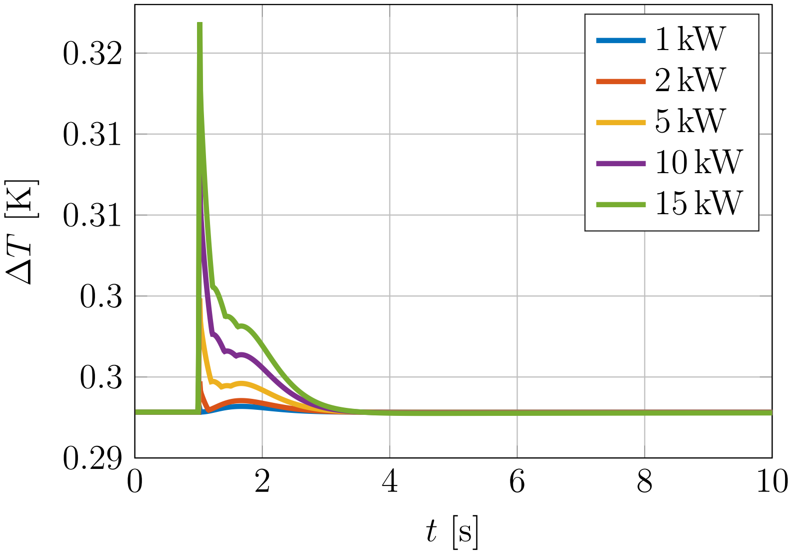

(d) System Pressure Difference

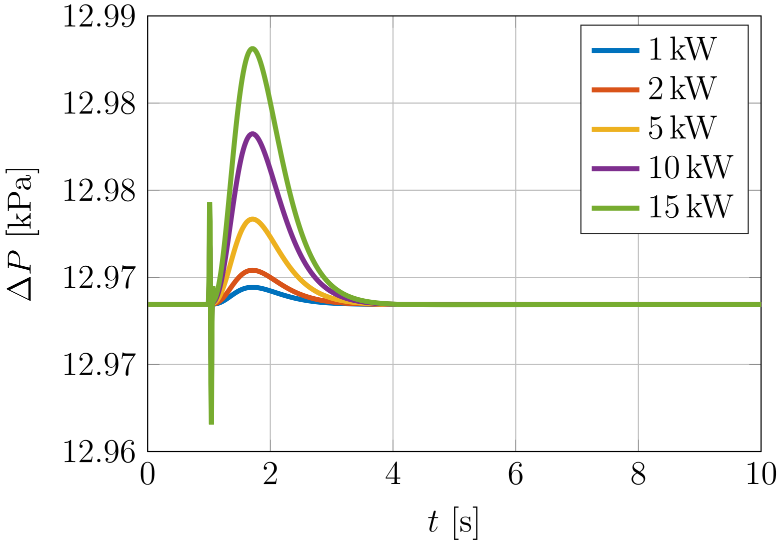

Chapter 4

Conclusion

The presented simulation results for a simple, closed loops over a number of single and two-phase states showed the system to be linearly stable under the models used and assumptions made. The simulations were performed using the highest fidelity equations-of-state currently available for water, solved using a modern fully, nonlinear solver which avoids need to form the true Jacobian for Newton-like convergence, and used a new FVM discretization scheme which emphasized precise and complete coverage of the computational domain for accurate integration of the entire computational domain for the stability analysis.

Future efforts will aim to refine the state space over which the steady-states are calculated to truly exhaust potential operation zones in which the systems may become unstable to small perturbations. Additionally, expanding the work to include larger systems in terms of both volume and path length is definitely an avenue that needs exploration. It would be interesting to study how the character of the system changes, if at all, in scaling the small loop presented in this work to the more modest scale of the UW–Madison RCCS or even large cooling loops, such as the future experiment at Argonne National Lab.

In simulating such large systems, however, pieces of the code used to perform the simulations of this work would need to be reimplemented in a faster computer language. The current implementation uses the MATLAB scripting language for all of the simulations and results. MATALB was chosen for its speed of development, ease of debugging, and flexibility of programming paradigm. Since all of the thermodynamics, solvers, etc. were written from scratch, MATLAB was used more as a prototyping language with the intent of moving to a faster language in the future. The main hits to speed comes from the continuous EOS in all fluid regimes. Massive speed increases would easily be seen if even just the two-phase checks and calculations were performed in a faster language, which is the next primary goal.

Also, the flexibility and generality of the solver is something to investigate and expand upon. Adding a simpler model to the code base for benchmarking the full nonlinear form or even providing an initial guess would be worthwhile. And then adding more complex models beyond HEM, such as a true two-fluid model and wall conduction/convection capabilities to the current framework would increase the usefulness of the code base and possibly provide a different picture of stability, both linear and not.

By adding more detailed models, increasing the computational efficiency of the tools, and allowing the model geometry to comes closer to reality, better investigations can be taken into the analysis of two-phase systems. Even adding a higher level of geometric specification and mathematical rigor can lead to a more thoughtful derivation of models and consideration of other methods to better analyze and explore these systems.

Appendix A

Thermophysical Properties

A.1 Equation of State

The EOS used for the simulations is the IAPWS Formulation 1995 for the Thermodynamic Properties of Ordinary Water Substance for General and Scientific Use (IAPWS-95) [36]. The specifics of the EOS are discussed in the following section. Also, the procedure for back-calculating the temperature given a density and internal energy from the formulation is outlined since the conservation laws for the simulations evolve the internal energy based on mechanical balance but the EOS uses temperature for explicit calculation of state properties.

A.1.1 IAPWS Formulation 1995

The IAPWS-95 is a fully non-ideal EOS for water that uses on an empirical curve fit of the Helmholtz Free Energy potential A_{FE}. The natural variables of the potential are density ρ and temperature T, and the formulation uses a dimensionless density δ and a dimensionless temperature τ defined by

$$\delta = \frac{\rho}{\rho_\mathrm{c}} \tag{A.1}$$

$$\tau = \frac{T_\mathrm{c}}{T} \tag{A.2}$$

where ρ_c and T_c are, respectively, the critical point density and temperature of water. The dimensionless form of the potential is the fundamental basis of the IAPWS formulation and has the form

$$\frac{A_\mathrm{FE}(\rho, T)}{RT} = \phi(\delta, \tau) = \phi^\mathrm{I}(\delta, \tau) + \phi^\mathrm{R}(\delta, \tau), \tag{A.3}$$

where ϕ^I is an ideal gas potential function, ϕ^R is a residual (i.e., non-ideal gas) potential function, and R is the specific gas constant of water. The actual functional form of $\phi(\delta, \tau)$ is cumbersome and will not be presented here (see [36] for a full description). Using this potential and its associated derivatives, all thermodynamic properties can be calculated for a given state. A select group of relationships between the potential and properties are presented in table A.1. The relationships are valid for the entire set of single phase states.

TABLE A.1: *Select thermodynamic properties and their Helmholtz free energy relationships in a dimensionless form.*

Property	Helmholtz Potential Relation
Pressure	$\frac{P}{R\rho_\mathrm{c}T_\mathrm{c}} = \left[1 + \delta\frac{\partial\phi^\mathrm{R}}{\partial\delta}\right]\frac{\delta}{\tau}$
Internal Energy	$\frac{i}{RT_\mathrm{c}} = \frac{\partial\phi}{\partial\tau}$
Entropy	$\frac{s}{R} = \tau\frac{\partial\phi}{\partial\tau} - \phi$
Enthalpy	$\frac{h}{RT_\mathrm{c}} = \frac{1}{\tau}\left[1 + \tau\frac{\partial\phi}{\partial\tau} + \delta\frac{\partial\phi^\mathrm{R}}{\partial\delta}\right]$

Additionally, the formulation permits calculation of saturated properties. Unlike the explicit, single phase equations above, saturated calculations involve a necessarily iterative procedure. Solving for a saturated condition involves leveraging the three equilibrium conditions of phase change: constant pressure, constant temperature, and phasic equality of Gibbs free energy. In terms of the non-dimensional Helmholtz free energy function $\phi(\delta,\tau)$, these equilibrium conditions form a system of equations that must be simultaneously satisfied:

$$\frac{P_{\text{sat}}}{R\rho_{\text{c}}T_{\text{c}}} = \left[1 + \delta_\ell \frac{\partial \phi^{\text{R}}}{\partial \delta}(\delta_\ell, \tau_{\text{sat}})\right]\frac{\delta_\ell}{\tau_{\text{sat}}} \tag{A.4a}$$

$$\frac{P_{\text{sat}}}{R\rho_{\text{c}}T_{\text{c}}} = \left[1 + \delta_g \frac{\partial \phi^{\text{R}}}{\partial \delta}(\delta_g, \tau_{\text{sat}})\right]\frac{\delta_g}{\tau_{\text{sat}}} \tag{A.4b}$$

$$\frac{P_{\text{sat}}}{R\rho_{\text{c}}T_{\text{c}}} = \left[\text{Ln}\left(\frac{\delta_\ell}{\delta_g}\right) + \phi^{\text{R}}(\delta_\ell, \tau_{\text{sat}}) - \phi^{\text{R}}(\delta_g, \tau_{\text{sat}})\right]\frac{\delta_\ell \delta_g}{\tau_{\text{sat}}(\delta_\ell - \delta_g)}. \tag{A.4c}$$

Equations A.4a and A.4b arise from the definition of pressure in terms of the Helmholtz free energy and the pressure equality of the functions given the saturated liquid density ρ_ℓ and gas density ρ_g at the saturation temperature. Equation A.4c is the Maxwell construction (i.e., equal area rule) of the Gibbs free energy equivalence ([57]). The above system consists of three equations and four unknowns: P_{sat}, τ_{sat}, δ_ℓ, and δ_g; therefore, the system can be solved once one of the saturation values is specified. A pressure-volume diagram is shown in figure A.1 calculated from an implementation of the IAPWS-95 formulation.

A.1.2 Back Calculation of Temperature

Temperature is a very powerful state variable because it is a directly measurable quantity that provides a qualitative measurement of a fluid's internal energy. However, in the balance equations presented in section 2.1, density and internal energy are the variables that are

Figure A.1: Pressure versus specific volume with several isotherms. The gray line denotes the phase coexistence curve.

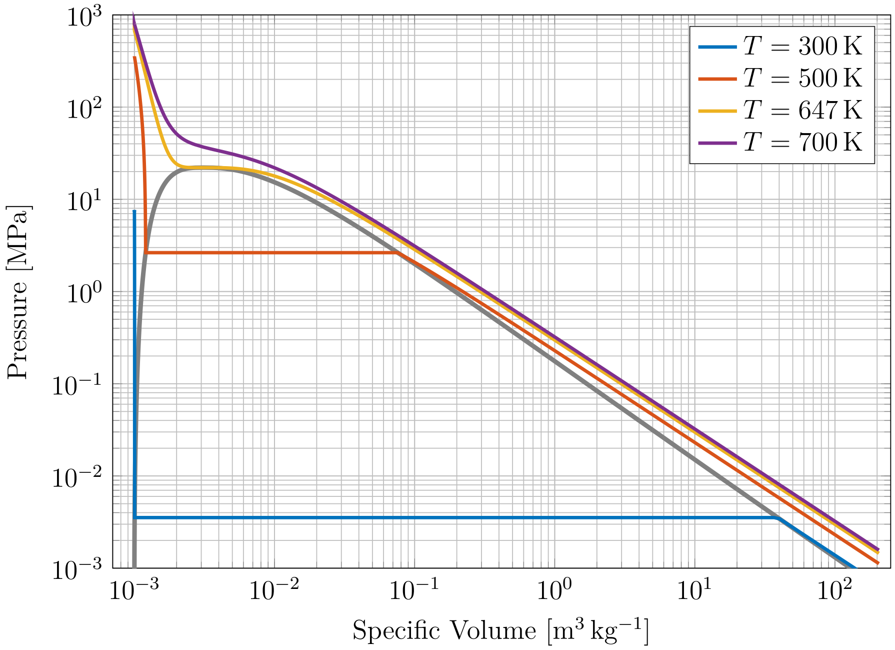

Figure A.2: Internal energy versus density with an arbitrary isochore. From the shape of the vapor dome in ρ-i space, it is clear that the saturation internal energy is always less than the single phase along an isochore.

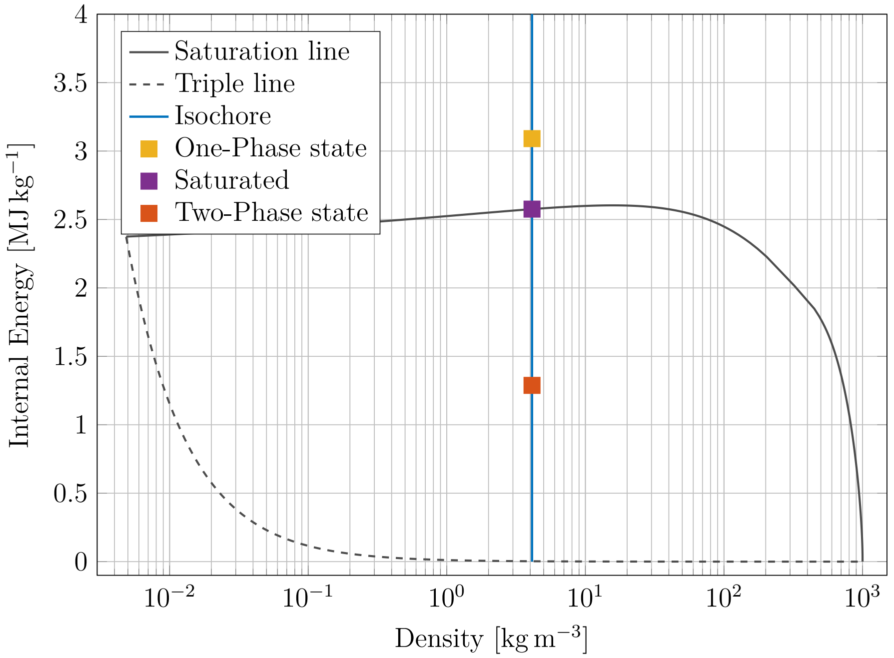

mechanically balanced, completely independent of thermodynamics. As such, it is most natural to update the thermodynamic and transport quantities with the mechanically specified density and internal energy to have a consistent evolution system. Furthermore, since density and internal energy are defined and independent in the two-phase region (unlike pressure and temperature), the time evolution may lead to mixture quantities.

The solution procedure chosen relies on one key fact about the relationship between internal energy and temperature: along an arbitrary isochore, internal energy is an injective, monotonic function of temperature. One result of this fact is that a single phase internal energy will always be higher than its saturation value at the current density; this allows for an explicit determination of one- or two-phase conditions (see figure A.2 for a phase diagram). Another result is that root-finding procedures can be readily used to calculate the temperature for a state defined by density and internal energy. In the single phase region with a given guess value, the dimensionless temperature is calculated by driving the following residual formula to zero through Newton's method:

$$r(\tau) = \frac{\partial \phi}{\partial \tau}(\delta, \tau) - \frac{i}{RT_{\mathrm{c}}}. \tag{A.5}$$

For the two-phase region, the situation is a bit more complicated since the mixture internal energy must be calculated at every temperature update and $\partial\phi/\partial\tau$ approximated numerically since no closed form exists. The full algorithm is outlined below. Once the temperature has been calculated, all other properties can be directly solved for using the natural variables of the Helmholtz potential.

Algorithm 4 is an outline of the temperature back calculation. The functions involving saturation properties solve equation A.4 through another Newton method. The residual r_{one} is the same as equation A.5. The residual r_{two} calculates the mixture internal energy at the current τ iterant and then approximates the derivative in the vapor dome since the closed

Algorithm 4: Temperature Back Calculation

```
function temperature($\delta$, $i_{\text{ND}}$ $\tau_{guess}$)
    $i_{\text{sat}} = $ getSaturationInternalEnergy($\delta$)
    $\tau = \tau_{\text{guess}}$
    $\mathrm{d}\tau = \mathrm{Inf}$
    if $i_{\text{ND}} > i_{sat}$
        % One Phase
        while $\mathrm{Abs}(\mathrm{d}\tau) > \varepsilon$ do
            $\mathrm{d}\tau = r_{\text{one}}(\tau)/r'_{\text{one}}(\tau)$
            $\tau = \tau - \mathrm{d}\tau$
        end
    else
        % Two Phase
        while $\mathrm{Abs}(\mathrm{d}\tau) > \varepsilon$ do
            $[P_{\text{sat}},\, \delta_\ell,\, \delta_g] = $ getSaturationProperties($\tau$)
            $\mathrm{d}\tau = r_{\text{two}}(\tau, P_{\text{sat}},\, \delta_\ell,\, \delta_g)/r'_{\text{two}}(\tau, P_{\text{sat}},\, \delta_\ell,\, \delta_g)$
            $\tau = \tau - \mathrm{d}\tau$
        end
    end
    return $\tau$
end
```

form derivative is very computationally expensive with little, if any, gain in convergence rate.

A.2 Transport Properties

Thermal conductivity κ, dynamic viscosity μ, and surface tension σ are thermophysical transport properties and have no direct relation to thermodynamic potentials. However, the IAPWS has curve fits that are functions of density and temperature and are meant to be used in conjunction with the IAPWS-95 EOS [58, 59, 60].

A.3 Mixture Properties

For homogenous simulations, a selection of interpolation scheme is needed to acquire, in some sense, an average thermodynamic value within the vapor dome for two-dimensional states. The most popular and arguably most natural type of interpolation for some two-phase property ψ_{mix} given a liquid saturation value ψ_ℓ and a gas saturation value ψ_g is the affine homotopy

$$\psi_{\text{mix}} = (1-w)\,\psi_\ell + w\,\psi_g \tag{A.6}$$

for some weight function $w \in [0,1]$. This method has the inherent property of creating a continuous transition between between the liquid and gas ends of the vapor dome along any isobar/isotherm. The only potential drawback being that the connection is only C^0 continuous, thus possessing a discontinuous derivative at the vapor dome boundary. However, the construction of such an interpolant would be quite burdensome at little gain to the physics of the approximation.

The two most popular choices for the weight function w are the quality x (i.e., gas mass fraction) of the state and the void α (i.e., gas volume fraction) of the state. The quality of a state can be derived given two independent properties within the vapor dome, which mostly excludes $\{T, P\}$ as a valid pair, and using one of the varying per mass properties, which will be naturally mixed, to compute the fraction:

$$x = \frac{\psi_{\text{mix}} - \psi_\ell}{\psi_g - \psi_\ell}. \tag{A.7}$$

It is noted that a mixture quantity such as internal energy or density is required to be known to perform this calculation. Evident by the construction, the value of x runs from zero to one as long as the saturated gas property is greater than the liquid one, which is true for per unit mass quantities. The void of a state can be derived using the definition of the quality to create the appropriate ratio of extensive volumes:

$$\alpha = \frac{x\,v_g}{(1-x)\,v_\ell + x\,v_g} = \frac{1}{1 + \left(\dfrac{1-x}{x}\right)\dfrac{v_\ell}{v_g}} = \frac{1}{1 + \left(\dfrac{1-x}{x}\right)\dfrac{\rho_g}{\rho_\ell}} \tag{A.8}$$

It is noted that this relation is typically called the *homogenous void fraction* since it lacks a phasic velocity ratio in the right-term of the denominator. Evident by the construction, the value of α runs from zero to one as long as x does, which was already guaranteed.

By default, all per unit mass thermodynamic properties use the quality for their mixture weight function. Also by default, all transport properties use the void for their mixture weight function.

Appendix B

Friction Factors

As mentioned in section 2.1.3, the mono-directional bulk momentum stress tensor is taken to have the algebraic form

$$\tau_{ij} z_i n_j = \Delta P_{\text{fric}} = \frac{1}{2} f_{\text{D}} \, \frac{L_{\text{char}}}{D_{\text{eff}}} \, \rho \, v^2, \tag{B.1}$$

where f_{D} is the Darcy friction factor, L_{char} is a characteristic (path) length, D_{eff} is an effective flow diameter, ρ is the fluid density, and v is the fluid velocity. For correctness, the method used to calculate the friction factor must account for different kinematic flow regimes and distinguish between single and two-phase flow. The following appendix outlines the methodology used in this work.

For slow or very viscous flows, the friction factor is found to be a function of its Reynolds number:

$$\text{Re} = \frac{\rho \, v \, D_{\text{eff}}}{\mu} \tag{B.2}$$

where μ is the dynamic viscosity. This is primarily due to the layered and ordered nature of the flow that results in much of the fluid's traction coming from its inherent viscosity [61]. The Darcy friction approximation used for Reynolds numbers at or below 2000, called *laminar flow*, is

$$f_{\mathrm{D}} = \frac{64}{\mathrm{Re}}. \tag{B.3}$$

For flows with Reynolds numbers above 4000, called *turbulent flow*, the Darcy friction factor is well-approximated by the Colebrook-White equation

$$\frac{1}{\sqrt{f_{\mathrm{D}}}} = -2\,\mathrm{Log}_{10}\left(\frac{\varepsilon_{\mathrm{rel}}}{3.7} + \frac{2.51}{\mathrm{Re}\,\sqrt{f_{\mathrm{D}}}}\right) \tag{B.4}$$

where $\varepsilon_{\mathrm{rel}}$ is the relative surface roughness and Re is the Reynolds number. The relative surface roughness is a material-dependent quantity determined by measuring how smooth the finished inner surface is and dividing that measure by the channel's hydraulic diameter. A constant value of 1×10^{-4} was used in this work. Despite its seemingly arbitrary nature, the Colebrook-White equation is derived from physical arguments in turbulent flow theory [62]; however, to avoid yet another level of implicit solution in this work, an explicit approximation to the implicit Colebrook-White equation due to Serghides is used

$$\frac{1}{\sqrt{f_{\mathrm{D}}}} = f_a - \frac{(f_b - f_a)^2}{f_c - 2f_b + f_a} \tag{B.5}$$

where

$$f_a = -2\,\mathrm{Log}_{10}\left(\frac{12}{\mathrm{Re}} + \frac{\varepsilon_{\mathrm{rel}}}{3.7}\right) \tag{B.6a}$$

$$f_b = -2\,\mathrm{Log}_{10}\left(\frac{2.51\,f_a}{\mathrm{Re}} + \frac{\varepsilon_{\mathrm{rel}}}{3.7}\right) \tag{B.6b}$$

$$f_c = -2\,\mathrm{Log}_{10}\left(\frac{2.51\,f_b}{\mathrm{Re}} + \frac{\varepsilon_{\mathrm{rel}}}{3.7}\right) \tag{B.6c}$$

The method is derived by applying Steffensen's Method to the Colebrook-White equation for a particular initial guess value, and the additional arithmetic overhead is balanced by its explicit nature and excellent comparison to Colebrook-White over a large sample space as detailed in [63, 64]. For flows between the upper and lower Reynolds number bounds of 2000 and 4000, the so-called *transition region*, a log-linear affine homotopy similar to the mixture property calculation was used

$$f_{\mathrm{D,tran}} = (1 - w_{\mathrm{D}}) f_{\mathrm{D}}(\mathrm{Re} = 2000) + w_{\mathrm{D}} f_{\mathrm{D}}(\mathrm{Re} = 4000) \tag{B.7}$$

where the weight function is

$$w_{\mathrm{D}} = \frac{\mathrm{Log}_{10}(\mathrm{Re}) - \mathrm{Log}_{10}(2000)}{\mathrm{Log}_{10}(4000) - \mathrm{Log}_{10}(2000)}. \tag{B.8}$$

The above functional forms and correlations are all based upon the presence of a single phase. There are a number of methods used to account for the increased frictional pressure drop due to the existence of another phase; the particular one chosen here is the two-phase multiplier. That is, the two-phase pressure drop is expressed as a scalar multiple of the saturated liquid drop:

$$\Delta P_{\mathrm{fric,two}} = \alpha_{\mathrm{two}} \, \Delta P_{\mathrm{fric},\ell} \tag{B.9}$$

where $\Delta P_{\mathrm{fric},\ell}$ is calculated per above and the two-phase multiplier α_{two} is calculated using the model proposed by Friedel:

$$\alpha_{\mathrm{two}} = \beta_1 + \frac{3.24 \beta_2 \beta_3}{\mathrm{Fr}^{0.045} \, \mathrm{We}^{0.035}} \tag{B.10}$$

where

$$\begin{aligned}
\beta_1 &= (1-x)^2 + x^2 \left(\frac{\rho_\ell}{\rho_g} \frac{f_{\mathrm{D},g}}{f_{\mathrm{D},\ell}} \right) \\
\beta_2 &= x^{0.78} (1-x)^{0.24} \\
\beta_3 &= \left(\frac{\rho_\ell}{\rho_g} \right)^{0.91} \left(\frac{\mu_g}{\mu_\ell} \right)^{0.19} \left(1 - \frac{\mu_g}{\mu_\ell} \right)^{0.7} \\
\mathrm{Fr} &= \frac{v^2}{g\, D_{\mathrm{eff}}} \\
\mathrm{We} &= \frac{\rho\, v^2\, D_{\mathrm{eff}}}{\sigma}
\end{aligned}$$

where x is the quality and σ is the surface tension [65]. The dimensionless quantities Fr and We are the Froude number and Weber number, respectively. As may seem evident, this correlation is extremely empirical but is the recommended correlation to use for the set of states expected to be seen in this work.

Appendix C

Extra Plots

This appendix is used to display all plots not shown in the results section.

C.1 Separated Single Phase Eigenvalue Maps

(a) 1 kW *heat load.*

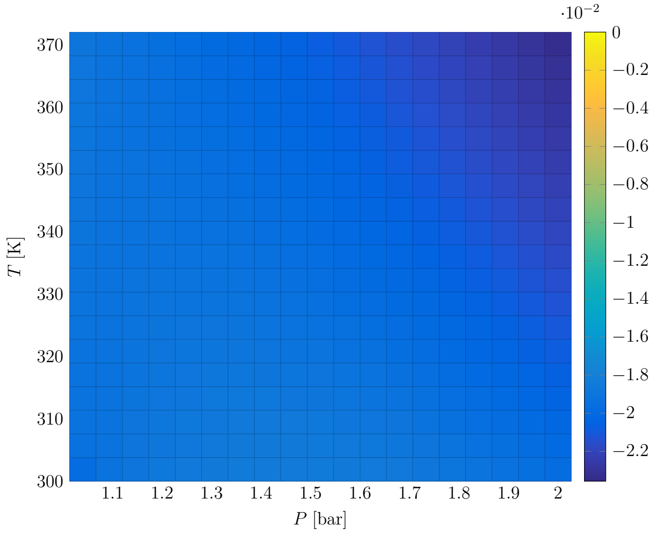

(b) 2 kW *heat load.*

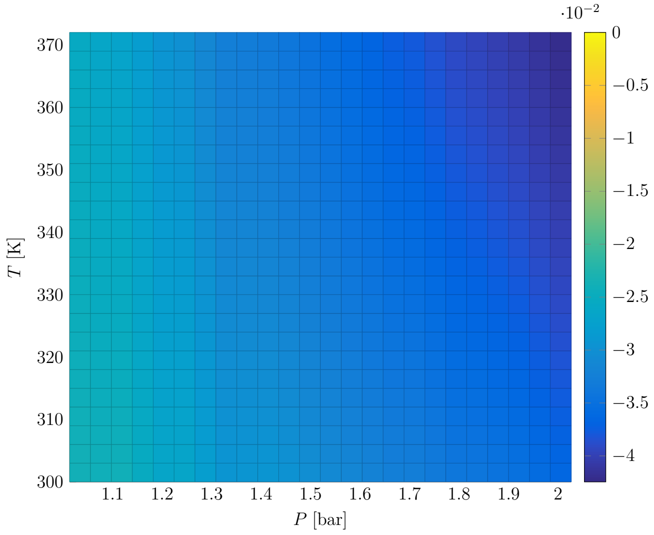

(c) 4 kW *heat load.*

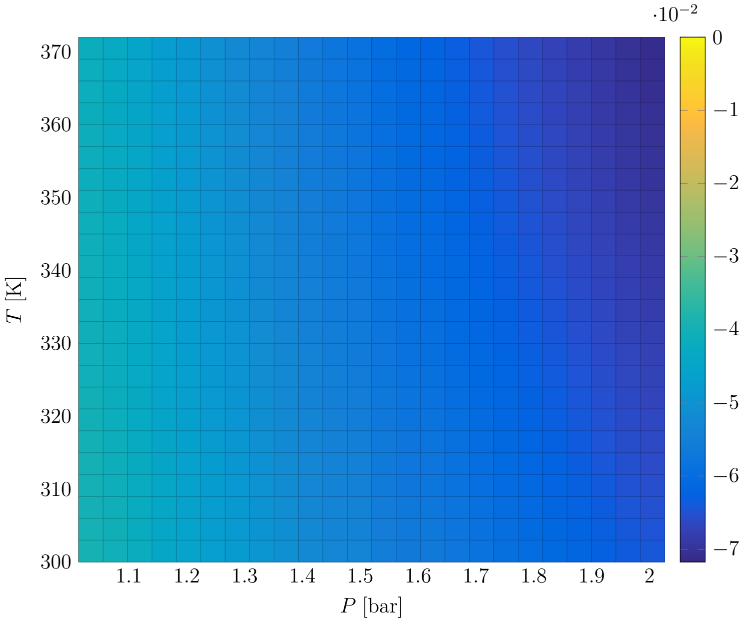

(d) 8 kW *heat load.*

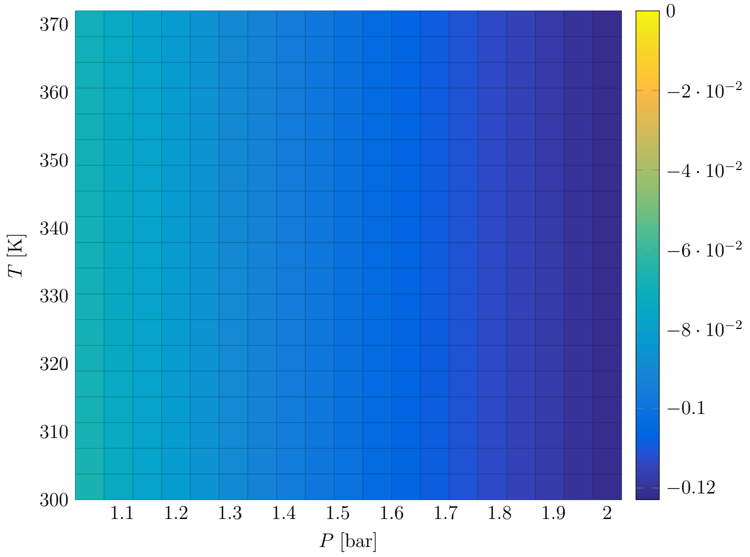

(e) 16 kW *heat load.*

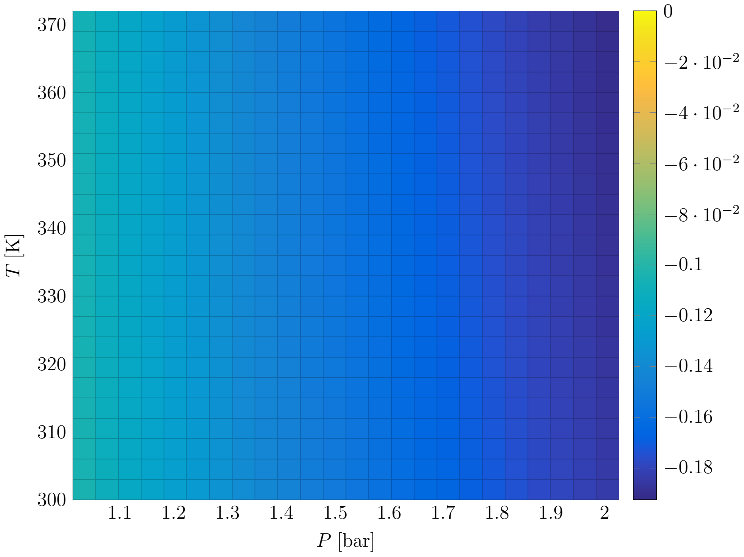

C.2 Short-time Dynamics of Steady-State Evolutions

Figure C.2: The initial dynamics of the steady-state time evolutions of the test loop with the cooled control volume fixed at a saturated liquid state at 372 K.

(a) Maximum Quality

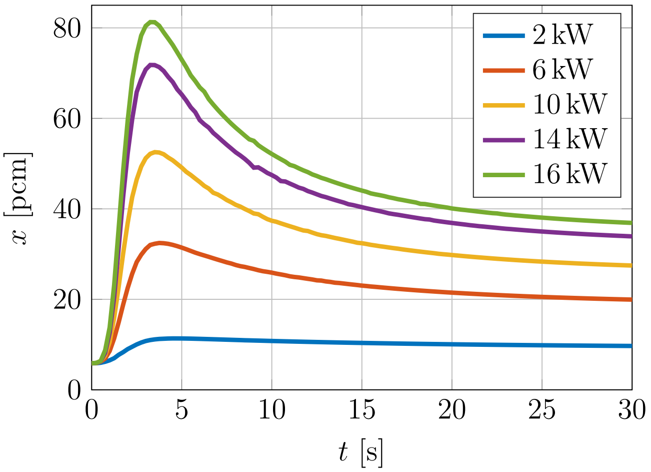

(b) Maximum Void Fraction

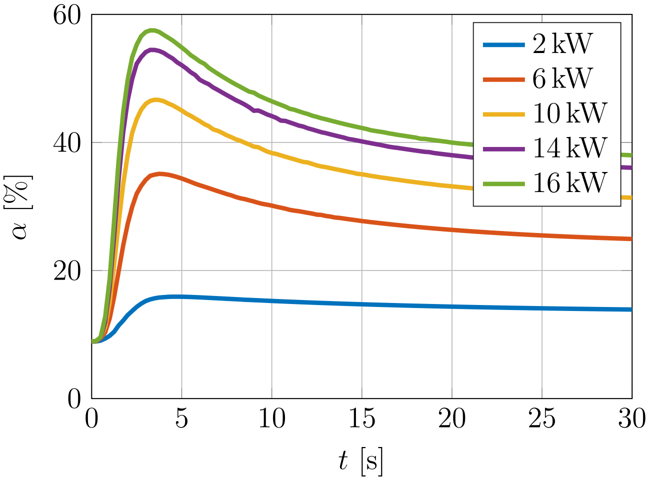

Figure C.2: *(cont.) The initial dynamics of the steady-state time evolutions of the test loop with the cooled control volume fixed at a saturated liquid state at* 372 K*.*

(c) System Temperature Rise

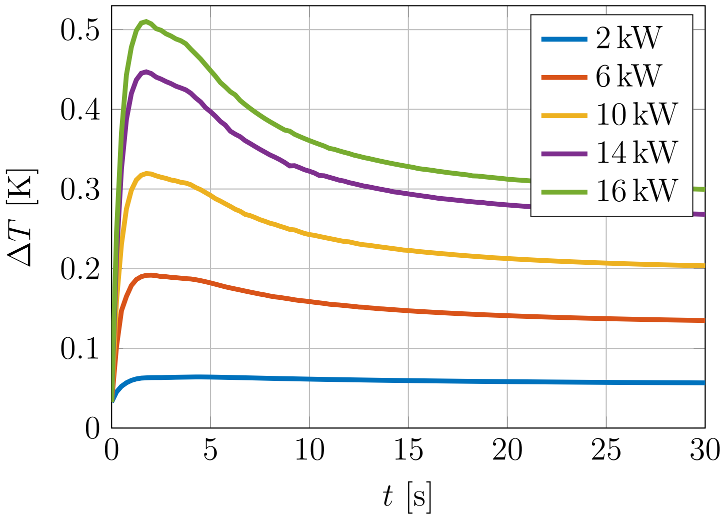

(d) System Pressure Difference

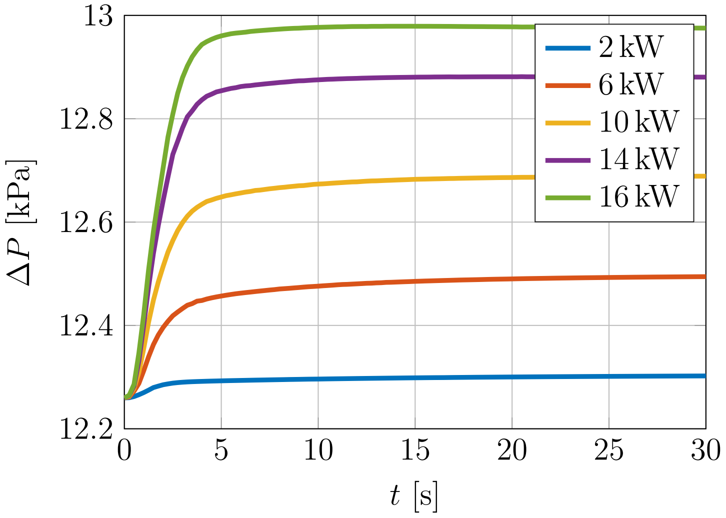

Figure C.3: The initial dynamics of the steady-state time evolutions of the test loop with the cooled control volume fixed at a saturated liquid state at 390 K.

(a) Maximum Quality

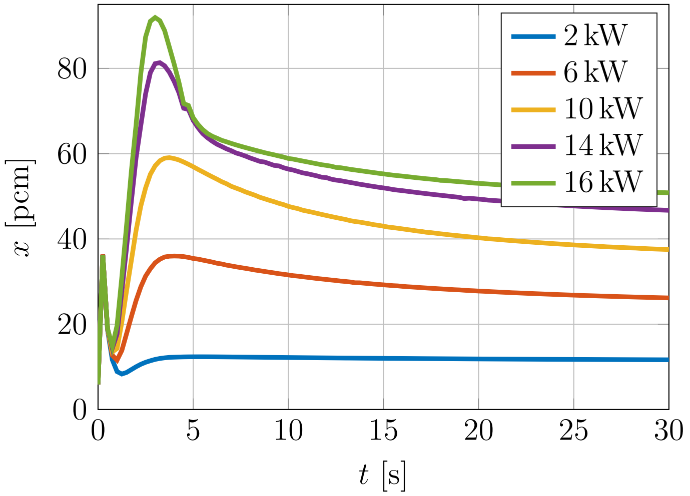

(b) Maximum Void Fraction

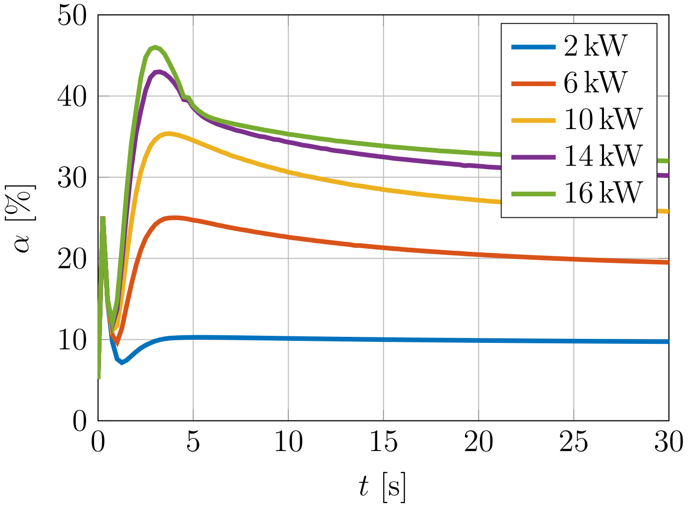

Figure C.3: (cont.) The initial dynamics of the steady-state time evolutions of the test loop with the cooled control volume fixed at a saturated liquid state at 390 K*.*

(c) System Temperature Rise

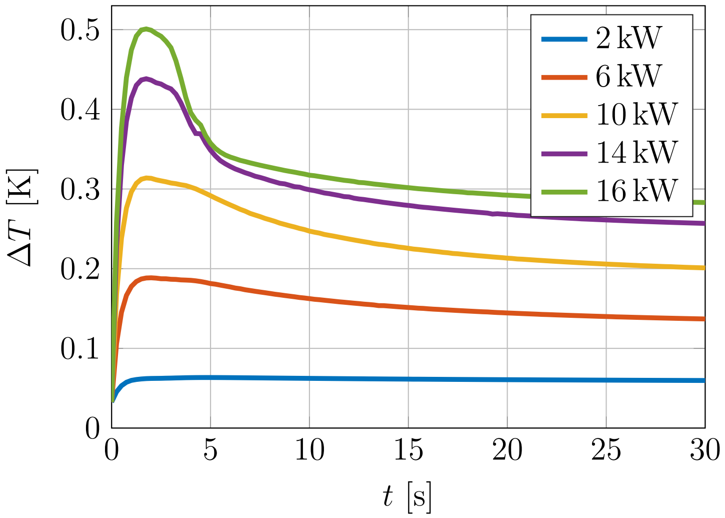

(d) System Pressure Difference

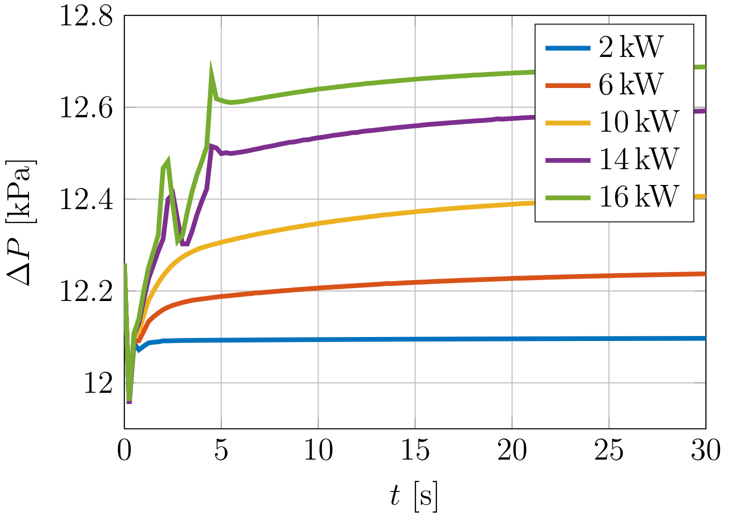

C.3 Long-time Dynamics of Pulse Evolutions

Figure C.4: Nonlinear response of the 1 kW *system to various point-power insertions.*

(a) Maximum Quality

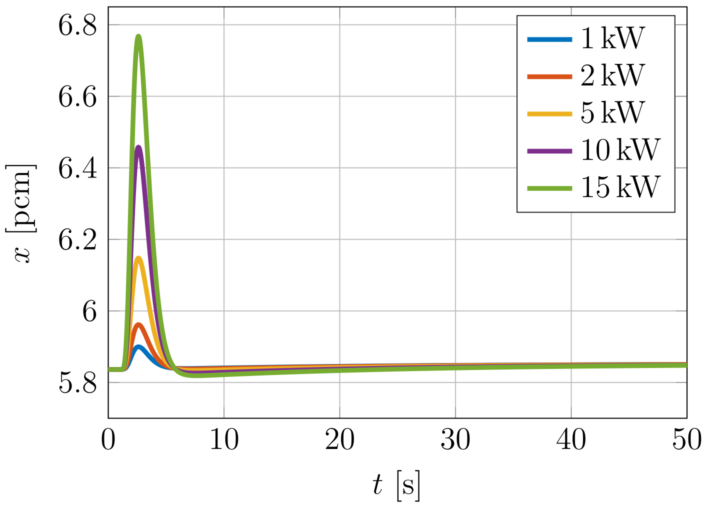

(b) Maximum Void Fraction

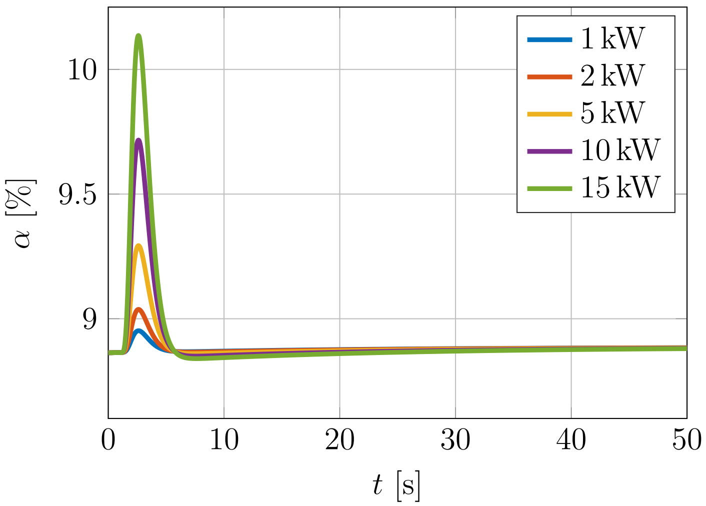

Figure C.4: (cont.) Nonlinear response of the 1 kW *system to various point-power insertions.*

(c) System Temperature Rise

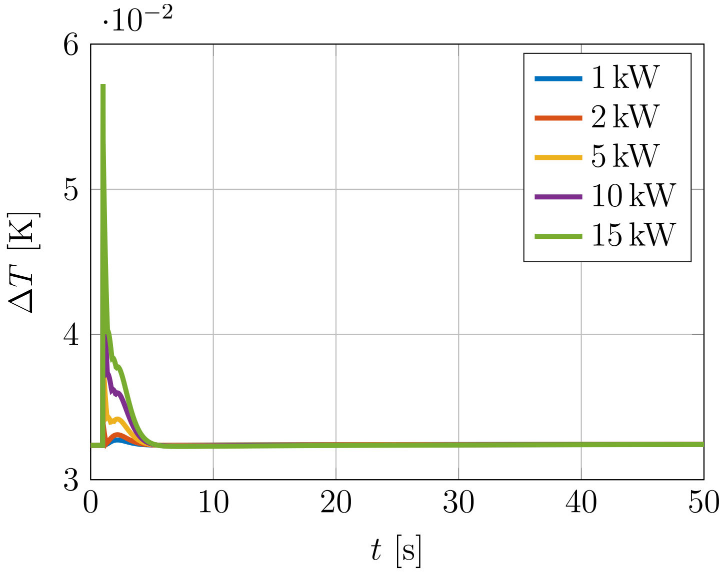

(d) System Pressure Difference

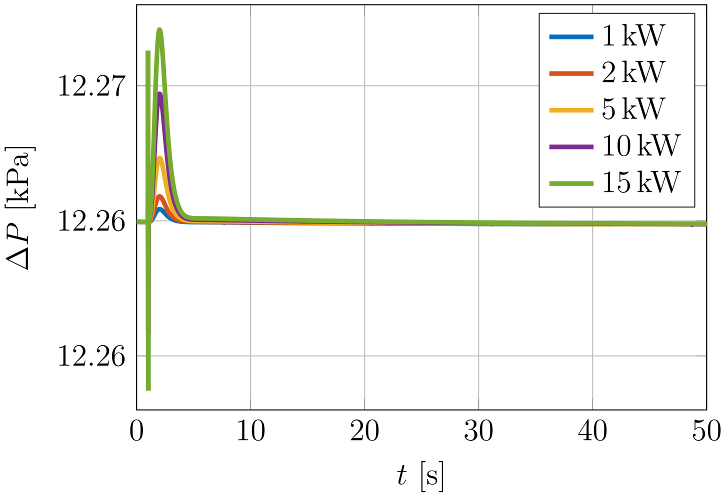

Figure C.5: Nonlinear response of the 16 kW *system to various point-power insertions.*

(a) Maximum Quality

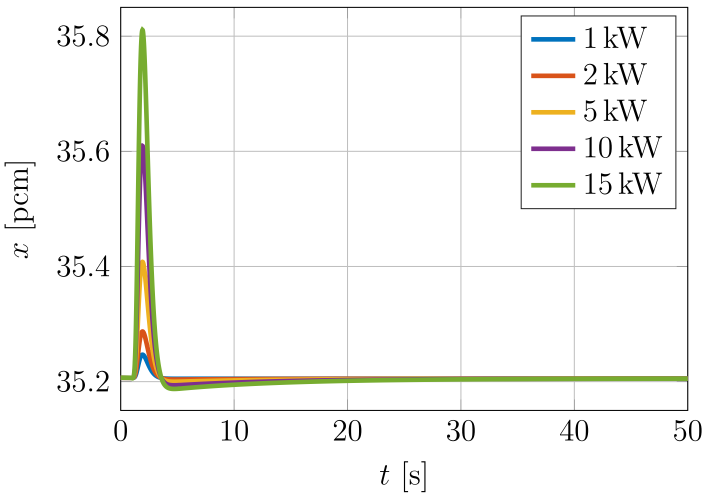

(b) Maximum Void Fraction

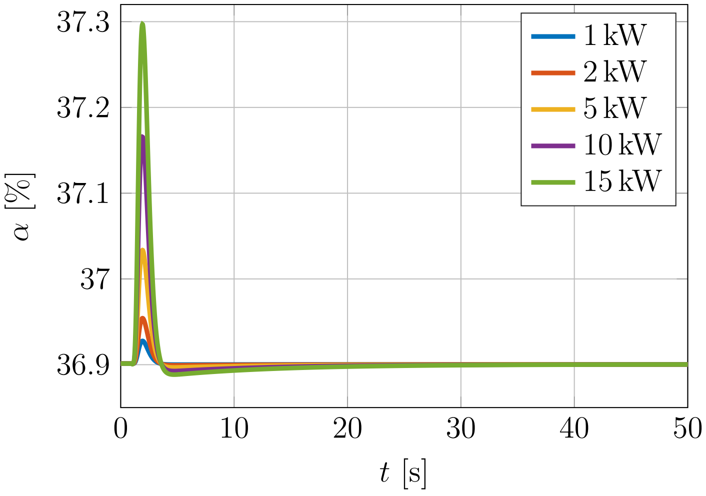

Figure C.5: *(cont.) Nonlinear response of the* 16 kW *system to various point-power insertions.*

(c) System Temperature Rise

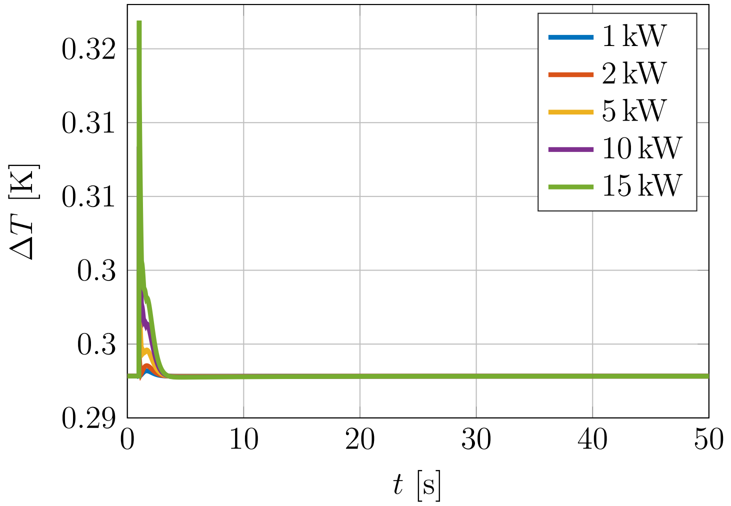

(d) System Pressure Difference

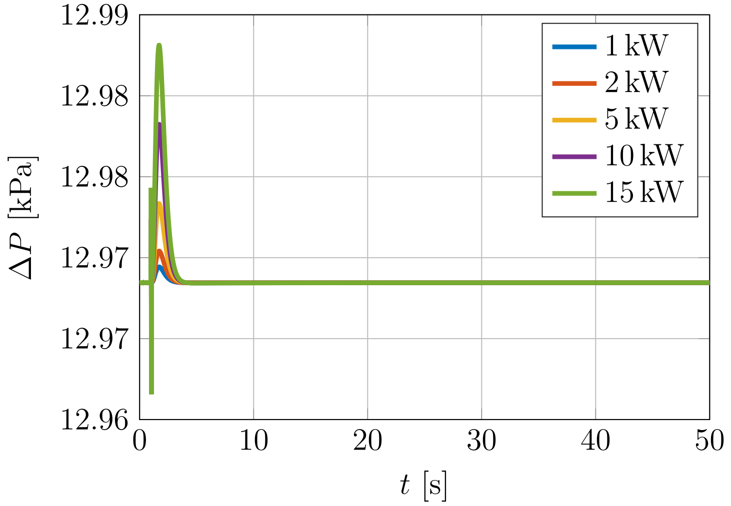

Bibliography

[1] I. Bechtel National, 450 MWt Reactor Cavity Cooling System Design Description, dOE-HTGR-90016, Revision 0 (Nov. 1993).

[2] G. Atomics, Gas Turbine-Modular Helium Reactor (GT-MHR) Conceptual Design Description Report, 910720 Revision 1 (Jul. 1996).

[3] Nuclear Regulatory Comminission, U.S. Nuclear Regulatory Commission Regulations: Title 10, Code of Federal Regulations (Aug. 2007).

[4] J. Achard, D. Drew, R. Lahey, Analysis of nonlinear density-wave oscillations in boiling channels., Journal of Fluid Mechanics 155 (1985) 213–232.

[5] A. Satoh, K. Okamoto, H. Madarame, Instability of Single-phase Natural Circulation Under Double Loop System, Chaos, Solitons & Fractals 9 (9) (1998) 1575–1585. doi:10.1016/S0960-0779(97)00117-3.

[6] J. Boure, A. Bergles, L. Tong, Review of two-phase flow instability, Nuclear Engineering and Design 25 (2) (1973) 165–192. doi:10.1016/0029-5493(73)90043-5.

[7] S. Kakac, B. Bon, A Review of two-phase flow dynamic instabilities in tube boiling systems, International Journal of Heat and Mass Transfer 51 (3–4) (2008) 399–433. doi:10.1016/j.ijheatmasstransfer.2007.09.026.

[8] G. V. Durga Prasad, M. Pandey, M. S. Kalra, Review of research on flow instabilities in natural circulation boiling systems, Progress in Nuclear Energy 49 (6) (2007) 429–451. doi:10.1016/j.pnucene.2007.06.002.

[9] A. K. Nayak, P. K. Vijayan, Flow Instabilities in Boiling Two-Phase Natural Circulation Systems: A Review, Science and Technology of Nuclear Installations 2008 (2008) 1–15. doi:10.1155/2008/573192.

[10] J. Thome, Chapter 12: Two-Phase Flow Patterns, in: Wolverine Engineering Data Book III, Wolverine Tube Inc, 2004, pp. 12–1–12–34.

[11] L. S. Tong, Y. S. Tang, Boiling Heat Transfer And Two-Phase Flow, 2nd Edition, CRC Press, 1997.

[12] S. M. Ghiaasiaan, Two-Phase Flow, Boiling, and Condensation: In Conventional and Miniature Systems, 1st Edition, Cambridge University Press, 2007.

[13] M. Aritomi, J. H. Chiang, M. Mori, Geysering in parallel boiling channels, Nuclear Engineering and Design 141 (1–2) (1993) 111–121. doi:10.1016/0029-5493(93)90096-R.

[14] L. Neal, S. Zivi, R. Wright, The Mechanisms of Hydrodynamic Instabilities in Boiling Channel, eURATOM Report, Pro-ceedings of Symposium on Two-Phase Flow Dynamics, Eindhoven (1967).

[15] J. Bouré, A. Mihaila, The oscillatory behavior of heated channels, An analysis of the density effect. Part I: the mechanism (nonlinear analysis). Centre d'Etudes Nucleaires de Grenoble, Report CEA 3049.

[16] C. P. Marcel, M. Rohde, T. Van Der Hagen, Experimental and numerical investigations on flashing-induced instabilities in a single channel, Experimental Thermal and Fluid Science 33 (8) (2009) 1197–1208. doi:10.1016/j.expthermflusci.2009.08.001.

[17] C. P. Marcel, M. Rohde, T. Van Der Hagen, Experimental investigations on flashing-induced instabilities in one and two-parallel channels: A comparative study, Experimental Thermal and Fluid Science 34 (7) (2010) 879–892. doi:10.1016/j.expthermflusci.2010.02.002.

[18] F. D'Auria, G. Galassi, Characterization of instabilities during two-phase natural circulation in typical PWR conditions, Experimental Thermal and Fluid Science 3 (6) (1990) 641–650. doi:10.1016/0894-1777(90)90081-H.

[19] M. Aritomi, J. H. Chiang, T. Nakahashi, M. Wataru, M. Mori, Fundamental Study on Thermo-Hydraulics during Start-Up in Natural Circulation Boiling Water Reactors, (I), Journal of Nuclear Science and Technology 29 (7) (1992) 631–641. doi:10.1080/18811248.1992.9731576.

[20] G. Yun, G. Su, J. Wang, W. Tian, S. Qiu, D. Jia, J. Zhang, Two-phase instability analysis in natural circulation loops of China advanced research reactor, Annals of Nuclear Energy 32 (4) (2005) 379–397. doi:10.1016/j.anucene.2004.11.002.

[21] R. W. Johnson, The Handbook of Fluid Dynamics, 1st Edition, Springer, 1998.

[22] G. B. Wallis, J. H. Heasley, Oscillations in Two-Phase Flow Systems, Journal of Heat Transfer 83 (3) (1961) 363. doi:10.1115/1.3682286.

[23] P. Welander, On the oscillatory instability of a differentially heated fluid loop, J. Fluid Mech 29 (1) (1967) 17–30.

[24] Y. Zvirin, R. Greif, Transient behavior of natural circulation loops: Two vertical branches with point heat source and sink, International Journal of Heat and Mass Transfer 22 (4) (1979) 499–504. doi:10.1016/0017-9310(79)90053-X.

[25] S. Y. Lee, M. Ishii, Thermally induced flow oscillation in vertical two-phase natural circulation loop, Nuclear Engineering and Design 122 (1–3) (1990) 119–132. doi:10.1016/0029-5493(90)90201-8.

[26] S. Y. Lee, D. W. Lee, Linear analysis of flow instabilities in an open two-phase natural circulation loop, Nuclear Engineering and Design 128 (3) (1991) 317–330. doi:10.1016/0029-5493(91)90169-I.

[27] S. Guanghui, J. Dounan, K. Fukuda, G. Yujun, Theoretical and experimental study on density wave oscillation of two-phase natural circulation of low equilibrium quality, Nuclear Engineering and Design 215 (3) (2002) 187–198. doi:10.1016/S0029-5493(01)00456-3.

[28] A. Knaani, Y. Zvirin, Bifurcation phenomena in two-phase natural circulation, International Journal of Multiphase Flow 19 (6) (1993) 1129–1151. doi:10.1016/0301-9322(93)90081-5.

[29] A. Nayak, P. Dubey, D. Chavan, P. Vijayan, Study on the stability behaviour of two-phase natural circulation systems using a four-equation drift flux model, Nuclear Engineering and Design 237 (4) (2007) 386–398. doi:10.1016/j.nucengdes.2006.05.009.

[30] J. D. Lee, C. Pan, Nonlinear analysis for a double-channel two-phase natural circulation loop under low-pressure conditions, Annals of Nuclear Energy 32 (3) (2005) 299–329. doi:10.1016/j.anucene.2004.08.012.

[31] A. T. J. Hayward, Compressibility equations for liquids: A comparative study, British Journal of Applied Physics 18 (7) (1967) 965. doi:10.1088/0508-3443/18/7/312.

[32] K. Muralidhar, G. Biswas, Advanced Engineering Fluid Mechanics, Alpha Science Int'l Ltd., 2005, google-Books-ID: zqpLiQ19Sg8C.

[33] R. J. LeVeque, Finite Volume Methods for Hyperbolic Problems, 1st Edition, Cambridge University Press, 2002.

[34] I. G. Currie, Fundamental Mechanics of Fluids, Fourth Edition, CRC Press, 2012.

[35] S. Klein, G. Nellis, Thermodynamics, 1st Edition, Cambridge University Press, New York, 2011.

[36] IAPWS, Revised Release on the IAPWS Formulation 1995 for the Thermodynamic Properties of Ordinary Water Substance for General and Scientific Use (Sep. 2009).

[37] R. W. Johnson, The Handbook of Fluid Dynamics, Springer Science & Business Media, 1998, google-Books-ID: JBTlucgGdegC.

[38] F. P. Incropera, D. P. DeWitt, T. L. Bergman, A. S. Lavine, Introduction to Heat Transfer, 5th Edition, Wiley, Hobokenm NJ, 2006.

[39] R. LeVeque, Finite Difference Methods for Ordinary and Partial Differential Equations, Other Titles in Applied Mathematics, Society for Industrial and Applied Mathematics, 2007.

[40] W. E. Schiesser, The Numerical Method of Lines: Integration of Partial Differential Equations, Elsevier, 2012, google-Books-ID: 2YDNCgAAQBAJ.

[41] O. C. Zienkiewicz, K. Morgan, Finite Elements and Approximation, Courier Corporation, 2013.

[42] C. Kelley, Solving Nonlinear Equations with Newton's Method, Fundamentals of Algorithms, Society for Industrial and Applied Mathematics, 2003.

[43] K. Eriksson, D. Estep, C. Johnson, Applied Mathematics: Body and Soul: Calculus in Several Dimensions, Springer Science & Business Media, 2003.

[44] L. Armijo, Minimization of functions having Lipschitz continuous first partial derivatives., Pacific Journal of Mathematics 16 (1) (1966) 1–3.

[45] Y. Saad, Iterative Methods for Sparse Linear Systems, Other Titles in Applied Mathematics, Society for Industrial and Applied Mathematics, 2003.

[46] G. S. Rao, Mathematical Methods, I. K. International Pvt Ltd, 2009.

[47] Y. Saad, M. Schultz, GMRES: A Generalized Minimal Residual Algorithm for Solving Nonsymmetric Linear Systems, SIAM Journal on Scientific and Statistical Computing 7 (3) (1986) 856–869. `doi:10.1137/0907058`.

[48] H. F. Walker, L. Zhou, A simpler GMRES, Numerical Linear Algebra with Applications 1 (6) (1994) 571–581. `doi:10.1002/nla.1680010605`.

[49] P. Jiránek, M. Rozložník, M. Gutknecht, How to Make Simpler GMRES and GCR More Stable, SIAM Journal on Matrix Analysis and Applications 30 (4) (2008) 1483–1499. `doi:10.1137/070707373`.

[50] P. Jiránek, M. Rozložník, Adaptive version of Simpler GMRES, Numerical Algorithms 53 (1) (2009) 93–112. `doi:10.1007/s11075-009-9311-2`.

[51] C. A. Floudas, P. M. Pardalos, Encyclopedia of Optimization, Springer Science & Business Media, 2008.

[52] B. N. Datta, Numerical Linear Algebra and Applications, Second Edition, SIAM, 2010.

[53] M. Giaquinta, S. Hildebrandt, Calculus of Variations I: The Lagrangian Formalism, Springer Science & Business Media, 1996.

[54] D. A. Knoll, D. E. Keyes, Jacobian-free Newton–Krylov methods: A survey of approaches and applications, Journal of Computational Physics 193 (2) (2004) 357–397. `doi:10.1016/j.jcp.2003.08.010`.

[55] J. Guckenheimer, P. Holmes, Nonlinear Oscillations, Dynamical Systems, and Bifurcations of Vector Fields, no. v. 42 in Applied Mathematical Sciences, Springer, 1983.

[56] V. Galaktionov, J. Vázquez, A Stability Technique for Evolution Partial Differential Equations: A Dynamical Systems Approach, Progress in nonlinear differential equations and their applications, Birkhäuser, 2004.

[57] H. Gould, J. Tobochnik, The Chemical Potential and Phase Equilibria, in: Statistical and Thermal Physics: With Computer Applications, Princeton University Press, 2010, pp. 357–388.

[58] IAPWS, Release on the IAPWS Formulation 2008 for the Viscosity of Ordinary Water Substance (Sep. 2008).

[59] IAPWS, Release on the IAPWS Formulation 2011 for the Thermal Conductivity of Ordinary Water Substance (Sep. 2011).

[60] IAPWS, Release on Surface Tension of Ordinary Water, `http://www.iapws.org/relguide/Surf-H2O.html` (2014).

[61] G. Nellis, S. Klein, Heat Transfer, Cambridge University Press, 2009, google-Books-ID: D4FFiD6hZ94C.

[62] G. D. Matthew, The colebrook-white equation - an oft cited result but neglected derivation ?, Proceedings of the Institution of Civil Engineers 89 (1) (1990) 39–45. `doi:10.1680/iicep.1990.5250`.

[63] R. Burden, J. Faires, Numerical Analysis, Cengage Learning, 2004, google-Books-ID: wmcL0y2avuUC.

[64] H. K. Winning, T. Coole, Explicit Friction Factor Accuracy and Computational Efficiency for Turbulent Flow in Pipes, Flow, Turbulence and Combustion 90 (1) (2012) 1–27. `doi:10.1007/s10494-012-9419-7`.

[65] J. G. Collier, J. R. Thome, Convective Boiling and Condensation, Clarendon Press, 1994.